



Department für Biotechnologie

**DIFFERENTIATION OF ADIPOSE DERIVED
MESENCHYMAL STEM CELLS USING
SPECIALIZED BIOREACTORS**

Masterarbeit
zur Erlangung des akademischen Grades
Diplomingeneurin
an der Universität für Bodenkultur Wien

Eingereicht von:
Couperus Anna Marejke, BSc

Wien, März 2014

Erstprüfer: Univ. Prof. Dipl.-Chem. Dr. Kasper Cornelia
Zweitprüfer: Univ. Prof. Mag. Dr. Obinger Christian

Statement of Authenticity

I certify, that all materials presented here are of my own creation, and that any work adopted from other sources is duly cited and referenced as such.

Vienna, December 23rd, 2013

Signature

Acknowledgement

Ich möchte mich an dieser Stelle bei allen bedanken, die mich bei der praktischen Arbeit und der Verfassung dieser Diplomarbeit unterstützt haben.

Besonderer Dank gilt Frau Univ. Prof. Dipl.-Chem. Dr. Cornelia Kasper für die Ermöglichung und Betreuung der vorliegenden Diplomarbeit. Ebenso bedanke ich mich bei Dipl.-Chem. Anne Neumann und der gesamten Arbeitsgruppe für deren tatkräftige Unterstützung während des gesamten Weges.

Ein herzlicher Dank ist auch an meine Freunde und Studienkollegen für viele wertvolle Kommentare und kritisches Korrekturlesen gerichtet.

Zuletzt möchte ich aus tiefstem Herzen meiner Familie danken, die mir mein Studium ermöglicht hat und mir auch immer liebevoll unterstützend zur Seite gestanden ist.

Abstract

Articular cartilage repair remains one of the most intensely studied orthopaedic topics. A promising future for the repair of damaged articular cartilage lies in the tissue engineering approach. To date, this field has introduced new perspectives and potent methodologies. The ideal cell source for cartilage tissue engineering would be one that can easily be accessed, isolated, expanded and differentiated towards the chondrogenic lineage, like human mesenchymal stem cells (hMSCs). There are various sources for hMSCs, including bone marrow tissue, umbilical cord and adipose tissue. Especially adipose tissue has received much attention because it is ethical without any severe concerns and abundantly accessible in course of most bariatric, abdominoplastic and liposuction surgeries. *In vivo* articular cartilage cells are exposed to mechanical forces due to joint movement. To better reflect the natural three-dimensional microenvironment, dynamic cultivations of hMSCs on biomaterials are performed, applying different bioreactor systems, to optimize the yield and quality of *in vitro* expanded cartilage constructs. In this regard, two different objectives were investigated in this thesis. First of all, the influence of oxygen tension on the static cultivation of adipose tissue derived mesenchymal stem cells (adMSCs) was explored. And second, a tailor-made bioreactor system in special focus on its dynamic cultivation factors, including fluid flow induced shear stress and scaffold porosity, was evaluated. Cultivation of adMSC in hypoxic conditions (5% O₂) was performed and cell proliferation, metabolic activity, differentiation capacity were studied. Hypoxic conditions (5% O₂) caused an increase in the proliferation activity and a higher degree of differentiation of adMSCs. Evaluation of dynamic cultivation characteristics showed that this bioreactor system is a potent tool for cartilage tissue engineering. However, the data suggested, that Matristypt® is a non-suitable matrix for dynamic cultivation in this particular perfusion bioreactor system. Further investigations must be conducted with special focus on finding a scaffold, which provides the same biological compatibility but with a more porous matrix.

Kurzfassung

Die Behandlung von Gelenksknorpelschäden zählt zu den meist untersuchten Forschungsgebieten in der Orthopädie. Tissue engineering bietet dafür eine vielversprechende Zukunft und liefert neue Perspektiven, wie Methoden zur erfolgreichen Therapie von Knorpeldefekten. Das ideale zelluläre Ausgangsmaterial sollte gut verfügbar, leicht isolierbar und expandierbar sein und chondrogenes Differenzierungspotential aufweisen. Menschliche mesenchymale Stammzellen (hMSCs) besitzen alle diese Eigenschaften. Sie sind in zahlreichen Geweben zu finden, wie zum Beispiel im Knochenmark, der Nabelschnur aber auch im Fettgewebe und besitzen hinreichendes *in vitro* Expansion- und Differenzierungspotential. Besonders das Fettgewebe bietet sich als potentielle Quelle an, es unterliegt keinerlei ethischen Bedenken und ist reichlich verfügbar im Verlauf von bariatrischen Eingriffen, sowie Fettabsaugungen und Bauchdeckenstraffungen. *In vivo* unterliegen Gelenksknorpelzellen starken mechanischen Belastungen, die im Zuge von normalen Gelenkbewegungen auftreten. Um diese komplexe dreidimensionale Mikroumgebung in der Zellkultur besser wieder zu spiegeln, kommen dynamische Bioreaktorsysteme in der modernen Zellkulturtechnik von hMSCs zum Einsatz. Diese ermöglichen eine größere Zellausbeute und eine höhere Qualität des expandierten Knorpelgewebes. Im Bezug dessen wurden in dieser Arbeit zwei Aufgabenstellungen untersucht. Zuerst wurde der Einfluss von Sauerstoffstress auf aus Fettgewebe isolierten mesenchymalen Stammzellen (adMSCs) in statischer Kultivierung evaluiert. Weiters wurde ein speziell angefertigtes Bioreaktorsystem, mit besonderem Augenmerk auf dynamische Faktoren, wie dem durchfluss-induzierten Scherstress und dem Einfluss der Porosität der verwendeten Biomatrix, untersucht.

adMSCs wurden statisch unter hypoxischen Bedingungen (5% O₂) kultiviert und im Hinblick auf ihre Zellproliferationsrate, Stoffwechselaktivität und Differenzierungskapazität getestet. Es konnte ein Anstieg der Proliferationsrate, sowie ein höherer Grad an Differenzierung festgestellt werden. Die Evaluierung der dynamischen Kultivierungsbedingungen führte zu dem Ergebnis, dass das Bioreaktorsystem zwar geeignete Grundvoraussetzungen bietet, jedoch die verwendete Biomatrix Matristypt® eine zu geringe Porosität aufweist um erfolgreich in diesem Perfusionbioreaktorsystem eingesetzt werden zu können. Weitere Studien sind von Nöten mit speziellem Fokus auf Entwicklung einer geeigneten Matrix, die die biologische Kompatibilität mit ausreichender Porosität verbindet.

Contents

List of Abbreviations	VIII
List of Tables	X
List of Figures	XI
1 Introduction	1
2 Objectives	2
3 Theory	3
3.1 Cartilage tissue engineering.	3
3.1.1 Articular cartilage.	3
3.1.2 Current and future applications	6
3.2 Adipose derived mesenchymal stem cells	7
3.2.1 Harvesting, Isolation and expansion	8
3.2.2 Differentiation potential.	9
3.3 Static cultivation versus dynamic cultivation	10
3.3.1 Oxygen tension.	13
3.3.2 Fluid flow induced shear stress	14
4 Experiments	16
4.1 Experiments under static culture conditions	16
4.1.1 Non invasive in situ monitoring of dissolved oxygen in culture media during cultivation.	16
4.1.2 Seeding strategies for growth on scaffolds.	23
4.1.3 Isolation of adMSCs from abdominoplastic surgery material	29
4.1.4 Proliferation of adMSCs(64m)	29
4.1.5 Differentiation of adMSCs(82f) and adMSCs(64m)	31
4.1.6 Monitoring of oxygen consumption during differentiation of adMSCs(64m).	36
4.2 Characterization of a specialized bioreactor system for dynamic cultivation	39
4.2.1 Medium evaporation behavior of a bioreactor setup	40
4.2.2 Fluid flow, back pressure and shear stress correlation for a bioreactor system	41
5 Discussion and Outlook	45
5.1 Experiments under static culture conditions	45
5.2 Characterization of a specialized bioreactor system for dynamic cultivation	48
Bibliography	50

A	Material	55
A.1	Cells	55
A.2	Disposables	55
A.3	Laboratory equipment and devices	56
A.4	Chemicals	57
A.5	Culture media and solutions.	58
B	Methods	59
B.1	Culture conditions	59
B.2	Non invasive in situ monitoring of dissolved oxygen in culture media during cultivation	59
B.2.1	Experimental setup.	59
B.2.2	Non invasive in situ monitoring of oxygen partial pressure distribution	60
B.3	Seeding Strategies for growth on scaffolds	61
B.3.1	MTT assay	61
B.3.2	DAPI nucleic acid staining	62
B.4	Isolation of adMSCs from abdominoplastic surgery material	62
B.5	Proliferation of adMSCs	63
B.6	Differentiation	63
B.6.1	Fixation	63
B.6.2	Oil Red-O.	64
B.6.3	Alcian blue	64
B.6.4	Von Kossa	64
B.6.5	Alizarin red	64
B.7	Monitoring of oxygen consumption during differentiation of adMSCs	64
B.8	Perfusion system	65
B.8.1	Perfusion bioreactor design	65
B.8.2	Experimental Setup	68
B.8.3	Fluid characteristic and shear stress.	68
B.8.4	Scaffolds	70

List of Abbreviations

μl	Microliter
2D	Two dimensional
3D	Three dimensional
\varnothing d	Diameter
adMSC	Adipose derived mesenchymal stem cells
AgNO_3	Silver nitrate
AMP	Adenosine monophosphate
BMP	Bone morphogenic protein - 2
CaCl_2	Calcium chloride
cAMP	Cyclic adenosine monophosphate
cm^2	Square centimeter
cm^3	Cubic centimeter
CO_2	Carbon dioxide
d	Day
DAPI	4',6-Diamidino-2- phenylindol
ddH ₂ O	Double deionized water
DMSO	Dimethyl sulfoxide
EU	European Union
FDA	U.S. Food and drug administration
FGF	Fibroblast growth factor
fig.	Figure
g	Gramm
g	Gravity
GAG	Glycosaminoglycans
h	Height
h	Hour
HCl	Hypochloric acid
hMSCs	Human mesenchymal stem cells

M	Molar
m ²	Square meter
MAPK	Mitogen activated protein kinase
MgCl ₂	Magnesium chloride
min	Minute
ml	Milliliter
mM	Millimolar
mm	Millimeter
MSC	Mesenchymal stem cell
MTT	3-[4, 5- dimethylthiazol-2yl]-2, 5-diphenyltetrazolium bromide
n	Quantity
N ₂	Nitrogen gas
Na ₂ NO ₃	Sodium carbonate
NaHCO ₃	Sodium hydrogen carbonate
O ₂	Oxygen
PBS	Phosphate buffered saline
PD	Population doubling
PFA	para-Formaldehyde
PLA	Polylactic acid
PLG	Polyglycolic acid
PLGA	Polylactic-co-polyglycolic acid
scf	Scaffold
SD	Standard deviation
SDS	Sodium dodecyl sulfate
sec	Second
SEM	Standard error of mean
std	Standard
TGF- β 1	Transforming growth factor β 1
TGF- β 2	Transforming growth factor β 2
U.S.	United States
ucMSCs	Umbilical cord derived mesenchymal stem cells

List of Tables

- 4.1 Half life of dissolved oxygen and established plateau values in culture supernatant at different seeding densities under normoxic conditions 19
- 4.2 Half life of dissolved oxygen and established plateau values in culture supernatant at different seeding densities under hypoxic conditions 22
- 4.3 Weight loss of bioreactor systems through evaporation 40
- 4.4 Resulting shear stress at various fluid flow levels 43

- B.1 Cell concentrations 61
- B.2 Cell concentrations 61

List of Figures

3.1	Illustration of the extracellular matrix organization of articular cartilage	3
3.2	Stratified structure of cartilage demonstrating zonal arrangement	4
3.3	Process for cultivation of tissue engineered cartilage	7
3.4	<i>In vitro</i> differentiation potential of MSCs	9
3.5	A: Spinner flask bioreactor system; B: Rotating wall bioreactor system (Maxson, Orr, and Burg 2011)	11
3.6	Simple perfusion bioreactor system (Yeatts and Fisher 2011)	12
3.7	Signaling influenced by culture conditions in a perfusion system (Yeatts, Choquette, and Fisher 2013)	13
4.1	Dissolved oxygen in culture supernatant during cultivation in normoxic conditions	17
4.2	Dissolved oxygen in the culture supernatant during specific time spans at a seeding density of 1×10^5 cells/ml	18
4.3	Mean half life and plateau of dissolved oxygen after seeding and established plateau values in culture supernatant at different seeding densities under normoxic conditions	19
4.4	Dissolved oxygen in culture supernatant during cultivation in hypoxic conditions	20
4.5	Dissolved oxygen in the culture supernatant during specific time spans at a seeding density of 1×10^5 cells/ml	21
4.6	Mean half life and plateau level of dissolved oxygen after seeding and established plateau values in culture supernatant at different seeding densities under hypoxic conditions	22
4.7	Progression of cell proliferation of ucMSCs seeded on scaffolds	23
4.8	Glucose concentration of ucMSCs seeded on scaffolds	24
4.9	Lactate production of ucMSCs seeded on scaffolds	25
4.10	DAPI staining of harvested scaffolds on study day 1 with different seeding densities	26
4.11	DAPI staining of harvested scaffolds on study day 4 with different seeding densities	27
4.12	DAPI staining of upper side of harvested scaffolds on study day 7 with different seeding densities after DAPI staining	28
4.13	Bottom side of harvested scaffolds on study day 7 with different seeding densities after DAPI staining	29
4.14	Cell proliferation of adMSCs(64m) under normoxic and hypoxic culture conditions	30
4.15	Population doubling PD and cumulative cell number of adMSCs(64m) over 10 passages	31

4.16 Adipogenic differentiation of adMSCs(64m) and adMSCs(82f) at normoxic and hypoxic culture conditions	32
4.17 Chondrogenic differentiation of adMSCs(64m) and adMSCs(82f) at normoxic and hypoxic culture conditions	33
4.18 Osteogenic differentiation of adMSCs(64m) and adMSCs(82f) at normoxic and hypoxic culture conditions stained with Von Kossa	34
4.19 Osteogenic differentiation of adMSCs(64m) and adMSCs(82f) at normoxic and hypoxic culture conditions stained with Alizarin Red	35
4.20 Metabolic activity of adMSCs(64m) during differentiation under normoxic and hypoxic culture conditions	36
4.21 Oxygen kinetics during differentiation of adMSCs(64m) under normoxic culture conditions	37
4.22 Oxygen kinetics during differentiation of adMSCs(64m) under hypoxic culture conditions	38
4.23 IT-3a cell culture incubator table (Fraunhofer IGB)	39
4.24 Percental weight loss of bioreactor systems over 10 days	40
4.25 Pressure regime for a bioreactor system at a constant fluid flow of 1.5 ml/min for 25 h	41
4.26 Back pressure and shear stress regime against fluid flow	43
4.27 Calculated intrinsic permeability of Matristypt [®]	44
B.1 Setup of the oxygen monitoring system	60
B.2 Mini perfusion bioreactor (A), Matristypt [®] scaffold (B) and stainless steel mesh (C)	65
B.3 Scheme of the bioreactor system	66
B.4 Image of the bioreactor system stored in the cell culture incubator table	66
B.5 Technical drawing of the mini perfusion reactor	67

1 Introduction

The field of regenerative medicine has grown dramatically over the past decades. Especially in articular cartilage repair, tissue engineering has introduced new perspectives and methodologies as an alternative treatment to total and partial joint replacements. Finding an adequate cell source and bioreactor systems, which are able to reflect the highly complicated *in vivo* environment of articular cartilage are still challenging. The cell source can be embryonic stem cells, adult stem cells, like mesenchymal stem cells, reprogrammed differentiated cells (induced pluripotent stem cells or adult tissue-specific differentiated cells). Despite of the great differential potential of embryonic stem cell, their use comes with several limitations, including ethical and unpredictable risks. Adult tissue-specific cells, can often not be easily isolated and lack in *in vitro* expansion capabilities. By contrast, MSC represent a promising cell source. There are very little or no ethical concerns using these cells. In addition, they still have high self-renewal and proliferation capacity and they can be differentiated into various cell lineages. There are different sources for human mesenchymal stem cells (hMSCs) such as bone marrow tissue, umbilical cord and adipose tissue. Especially adipose tissue has received much attention because it is ethical without any severe concerns and abundantly accessible in course of most bariatric, abdominoplastic and liposuction surgeries. Modern expansion techniques involve highly specialized dynamic bioreactor systems and include adapted cell culture media, addition of signaling molecules, variation of physical and chemical factors and mechanical stimulation. Further knowledge of *in vivo* mechanisms which dictate cell fate, will help to mimic these initiating factors *in vitro*. Oxygen tension appears to be a crucial factor which influences MSC proliferation and differentiation capacity. *In vivo*, only a few cell types are exposed to atmospheric oxygen concentrations. Most tissues experience significant lower oxygen values. In case of cartilage tissue, mechanical stress also has to be taken into account. During every joint movement cells are exposed to various stress factors, including tensile, shear, compressive stresses and strains. All together these factors have a high impact on tissue modeling and development. In conclusion, invasive online monitoring and control of important cultivation parameters like pH, temperature, O₂, CO₂, metabolite concentrations and mechanical stimuli will help to provide the optimal growth conditions for the cells to create an artificial tissue.

2 Objectives

This study focuses on demonstration of *in vitro* proliferation and differentiation ability of adMSCs under normoxia (21% O₂) and hypoxia (5% O₂) and the eligibility of bioreactor systems to improve clinical cartilage therapies.

First of all, to optimize *in vitro* static cultivation a number of variables are investigated. The effect of reduced oxygen tension on proliferation capacity, metabolic activity and oxygen consumption rates in comparison to their differentiation lineage is evaluated. Moreover the multipotential character of adMSCs via specific histological staining methods is determined.

In addition, dynamic cultivation factors of a dynamic bioreactor system are evaluated and characterized with special focus on cartilage tissue engineering. In order to further optimize the *in vitro* 3D microenvironment and implement a cultivation strategy for adMSCs on 3D scaffolds the possibilities for controlling the culture conditions are explored. In particular the influence of fluid flow and scaffold porosity on resulting shear stress levels are investigated.

3 Theory

3.1 Cartilage tissue engineering

Articular cartilage repair remains one of the most intensely studied orthopaedic topics. To date the field of tissue engineering has introduced a new perspective and methodologies for the treatment of cartilage defects. An alternative therapy for the repair of damaged articular cartilage lies in the tissue engineering approach. However, routine tissue culture methodologies can hardly accomplish the high yield of cell production required for the manufacture of engineered cartilage tissue products. Thus, *in vitro* cell expansion has become a crucial step in tissue engineering of articular cartilage. Optimization of expansion protocols is a fundamental issue that needs to be improved. In particular, the finding of adequate sources of stem cells, selection of proper biomatrices and the development of large scale cell expansion processes are mandatory requirements for a sufficient production of chondrocytes (Melero-Martin and Al-Rubeai 2007).

3.1.1 Articular cartilage

Articular cartilage is a specialized, charged and hydrated soft tissue with a characteristic structural organization. It is a thin white tissue and covers the surface of all synovial joints in the human body (Goldring 2006). By its incredibly low coefficient of friction coupled with its ability to bear very large compressive loads, it is perfectly suited for placement in joints, like the knee and hip (Swieszkowski et al. 2007). Smoothness and thickness of the cartilage determines the load-bearing features and painless mobility of the joints. Its mechanical properties depend on the location within the cartilage, on the specific biochemical composition and structural arrangement of the extracellular matrix (Carey-Beth and Uhl 2001). The main extracellular components are collagen, proteoglycans, hyaluronan, non-collagenous proteins and water. All together they provide the shear, compressive, and permeability characteristics of the articular cartilage (Archer and Francis-West 2003). An illustration of the extracellular matrix organization of articular cartilage is given in figure 3.1. Articular cartilage does not contain any blood vessels, nerve endings and lymphatic vessels. Required nutrients are only provided by the surrounding tissues via diffusion, osmosis and perfusion. But this is a very slow process due to the thickness of the cartilage tissue (Archer and Francis-West 2003, Chung and Burdick 2008).

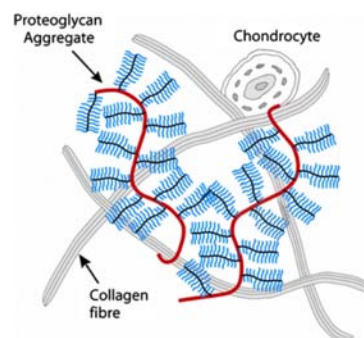


Figure 3.1: Illustration of the extracellular matrix organization of articular cartilage (Schulz and Bader 2007)

Chondrocytes are the only cells of articular cartilage and are responsible for the production of the extracellular matrix. However, they account for just between 5-10% of the entire wet weight. Water constitutes between 65-80% of the entire wet weight and is about 15% more concentrated at the surface than in the deeper zones. Collagen makes up about 15-22% of the wet weight and contains 90-95% type II collagen fibers with a small amount of types IX and XI. It provides the high tensile stiffness, strength and resistance of the tissue (Temenoff and Mikos 2000). Proteoglycans constitute about 4-10% of the total wet weight and are a mix of large aggregating (50-85%) and large non-aggregating (10-40%) proteoglycans (Melero-Martin and Al-Rubeai 2007). They are responsible for pressure elasticity and charged interactions with water. Incorporated non-collagenous proteins, elastins, integrins are responsible for the matrix organization and its maintenance. However, distribution and arrangement within the cartilage tissue is not uniform (Wescoe et al. 2008). Under the light microscope, four zones can be distinguished, namely the superficial zone, the middle zone, the deep zone and the calcified zone (figure 3.2). Each zone varies in structure and function, responds to different stimuli, and secretes different proteins (Carey-Beth and Uhl 2001).

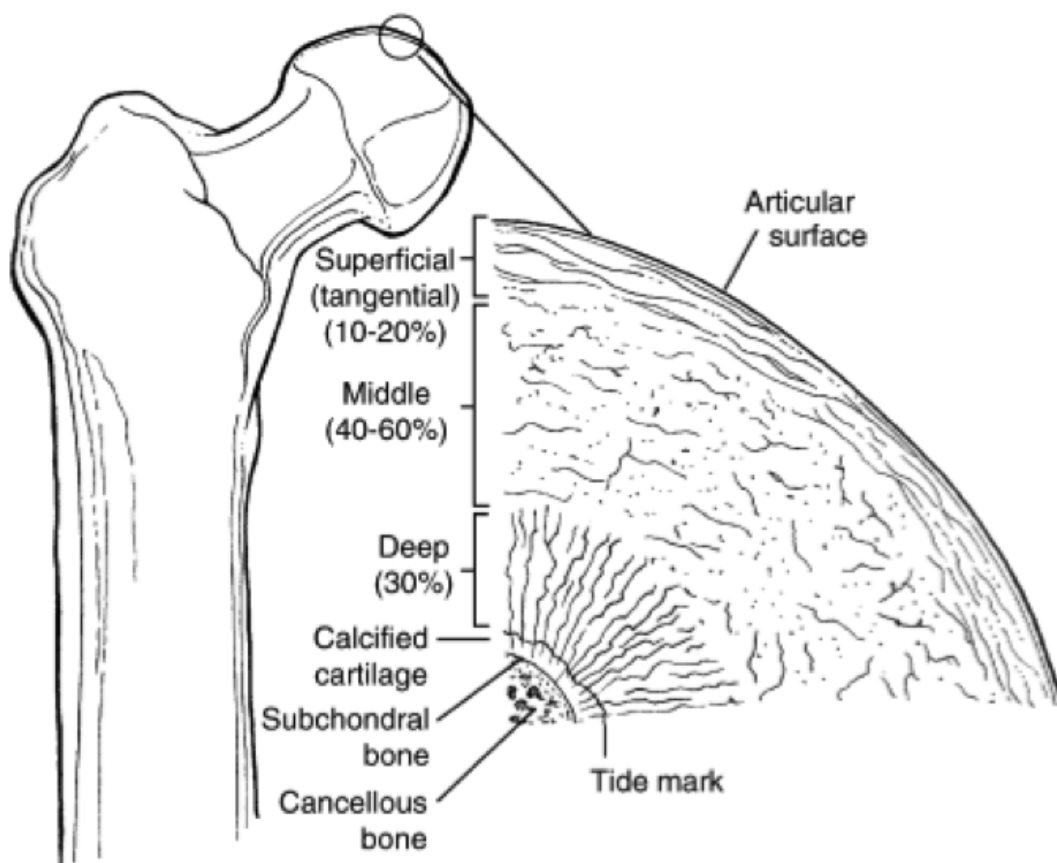


Figure 3.2: Stratified structure of cartilage demonstrating zonal arrangement (Pearle, Warren, and Rodeo 2005)

The superficial zone is responsible for the compressive strength of the tissue and provides the gliding surface. It is the thinnest zone, composed of two layers and is characterized by flattened chondrocytes. A acellular sheet with high quantities of collagen fibrils and relatively low quantities of proteoglycans covers the surface of the joint. Under this, the second layer of flattened and relatively inactive chondrocytes with their long axis to articular cartilage surface

is found. Also large amounts of fibronectin and water are found in this zone (Melero-Martin and Al-Rubeai 2007, Pearle, Warren, and Rodeo 2005, Carey-Beth and Uhl 2001).

The middle zone is larger than the superficial zone. In contrast, it consists of round, larger chondrocytes, which are biochemically more active than those in the superficial zone. The proteoglycan level is the highest among all four zones and collagen fibers show a more random arrangement compared to the superficial zone (Melero-Martin and Al-Rubeai 2007, Pearle, Warren, and Rodeo 2005, Carey-Beth and Uhl 2001).

The deep zone consists of collagen fibrils. In this area the collagen fibrils have the largest size among all zones. It is characterized by a high proteoglycan content and the lowest water content of all zones. The chondrocytes are aligned in radial columns and their synthetic activity is the largest (Melero-Martin and Al-Rubeai 2007, Pearle, Warren, and Rodeo 2005, Carey-Beth and Uhl 2001).

The calcified zone is partly mineralized with calcium. It is the thinnest layer and functions as the transition between cartilage and the underlying subchondral bone. The collagen fibrils from the deep zone extend into the calcified zone providing a strong anchoring system for the tissue on the subchondral bone. The calcified zone serves for structural and mechanical integration of articular cartilage to the underlying bone (Melero-Martin and Al-Rubeai 2007, Pearle, Warren, and Rodeo 2005, Carey-Beth and Uhl 2001).

It is the composition and highly complicated interaction of these components that makes regeneration and replacement techniques of articular cartilages challenging. Typically, articular cartilage engineering studies use homogenous cell assays, which purveys chondrocytes that produce large amounts of extracellular matrix, but lack in zonal organization. More attention has to be given on the differences between these zones. Especially methods of recreating zonal organization *in vitro* have to be developed.

Articular cartilage has a limited ability to recover after injuries and lesion. The combination of no blood supply and only a few cells distributed widely among a dense extracellular matrix leads to a limited healing ability (Melero-Martin and Al-Rubeai 2007). Common inflammatory response of hemorrhage, formation of fibrin clots, cellular production and migration of mesenchymal cells are missing (Buckwalter and Mankin 1999). The spontaneous repair of articular cartilage may occur depending on depth of the lesion. Superficial defects which do not affect the subchondral bone rely on the rarely spread chondrocytes for matrix remodeling. Deeper lesions require a blood supply from the well vascularized subchondral bone, which demands damage of blood vessels, bleeding and hematoma formation. With the resulting blood stream various types of stem cells and fibrocytes are provided. They further modulate to fibrochondrocytes (Hunziker 2002). In addition, large quantities of growth factors are also released from the bone tissue, which play an important role in initiating the repair response (Jackson et al. 2001). Nevertheless, these combinations of cells and growth factors produce a relatively disorganized network of collagen fibers, which only partially fills the defect with a structural weak and imperfect tissue. This heterogeneous composition and the consequential fragile biomechanical properties contribute primarily to its functional disability (Jackson et al. 2001). Except from the depth and degree of the lesion, factors like age, chronic conditions, associated instability and genetic predisposition are also factors which influence healing of cartilage (Buckwalter and Mankin 1999). For example, age drastically affects healing. In newborns, the mesenchymal stem cells, which are needed for healing occur 1 in every 10,000 cells in the bone marrow. This ratio reduces to 1 in 100,000 in teens, 1 in 400,000 by the age of 50 and 1 in 2 million in an 80 year old (Hunziker 2002).

Articular cartilage lesions occur during the course of many joint diseases. They result of either traumatic mechanical destruction or progressive mechanical degeneration. Diseases of hyaline cartilage represent one of the major health problems especially in industrialized countries with a high life expectancy (Schulz and Bader 2007). Some of the most common diseases deriving from articular cartilage lesions are arthritis, osteoarthritis and rheumatoid arthritis. Arthritis is a term for disorders that are characterized by inflammation of one or more joints including the knee, the shoulder, elbow, hip, and ankle joint (Leavitt M 2005). The term arthritis includes more than 100 different disease patterns. More than 40 million US American citizens (approximately 15% of the overall population of the USA) suffer from arthritis. It is estimated that nearly 80 million US American citizens will be affected by the year 2020 (Schulz and Bader 2007). For example osteoarthritis, which is an erosion of articulated surfaces, causes massive joint pain and stiffness. Progressive mechanical degeneration of the articular cartilage leads to successive loss of the normal cartilage structure and function. It begins with cartilage softening and proceeds to actual fragmentation of the cartilage. A loss of articular knee cartilage results. The underlying bone has no protection from daily living and starts to degrade, an event that may lead to osteoarthritis. In Germany 150,000 to 180,000 arthroscopic operations are conducted every year, while there are 1,500,000 such operations in the US and 350,000 among the EU. This has major economic consequences, creating direct and indirect costs of 8 billion Euros per year, solely in Germany (Csaki, Schneider, and Shakibaei 2008).

Currently, no reliable long term curative strategies have wide clinical acceptance. The traditional treatments are: 1) microfracture surgery; 2) autologous chondrocyte implantation; 3) transplants to fill the defect with autografts or allografts; 4) cell-based therapy (total and partial joint replacements) (Zhang, Hu, and Athanasiou 2009). Nowadays the most popular therapies are microfracture surgery and autologous chondrocyte implantation. In the microfracture technique, tiny fractures are caused by drilling small holes into the subchondral bone until bleeding occurs, which may induce spontaneous repair responses (Melero-Martin and Al-Rubeai 2007). In 75% of young patients, with even higher success rates in young athletes an improvement in joint function and pain relief was observed (Wu et al. 2013). Autologous chondrocyte implantation was first introduced by Brittberg et al. in 1994. The basic idea is to fill the defect or lesion with autologous chondrocytes, which are harvested by biopsies from low-weight bearing and healthy cartilage. After isolation and *in vitro* expansion of chondrocytes, they are injected in form of a cell-suspension into the injured area (Brittberg et al. 1994).

3.1.2 Current and future applications

Current techniques can, to a certain degree, repair cartilage, but until now there has been no technique that could sufficiently reproduce the structure and biomechanical function of normal articular cartilage. A new technique, namely matrix-induced autologous chondrocyte implantation has become more popular. Instead of using a cell suspension, cells are seeded on a collagen (type III) matrix, a 3D biomaterial scaffold. Clinical studies with a follow-up period of 2-10 years revealed that 90% of treated patients developed well-integrated new cartilage tissue (Wu et al. 2013). Nevertheless this therapy has some drawbacks. One limiting factor is the age of patients, since this treatment is only successfully implied for patients under 50 years. Another major drawback is the phenomenon of de-differentiation of chondrocytes during *in vitro* expansion. However, *in vitro* expansion is required due to the large amount of chondrocytes needed. To overcome these barriers, a possible solution is the use of mesenchymal stem cells as an alternative cell source rather than using adult chondrocytes. In figure 3.3 one approach

for the development of functional tissue engineered cartilage is presented (Wu et al. 1999). Adequate donor tissue is harvested and MSCs are isolated by enzymatic digestion. After cell expansion, cells are seeded onto a suitable biodegradable polymer scaffold and cultured within a bioreactor system. During cultivation, cells proliferate, differentiate and evolve the typical matrix, resulting in a construct that can be implanted to treat articular surface defects.

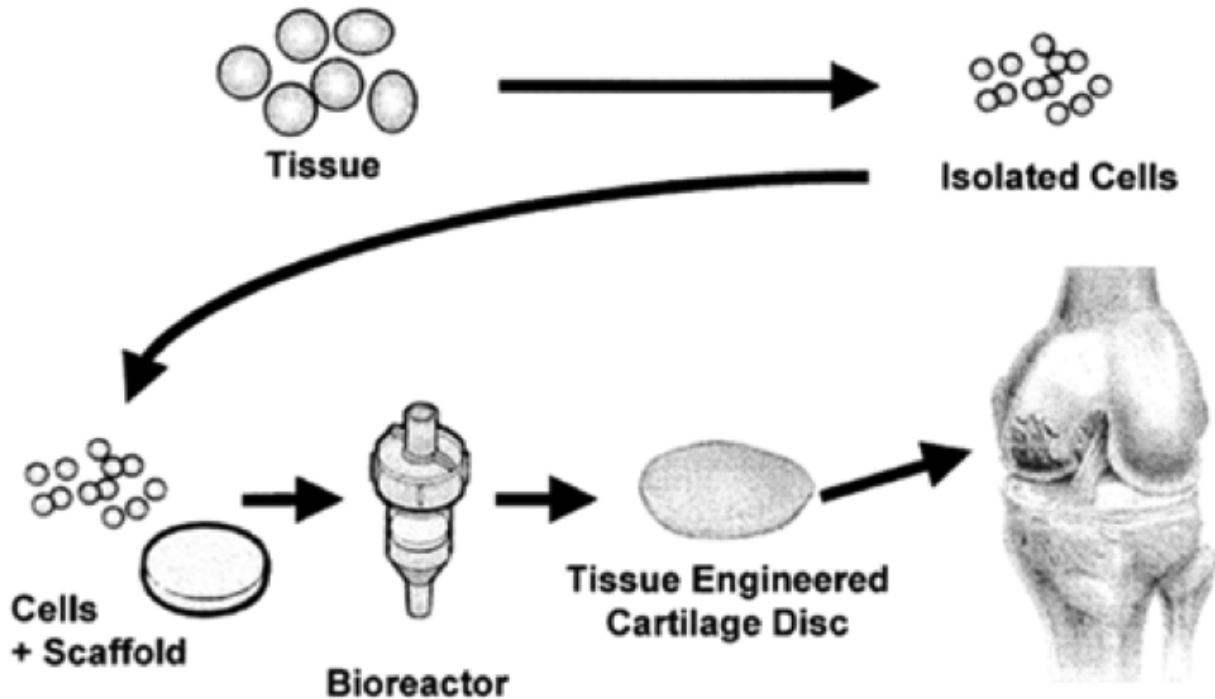


Figure 3.3: Process for cultivation of tissue engineered cartilage (Wu et al. 1999)

3.2 Adipose derived mesenchymal stem cells

The ideal cell source for cartilage tissue engineering is one that can easily be accessed, isolated and expanded and which synthesizes abundant cartilage-specific extracellular matrix components. Stem cells such as adult mesenchymal stem cells are a promising cell sources for articular cartilage tissue engineering. MSCs can conveniently be differentiated into chondrocytes *in vitro* (Pelttari, Steck, and Richter 2008). They have a high enough proliferation capacity to obtain a sufficient quantity of cells, without losing their MSC phenotype (Csaki, Schneider, and Shakibaei 2008). In addition, they do not induce an immune response like allografts do (Zhang, Hu, and Athanasiou 2009). MSCs can be harvested from a variety of human tissues, such as bone marrow, adipose tissue, umbilical cord, synovium, skeletal muscle, skin, etc. Especially the possibility of minimally invasive procedures to isolate MSCs from adipose tissues make them an attractive choice as an alternative cell source for adult chondrocytes in cartilage engineering. Even high amounts can be harvested from waste adipose tissue by liposuction or abdominoplastic surgery material. However, *in vitro* studies have shown that adipose-derived stem cells may have lower chondrogenic differentiation potential than bone marrow-derived MSCs (Zhang, Hu, and Athanasiou 2009). Moreover, the quality of cartilage produced by MSCs is still less compared to that produced by adult chondrocytes (Mahmoudifar and Doran 2012). Nevertheless adMSCs are attractive as a distinguished cell source because of their chondrogenic differentiation capability on diverse biomaterial scaffolds including agarose, alginate, and biologically active gelatin to create tissue engineered cartilage constructs (Chung

and Burdick 2008). Furthermore, ethical issues regarding embryonic stem cells in addition to safety concerns, make tissue derived MSCs the most favorable candidate for clinical cartilage tissue engineering (Mahmoudifar and Doran 2012).

3.2.1 Harvesting, Isolation and expansion

adMSCs can be isolated from liposuctions or abdominoplastic surgery in large numbers. After tissue digestion with collagenase, several centrifugation steps follow to isolate the stromal vascular cells from the primary adipocytes. Then cells can be easily grown under standard tissue culture conditions (Baer and Geiger 2012). These cells, called adipose derived MSCs, can differentiate into adipocytes, osteoblasts, chondrocytes and myocytes under specific culture conditions *in vitro* (Wu et al. 2013). The main advantages to methods of obtaining MSCs are adipose tissue can be obtained by minimal invasive procedures and MSCs yields are higher in contrast to other sources like bone marrow or umbilical cord blood (Csaki, Schneider, and Shakibaei 2008).

Conventional expansion of adMSCs involves flat, two-dimensional cell cultures in plastic flasks. Because of the limited available surface area only low yields can be achieved. To obtain large quantities of cells, the number of T-flasks or Petri-dishes have to be increased drastically. This leads to a not only time-consuming procedure but also to a higher risk of contamination. For tissue engineering a 3D environment need so be provided since the goal is to create a 3D tissue. The main focus lies on polymeric materials in form of hydrogels, sponges and fibrous meshes (Mauk and Burdick 2011). An optimal scaffold for cartilage tissue engineering provides the cells with an environment that contains niches which supports cell proliferation and stimulates cells to synthesize cartilage matrix. It substitutes the function of the native matrix until new cartilage has formed (Kock, Donkelaar, and Ito 2012). Such a 3D environment needs to:

- be biodegradable, without toxic metabolites
- have a porosity that allows diffusion of nutrients and waste products
- support cell viability, proliferation, differentiation and extra cellular matrix production
- be able to fix to and integrate with the tissue at the lesion
- provide mechanical support and stability.

A range of biomaterial scaffolds, including natural polymers extracted from living organisms and synthetic materials obtained from various chemical processes, have been widely investigated for tissue repair and regeneration (Zhang, Hu, and Athanasiou 2009). There are two main groups: natural and synthetic scaffolds. Natural scaffolds constituted from hyaluronan, agarose, alginate, chitosan and collagen are widely used in articular cartilage engineering (Frenkel and Cesare 2004). They are known for their good biocompatibility, cell attachment properties and support of differentiation (Flynn et al. 2008). Especially non-sulfated glycosaminoglycans and hyaluroans are used to support chondrogenesis (Stillaert et al. 2008). Agarose and alginate are polysaccharides derived from seaweed and are used to encapsulate cells (Awad et al. 2004). Both of these materials exhibit excellent cytocompatibility for cell growth. Their major drawbacks are their poor degradation properties. Collagens are main protein components of extra cellular matrix in natural cartilage. They contribute to cell adhesion, proliferation and differentiation and the most common scaffold materials used for cartilage tissue engineering (Zhang,

Hu, and Athanasiou 2009). Synthetic materials are highly investigated due to the desire to design a tailor-made scaffold. The biodegradable polymers polylactic acid (PLA), polyglycolic acid (PLG) and their co-polymer polylactic-co-polyglycolic acid (PLGA) are used (Frenkel and Cesare 2004) and FDA approved (Zhang, Hu, and Athanasiou 2009). Fabricated polymers are characterized by their uniform and reproducible structure. Their main advantage is their controllable porosity and crafted surface structure to enhance cell attachment, proliferation and differentiation (Frenkel and Cesare 2004). However, they don't provide the same cytocompatibility as natural derived scaffolds and may induce an immune response caused by metabolites during degradation of the material (Chung and Burdick 2008).

3.2.2 Differentiation potential

Adipose tissue has proven to be a reasonable source for adult stem cells with multipotent character such as MSCs. Differentiation is commonly induced by insulin, dexamethasone, cyclic AMP agonist, β -glycerophosphate, heparin, ascorbate and various cytokines depending on the cell lineage. adMSCs can be differentiated *in vitro* along various cell lineages, including adipogenic, chondrogenic, osteogenic and myogenic cells (Zuk et al. 2002). Furthermore, neuro-genetic marker expressions have been reported, but to date no studies have clearly shown that adMSCs demonstrate the full functionality profile of mature neuronal or glial cells (Trempe et al. 2011, Baer and Geiger 2012, Gimble et al. 2008, Liu, Zhuge, and Velazquez 2009). MSCs are characterized by their intrinsic self-renewal capability, their multilineage differentiation potential is illustrated in figure 3.4.

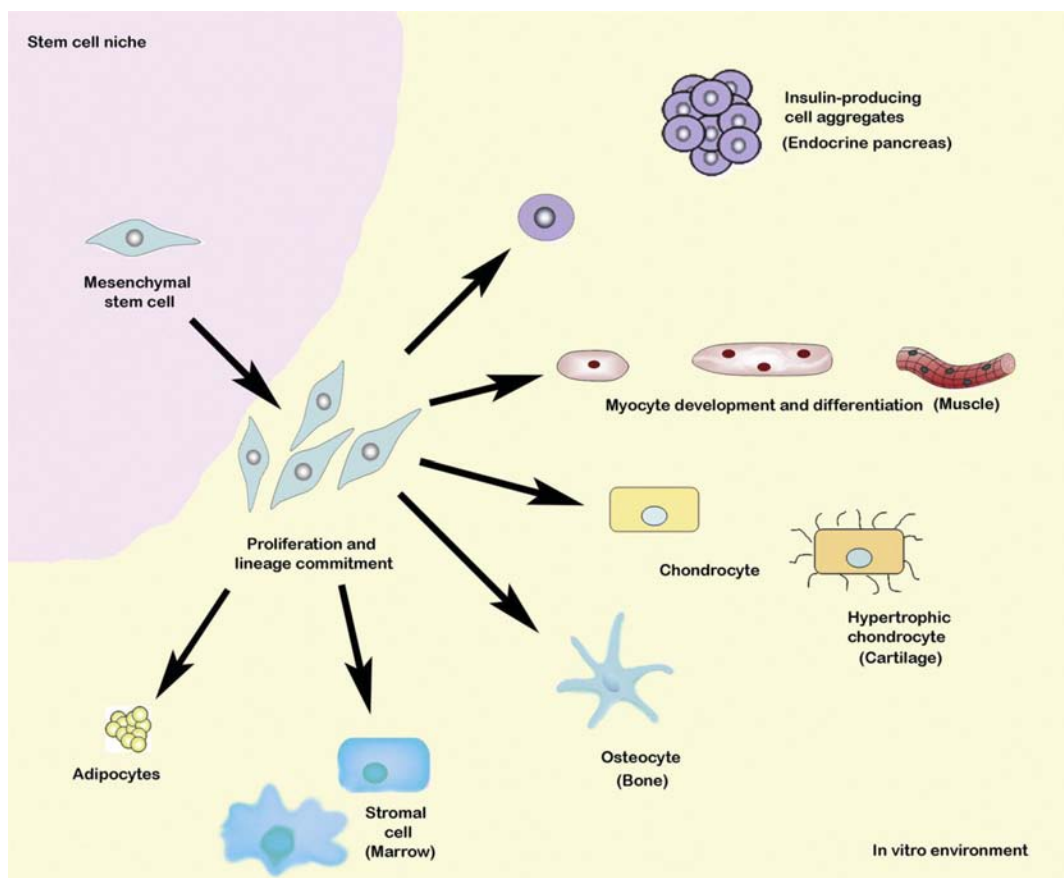


Figure 3.4: *In vitro* differentiation potential of MSCs (Kode et al. 2009)

Adipogenic differentiation

adMSCs can be induced to undergo adipogenesis by a number of stimuli. The most prominent are those which increase intracellular levels of cAMP, e.g. forskolin (Gimble et al. 2008). Additional inductive compounds are glucocorticoid receptor ligands, such as dexamethasone and insulin. First of all, cells reduce their proliferation rate and differentiate into preadipocytes. In the second step, the preadipocytes undergo another differentiation and begin to form small vacuoles filled with lipids (Jones et al. 2007). Within about two weeks of *in vitro* cultivation the morphology of adMSCs changes completely from fibroblast-like stromal cells to oval, neutral lipid droplet-filled cells (Lindroos, Suuronen, and Miettinen 2011). This process can be enhanced by adding linoleic, palmitic and oleic fatty acids supplements to the medium. The resulting differentiated adMSCs show the typical biochemical features characteristic of mature adipocytes, including the expression of gene markers (fatty acid-binding protein 4, lipoprotein lipase), secretion of adipokines (adiponectin, leptin) (Rodriguez et al. 2005). Adipocyte characteristic lipid-filled vacuoles can be visualized by histological staining with Oil Red-O (Bunnell et al. 2008).

Osteogenic differentiation

adMSCs differentiate along the osteocyte lineage in the presence of ascorbic acid-2-phosphate, β -glycerophosphate, dexamethasone and vitamin D3 (Gimble et al. 2008). During induction, cells quickly form slightly packed colonies and deposit calcium phosphate mineral within their extracellular matrix (Lindroos, Suuronen, and Miettinen 2011). A mineralization structure can be observed after one week. Osteogenic differentiation is accompanied with expression of osteogenic genes and proteins, such as osterix, cbfa1, osteopontin, osteonectin, osteocalcin collagen type I, BMP-2 and BMP-4 (Jones et al. 2007). Characteristic calcium deposition can be visualized by staining with Alizarin Red solution or Von Kossa staining (Bunnell et al. 2008).

Chondrogenic differentiation

adMSCs display chondrogenic characteristics following induction with ascorbate, dexamethasone and TGF- β 1. Common media additives are sodium pyruvate, proline, L-glutamine (Gimble et al. 2008). Chondrogenic differentiation occurs in three stages. First, the dividing adMSCs begin to express extracellular matrix proteins, which initiate the cells to form nodules. Next, cells within these nodules become chondrocytes and then start to secrete collagen and proteoglycan, which are the main components of the extracellular matrix of cartilage (Lindroos, Suuronen, and Miettinen 2011). In particular they express aggrecan, chondroitin sulfate, collagen type II and IV and proteoglycans (Jones et al. 2007). Accumulation of chondrocyte matrix can be detected with alcian blue staining (Bunnell et al. 2008).

3.3 Static cultivation versus dynamic cultivation

Successful *in vitro* engineering of cartilage tissue requires to mimicking the natural *in vivo* environment. Dynamic culture systems, like bioreactors are a promising tool to generate and adapt this environment on a level which cannot be provided by static cultivation. Bioreactors with integrated sensors are important to gather information about cell growth, viability and

nutrient consumption. In addition, it is possible to control and monitor cultivation parameters such as nutrient supply, gas and metabolite concentrations, pH, temperature, pressure, shear forces and cell mass growth. However, an understanding of the signaling pathways that induce proliferation and a guided differentiation is essential. During differentiation, chemical, biological and mechanical signals dictate the cells fate. Key signaling cascades for adMSCs differentiation are the MAPK, Wnt, and SMAD pathways (Yeatts, Choquette, and Fisher 2013). All these pathways are mediated by growth factors including bone morphogenic protein 2 (BMP-2), transforming growth factor β 2 (TGF- β 2), and fibroblast growth factor (FGF). *In vivo* these factors are released by surrounding cells or induction by physical stimuli. *In vitro* this influencing factors need to be substituted. Due to the adding of growth factors to the culture media and mechanical stimuli deriving from the bioreactor system an *in vivo*-like environment can be created.

A broad variety of bioreactor systems are used in tissue engineering. While the process of tissue engineering is not yet fully understood and the perfect culturing conditions are still unknown, current research focuses on operation strategies and on bioreactor design. Typical bioreactor systems are spinner flasks, rotating wall bioreactors and perfusion bioreactors. In spinner flasks scaffolds seeded with cells are attached to needles hanging from the stopper of the flask (figure 3.5 A). Media is added to cover the scaffolds and mixing is maintained with a magnetic stir bar in the bottom of the flask (Martin, Wendt, and Heberer 2004). Media is changed every few days to ensure sufficient nutrient supply. The rotating wall bioreactor is designed by NASA to simulate the effects of microgravity (figure 3.5 B). The most common type is the slow turning lateral vessel. This bioreactor consists of two concentric cylinders. The stationary inner cylinder has a membrane that allows gas exchange while the outer cylinder, made from a non-permeable material, rotates. The space between the two cylinders is perfused continuously with media. Pre-seeded scaffolds or microcarriers are kept in a state of constant free-fall. This is done by adjusting the speed of rotation of the outer cylinder so that the centrifugal force just balances the force of gravity and the fluid drag on the objects inside. Mixing occurs due to the small amount of unavoidable settling which creates movement of the scaffold/microcarrier relative to the media. But both system do not provide full control of culture parameters and do not perfuse media into the scaffold.

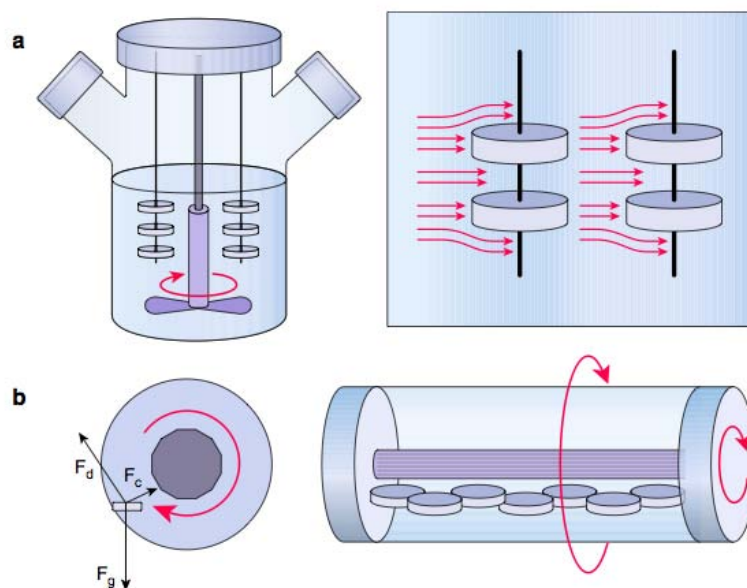


Figure 3.5: A: Spinner flask bioreactor system; B: Rotating wall bioreactor system (Maxson, Orr, and Burg 2011)

Perfusion bioreactor systems feature a greater range of regulative options. Media perfusion is realized via a pump system, which directly perfuses medium through a porous scaffold. This ensures a homogenous nutrient supply and oxygen concentration for all cells. In static cultures nutrient deprivation and varying oxygen tension within scaffolds occur. Various different perfusion bioreactor systems have been developed but most consist of the same basic components: a media reservoir, a pump, a tubing circuit and a perfusion chamber (figure 3.6). The perfusion chamber accommodates the scaffold, which is fixed so that medium cannot flow around it. As a consequence the media perfuses directly through the pores of the scaffold. Silicone tubing is commonly used throughout the system to enable gas exchange and oxygenation. Due to this direct perfusion, developing such systems is quite challenging because the perfusion chamber must be tailor-made for a specific scaffold and the scaffold must have the right porosity. Those bioreactor systems have a great potential to mediate signaling pathways to induce and enhance both adMSC proliferation and differentiation.

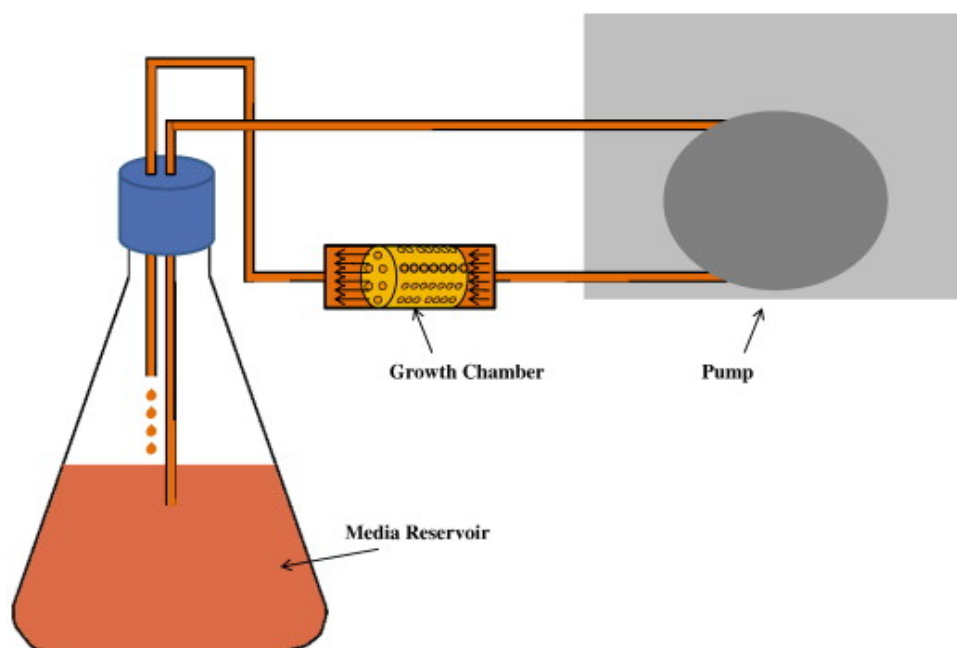


Figure 3.6: Simple perfusion bioreactor system (Yeatts and Fisher 2011)

The most promising dynamic parameters in cartilage tissue engineering are mechanical shear stress and oxygen tension, which can be controlled using such bioreactor systems. In figure 3.7 an illustration of signaling pathways influenced by both stimuli is given. Shear stress is achieved by the medium perfusion through the scaffold within the bioreactor system. The amount of shear stress, which the cells are exposed to depends on several variables, including flow rate, port size, and scaffold porosity. Various oxygen tensions are usually achieved by substitution of ambient air with nitrogen. The general mechanism consists of three kinase cascades that bridge the cellular signal, such as the binding of growth factors to their receptor or mechanical stimuli, into the cytoplasm and nucleus, where differentiation specific genes are transcribed and translated.

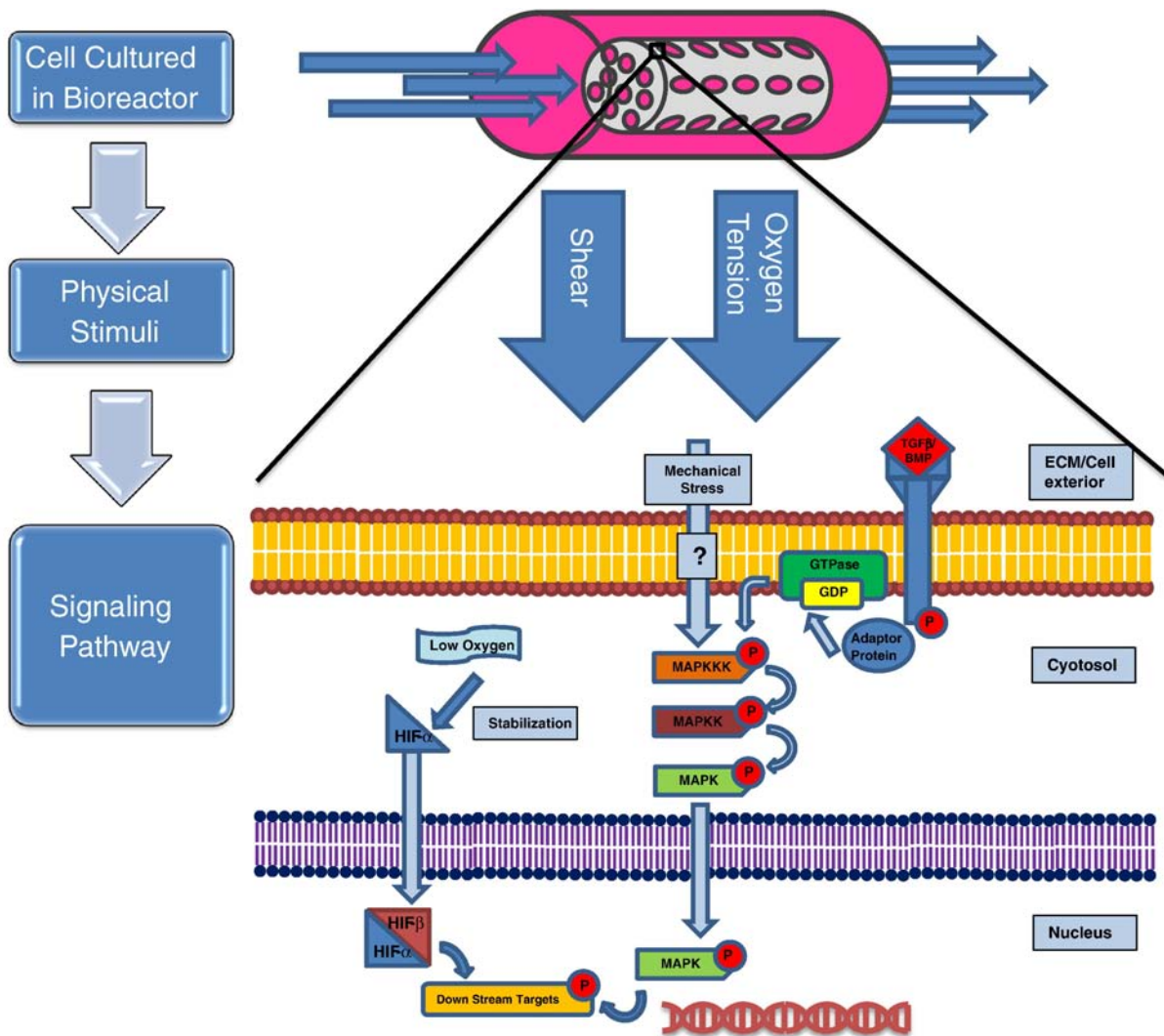


Figure 3.7: Signaling influenced by culture conditions in a perfusion system (Yeatts, Choquette, and Fisher 2013)

3.3.1 Oxygen tension

Only few cell types in the human organism are exposed to atmospheric oxygen tension, for instance keratinocytes and melanocytes in the epidermis, pneumocytes and macrophages in lung alveoli and cells of the corneal epithelium (Ivanovic 2009). The partial oxygen pressure in various organs and tissues depends on the consumption rate and tissue vascularization:

- Adipose tissue: 10-15% (Symonds 2012)
- Articular cartilage: 7% on the surface; less than 1% in the deep zones (Archer and Francis-West 2003)
- Bone marrow: 6-7% (Fehrer et al. 2007)

Together, these data indicate that low oxygen tensions (1- 15%) are physiological "normoxic" for MSCs (Mohyeldin, Garzón-Muvdi, and Quiñones-Hinojosa 2010). This means that MSC develop under significantly lower oxygen tensions compared to those used in standard cell culture techniques (Hansen et al. 2001). Due to the avascular nature of cartilage, the relatively

low levels of O₂ in the synovial fluid and the large O₂ diffusion distance, the chondrocytes' environment is subject to lower O₂ tension than in most other tissues (Malladi et al. 2006). Nevertheless the tissue requires O₂, but it consumes it with a low rate because of its primary glycolytic metabolism. *In vitro* cultivation of adMSCs under hypoxic culture conditions have shown an increased proliferation and expression of chondrogenic markers as compared to cultivation under normoxic conditions (Valorani et al. 2012; Yamamoto et al. 2013; Wang et al. 2005). Additionally, hypoxia supports chondrogenic rather than osteogenic differentiation of adMSCs and enhances cartilage matrix synthesis (Meyer et al. 2010; Mohyeldin, Garzón-Muvdi, and Quiñones-Hinojosa 2010). These findings suggest that oxygen tension could play an important role in regulating the proliferation and differentiation of adMSCs *in vitro*. Further understanding of the basic metabolism of articular cartilage and chondrocytic progenitor cells is necessary, before oxygen can be successfully utilized as a functional tool in cartilage tissue engineering. Further investigations are necessary to understand how different levels of oxygen tension can affect chondrogenesis. Alterations in the oxygen tension could then be used to enhance chondrogenic differentiation. In conclusion standard cell culture conditions with 21% oxygen do not mimic the physiological situation of cartilage. Cultivations under standard cell culture conditions lead to different biochemical characteristics and a less differentiated cell population (Grayson et al. 2006, Baumgartner et al. 2010). The availability of oxygen may possibly limit the chondrocytes metabolism. Nevertheless it is known that normoxic in comparison to hypoxic conditions supports the proliferation and stimulate collagen type II secretion in cultured chondrocytes (Hansen et al. 2001; Grayson et al. 2006; Krinner et al. 2009).

3.3.2 Fluid flow induced shear stress

Musculoskeletal tissues respond very sensitively to their mechanical environment, which allows them to adapt perfectly to their physical demands. Mechanical stimuli influence structure and function of tissues during their entire life cycle, including development, growth, remodeling, injury, disease and repair (Liu, Yuan, and Wang 2010). In particular, chondrocytes and chondroprogenitor cells have been shown to interact with a lot of mechanical factors such as deformation, shear forces, fluid flow, hydrostatic and osmotic pressure (Schmidt and Baier 2000). Bioreactors used for cultivating cartilage tissue try to mimic the mechanical load of cartilage, which results from the motion of and forces on joints. Joint movement produces a complex environment in articular cartilage *in vivo*, including tensile, shear and compressive stresses and strains (Carter and Wong 2003). Accordingly, bioreactors which provide the possibility of mechanical stimulation have been developed and examined for their potential to further induce and support chondrogenic differentiation (Maxson, Orr, and Burg 2011, Grad et al. 2011). Exposure of MSCs to mechanical stress influence cell signaling and have an impact on their differentiation (Bjerre et al. 2008). Shear stress induced by fluid flowing across a construct surface and into the cellular porous space is believed to be a very effective mechanical stimulus in activating mechanotransduction signaling (Huang, Farrell, and Mauck 2010, Yeatts, Choquette, and Fisher 2013). In addition, it increases mass transport of nutrients and oxygen is distributed more efficiently via medium perfusion (Martin, Wendt, and Heberer 2004). But flow through the scaffold is highly non-uniform, the highest speeds are at the center, while the lowest speeds occurred at scaffold surfaces and chamber wall. This results in a parabolic shear stress distribution (Yeatts et al. 2012, Porter et al. 2005). The resulting shear stress depends not only on the culture medium flow rate, but also on the scaffold 3D geometry, in particular porosity (Boschetti et al. 2006). The shear forces on human articular cartilage have been measured in terms of

the equilibrium shear modulus. It was about 2.6 MPa (Schulz and Bader 2007). Fluid flow induced shear stress applied to adult chondrocytes resulted in high-density monolayer culture with shifts in matrix gene expression and protein production within hours of exposure (Mawatari et al. 2010). Shear stress is also a potent modulator of the amount and type of extracellular matrix synthesized. Perfusion and rotating wall bioreactors have been shown to enhance extracellular matrix accumulation by chondrocytes seeded in porous polymeric scaffolds (O'Connor, Case, and Guilak 2013). Culture in an oscillating bioreactor that delivered slow, directional perfusion to MSC constructs improved functional properties, increased type II collagen content, and supported a more homogeneous matrix deposition (Wescoe et al. 2008). These studies indicate the importance of fluid flow in tissue engineering, although it is still unclear whether fluid flow induced nutrient transport, growth factor activation and/or direct cellular stimulation are influencing the different cellular behavior (O'Connor, Case, and Guilak 2013). Nevertheless successful production of engineered cartilage with MSCs may require mechanical conditioning to induce, maintain, and optimize chondrogenic activity.

4 Experiments

4.1 Experiments under static culture conditions

The aim of the following experiments was to prove the potential of differentiation and proliferation of freshly isolated adMSCs. First, the need of preconditioned medium for cultivation under hypoxic culture conditions was evaluated by a non invasive monitoring of dissolved oxygen in standard culture media during short term cultivation of ucMSCs. Furthermore, to optimize growth on scaffolds, a seeding strategy experiment was performed with ucMSCs. Proliferation potential of adMSCs(64m) was determined under varying oxygen tensions (5% and 21%). Effects of reduced oxygen level on the differentiation capability of adMSCs(64m) and adMSCs(82f) were also investigated. In addition, oxygen consumption during differentiation of adMSCs(64m) under normoxic and hypoxic culture conditions was monitored.

4.1.1 Non invasive in situ monitoring of dissolved oxygen in culture media during cultivation

The focus in this experiment lay in evaluating dissolved oxygen levels in the culture media during cultivation, especially finding out when an equilibrium of dissolved oxygen is reached. The experimental setup is described in B.2. Briefly, ucMSCs were plated in 24 well plates with an integrated O₂ sensor spot in the base of each well. Cells were seeded in 4 different initial concentrations (1×10^5 to 1×10^2 cells per ml). The study consisted of 2 groups and was conducted for 7 days with medium changes on day 2 (48 h) and day 5 (120 h). The first group was cultivated under normoxic conditions and the second group under reduced oxygen tension (5%). Dissolved oxygen was measured and automatically recorded online at intervals of 2 min over the whole study time. After seeding and after each medium change, the half life and plateau level of dissolved oxygen were calculated. The half life of oxygen decrease was used to characterize the duration until the oxygen equilibrium after seeding oder media replacements is reestablished. It was chosen as parameter because of its independence and autonomy regarding the height of amplitude. Thus, the duration of medium replacement and initial cell concentration had no influence on further calculations.

Normoxic environment

An overview of dissolved oxygen levels over cultivation is shown in figure 4.1. Data are presented as mean values of sixfold measurements and are plotted against time. Time points of medium changes are indicated as arrows in the figure. As general trend it can be observed that the higher the number of cell density, the lower dissolved oxygen values decreased during cultivation. Directly after seeding the dissolved oxygen level decreased below the plateau levels of each assay, indicating a faster rate of cellular consumption than gas diffuses into the medium. Moreover, the dissolved oxygen values in the cell culture supernatant progressively decreased during cultivation time in parallel to an increasing cell number. At a seeding density of 1×10^5 cells/ml the measured oxygen value dropped to a minimum of 10%. After the first medium replacement a more stable oxygen environment was observed. Only after more extended cell growth a further decrease of the oxygen concentration occurred. Furthermore, at the end of the

cultivation only a marginal decrease of the oxygen level can be seen. The experiment with 1×10^4 cells/ml showed a stable behavior after seeding. Over the course of cultivation the measured oxygen value progressively decreased after the first medium replacement. Even after a further medium change no stabilizing effect or reaching of the initial plateau level of dissolved oxygen in the supernatant could be observed. In both groups with lower seeding densities (1×10^3 and 1×10^2 cells/ml) a more stable oxygen environment could be seen until the end of cultivation. Only in the group with a seeding density of 1×10^3 cells/ml a slight decrease could be observed after the second medium replacement.

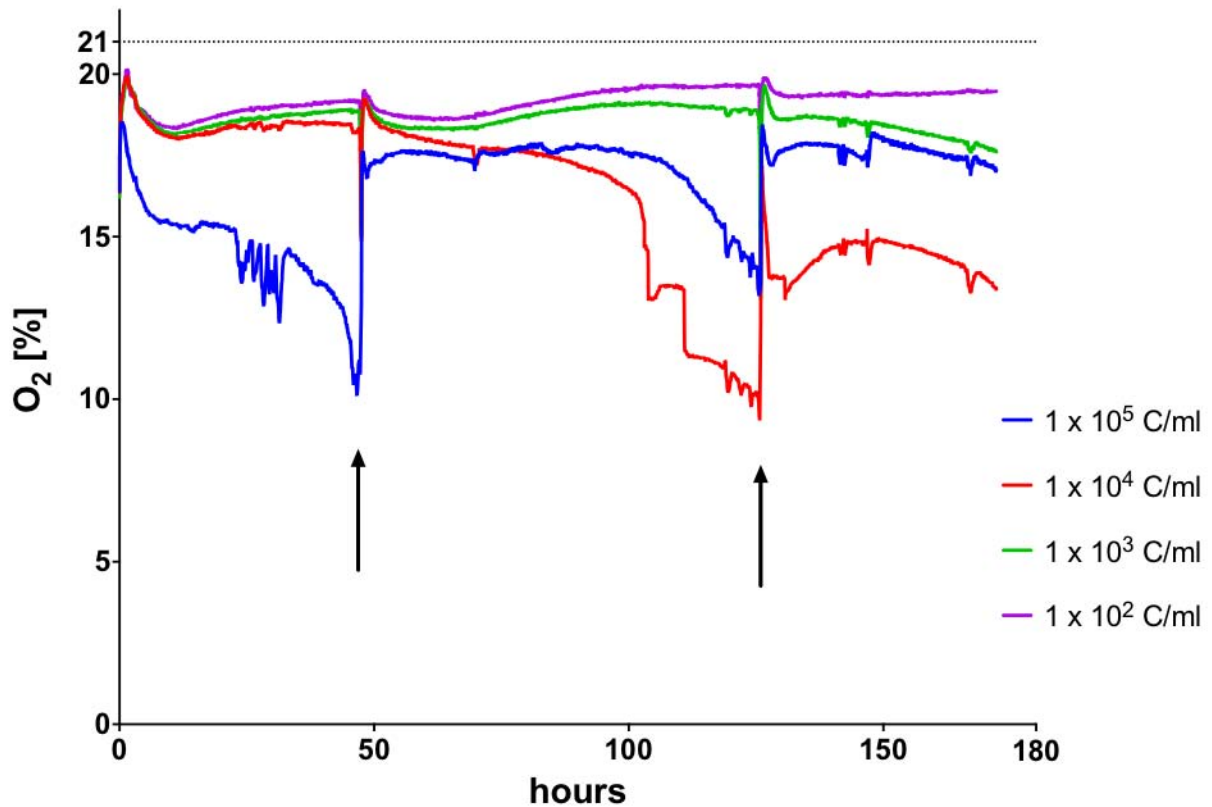


Figure 4.1: Dissolved oxygen in culture supernatant during normoxic cultivation of ucMSCs with different seeding densities under normoxic culture conditions. Data are the means of six-fold measurements for each seeding density. Medium changes are indicated by arrows.

Each seeding density assay was conducted in 6 fold measurements, whereby an exemplary analysis of data with a seeding density of 1×10^5 cells per ml is given in figure 4.2. Analysis of the other groups was assessed in similar way. The six data sets are represented in different colors and labeled with capital letters from A to F. Figures 4.2 A to C present the measured oxygen levels directly after seeding, as well as after the first and second medium replacement. Recorded data sets in the time span after seeding were exponentially fitted (one phase decay) (figure 4.2 A). The fitted curve is plotted in the same color as the corresponding data set. Via the received equation:

$$Y = (Y_0 - Plateau) \cdot e^{(-K \cdot X)} + Plateau \quad (4.1)$$

the established equilibrium (plateau) level was determined. Data are shown in figure 4.3 B. The half life of oxygen (figure 4.2 D and figure 4.3 A) was calculated using following equation:

$$t_{1/2} = \frac{\ln(2)}{K} \quad (4.2)$$

The plateau value after first and second medium replacement were calculated as mean value over a time span of 10 hours of cultivation. Half life values were neglected because the oxygen level revealed no decrease due to medium replacement.

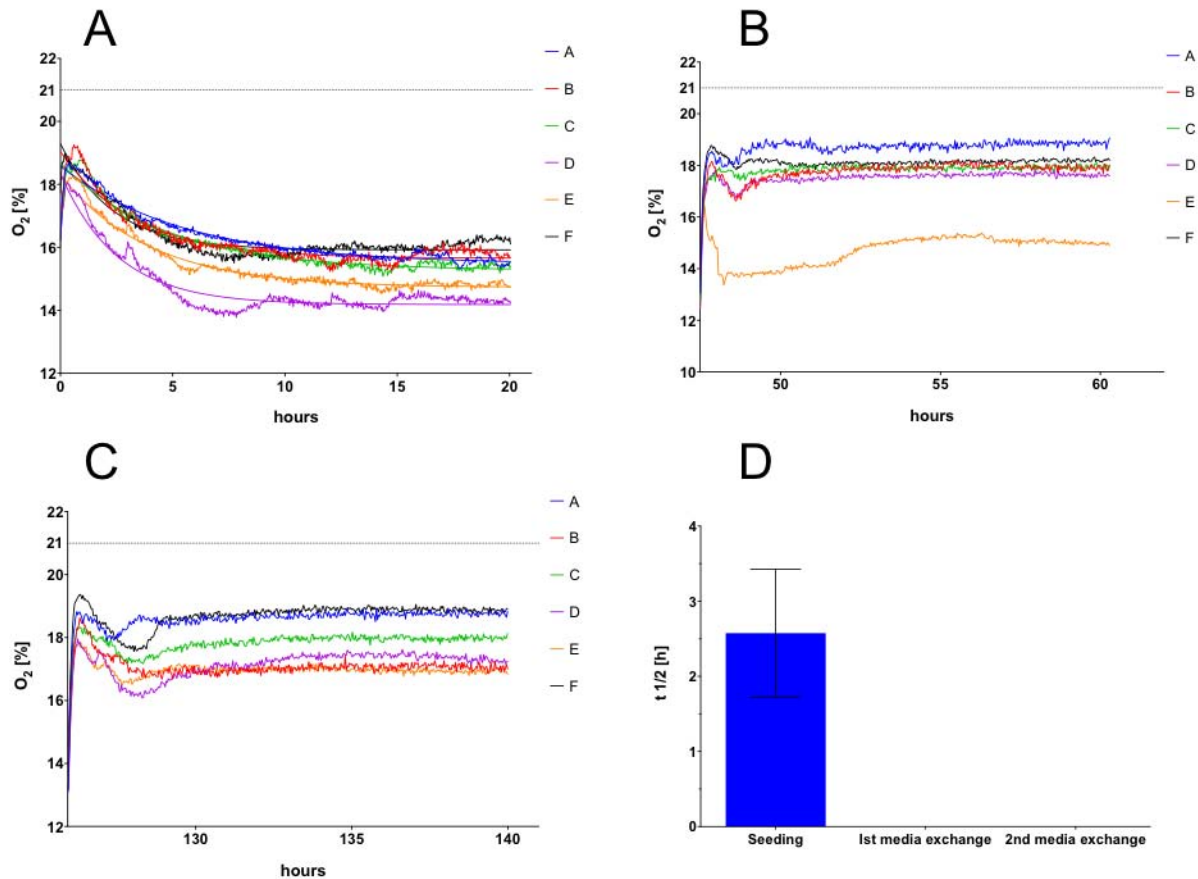


Figure 4.2: Exemplary analysis of dissolved oxygen in the culture supernatant during specific time spans at seeding density of 1×10^5 cells/ml: after seeding (A); after first media replacement (B) and after second media replacement (C). In each figure the six data sets are represented with capital letters from A to F. The origin in each figure is the time point of seeding (A), first media replacement (B) and second media replacement. Figure D demonstrates the mean \pm std. error of mean for sixfold measurements of half life of oxygen decrease.

The calculated half life of oxygen after seeding is presented for all groups in figure 4.3 A. In table 4.1 the corresponding values are shown. The group with the highest seeding density revealed the highest mean half life value of 2.5 ± 0.35 h versus 1.74 ± 0.13 , 1.90 ± 0.12 , 1.87 ± 0.10 h in the other assays. Accordingly, the measured mean plateau values of dissolved oxygen in the supernatant during cultivation were between 16.90 ± 0.85 , 18.13 ± 0.07 , 18.43 ± 0.11 and 19.16 ± 0.35 % O₂ increasing in parallel to the increasing seeding density.

Hyoxic environment

An overview of dissolved oxygen levels over cultivation is presented in figure 4.4. Data are presented as mean values of sixfold measurements plotted against time. Time points of medium

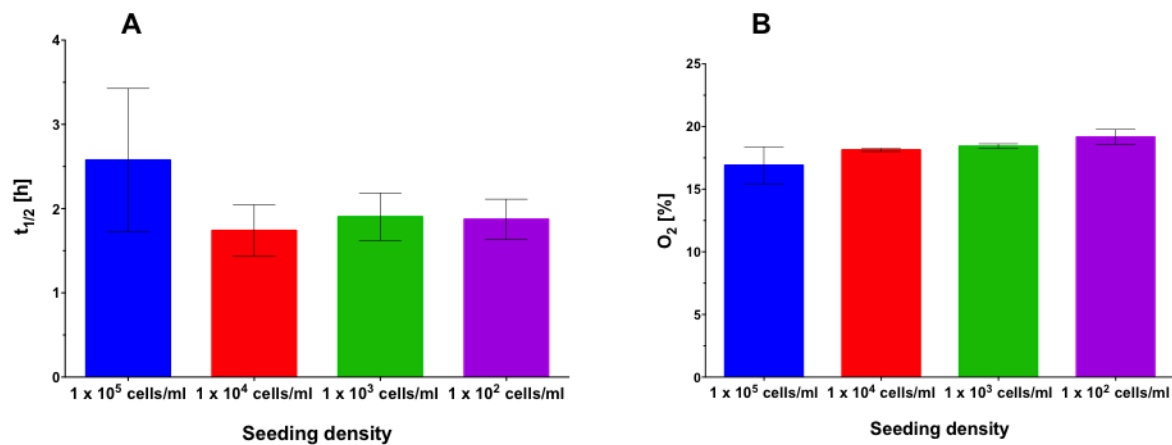


Figure 4.3: Mean half life of dissolved oxygen $t_{1/2} \pm$ SD in culture supernatant after seeding with different seeding densities (A) and oxygen plateau values \pm SD during cultivation period of 7 days (B).

Table 4.1: Half life of dissolved oxygen in culture supernatant with different seeding densities under normoxic conditions after seeding and oxygen plateau values during cultivation period of 7 days.

	1 x 10 ⁵ cells/ml	1 x 10 ⁴ cells/ml	1 x 10 ³ cells/ml	1 x 10 ² cells/ml
Half life $t_{1/2}$ [h]				
Mean	2.58	1.74	1.90	1.87
SD	0.85	0.31	0.28	0.24
Std. Error of Mean	0.35	0.13	0.12	0.10
Plateau O₂ [%]				
Mean	16.90	18.13	18.43	19.16
SD	1.47	0.12	0.20	0.60
Std. Error of Mean	0.85	0.07	0.11	0.35

changes are indicated by arrows in the figure. Likewise, the same trend as under normoxic conditions can be observed: the higher the initial cell density, the lower dissolved oxygen values during cultivation, indicating a faster rate of cellular consumption than gas diffusion into the medium. In the assay with the highest seeding density (1×10^5 cells/ml) the dissolved oxygen values in the cell culture supernatant progressively showed a lower plateau level versus the other groups. After the first medium replacement a more stabilized oxygen environment could be observed, but the dissolved oxygen value decreased during cultivation time in parallel to cell expansion. A difference of about 3% dissolved oxygen compared to initial and plateau values was measured. At the end of cultivation, after the second medium change no further decrease could be seen. The second most dense seeding assay (1×10^4 cells/ml) showed a stable behavior after seeding. Over the course of cultivation the measured oxygen value progressively decreased after the first medium replacement. Second medium change resulted in a constant dissolved oxygen level in the supernatant. Both groups with lower seeding densities (1×10^3 and 1×10^2 cells/ml) showed stable oxygen environment until the end of cultivation. Only in the group with a seeding density of 1×10^3 cells/ml a slight decrease could be observed after the second medium replacement.

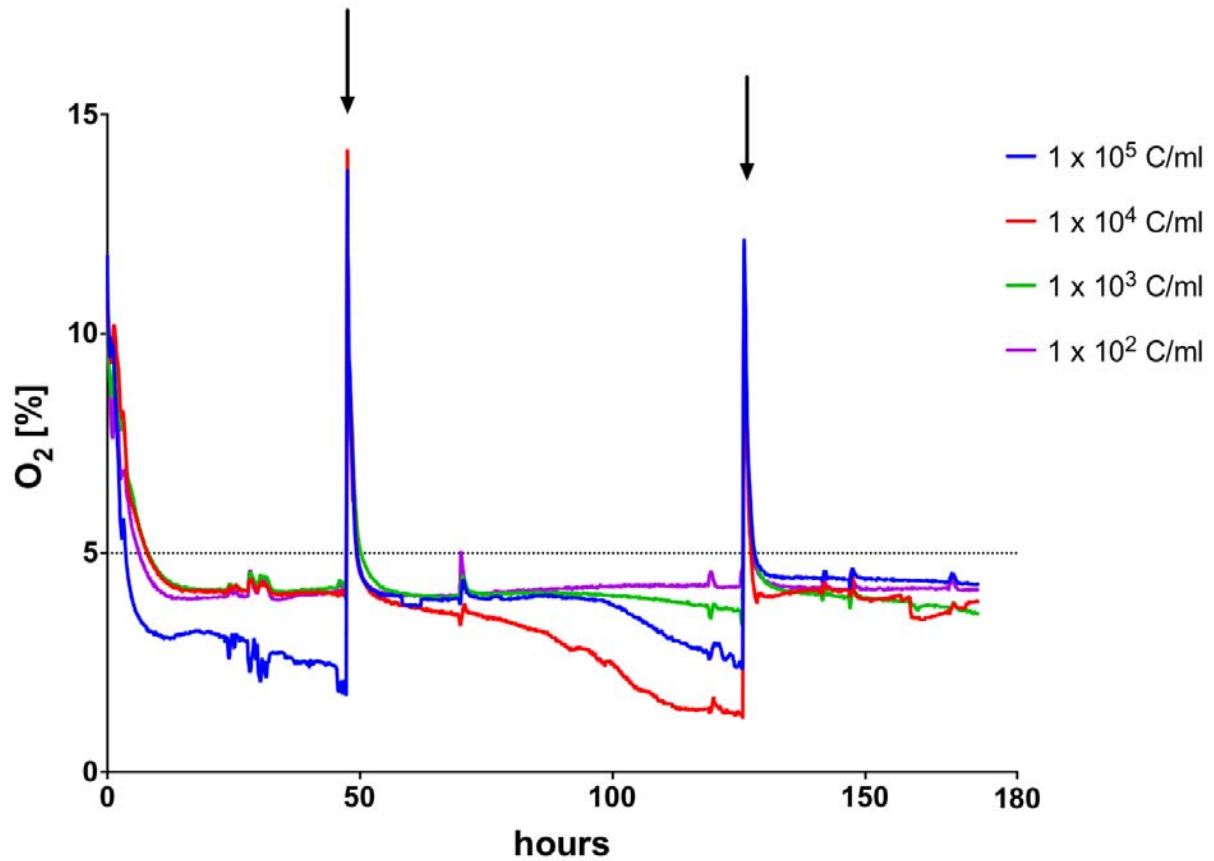


Figure 4.4: Dissolved oxygen in culture supernatant during hypoxic cultivation of ucMSCs with different seeding densities. Data are the means of sixfold measurements for each seeding density. Medium changes are indicated by arrows.

Each seeding density assay was conducted in 6 fold measurements. A representative analysis of data with a seeding density of 1×10^5 cells per ml is given in figure 4.5. Analysis of the other groups was assessed in an identical way. The six data sets are represented in different colors and labeled with capital letters from A to F. Figures A to C present the measured oxygen levels directly after seeding, respectively first and second medium replacement. The recorded data in the time span after seeding and both media exchanges were exponentially fitted (one phase decay). Via the received equation, mentioned above (4.1) the achieved plateau level was determined. Data are shown in figure 4.6 B. The half life of oxygen (figure 4.6 A) was calculated using the equation 4.2.

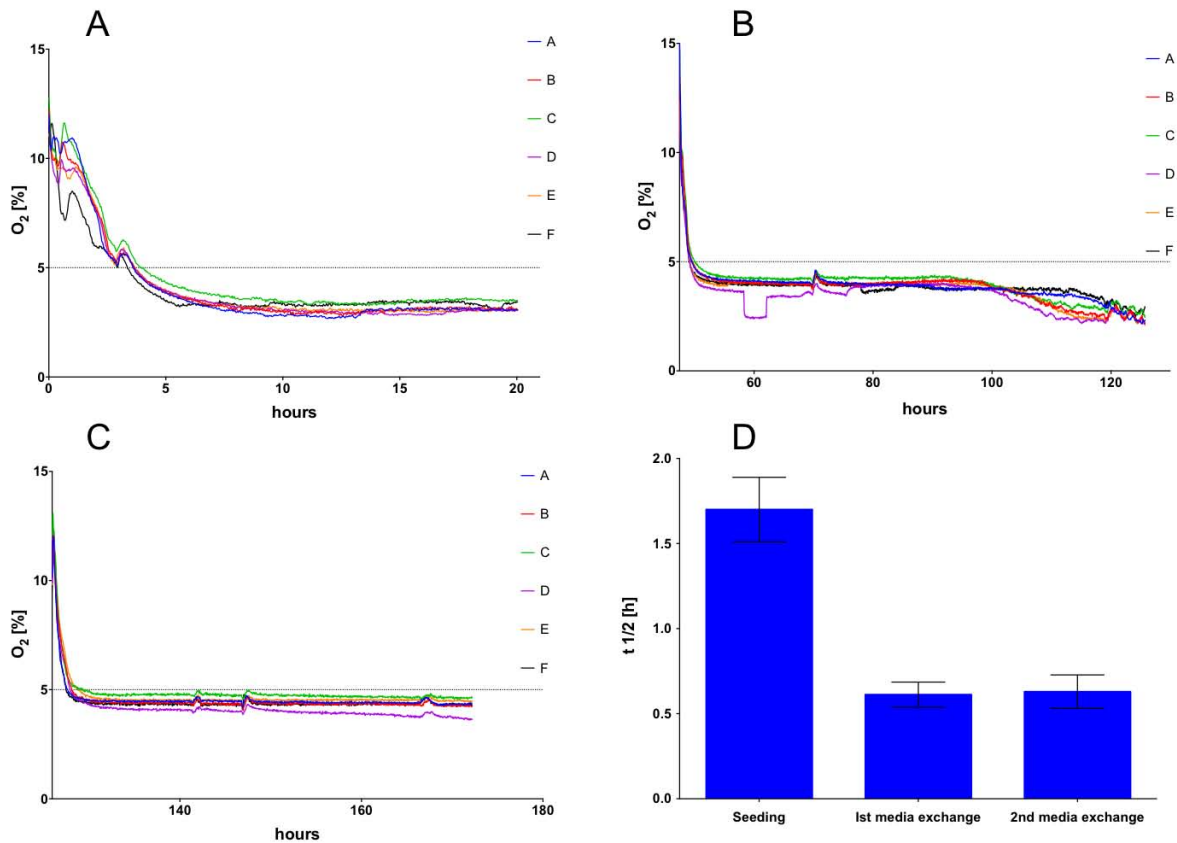


Figure 4.5: Exemplary analysis of dissolved oxygen in the culture supernatant during specific time spans at seeding density of 1×10^5 cells/ml: after seeding (A); after first media replacement (B) and after second media replacement (C). In each figure the six data sets are represented with capital letters from A to F. The origin in each figure is the time point of seeding (A), first media replacement (B) and second media replacement. Figure D demonstrates the mean \pm SD for sixfold measurements of half life of oxygen decrease.

Half life of oxygen after seeding and after medium changes are presented in figure 4.6 A and respectively 4.6 B. In table 4.2 the corresponding values are shown. The group with the second highest initial cell concentration revealed the highest mean half life value after seeding of 3.09 ± 0.19 h followed by 2.71 ± 0.012 of the lowest seeding density. The other groups, 1×10^5 cells/ml and 1×10^3 cells/ml initial density, showed both lower values of 1.70 ± 0.08 and 0.80 ± 0.06 h. Mean half life after medium exchanges resulted in drastically lower values of 0.62 ± 0.01 h, (1×10^5 cells/ml) 0.72 ± 0.02 h (1×10^4 cells/ml), 0.86 ± 0.04 h (1×10^3 cells/ml) and 0.55 ± 0.02 h (1×10^2 cells/ml). Moreover, the measured mean plateau values of dissolved oxygen in the supernatant during cultivation was between 3.82 ± 0.41 , 4.05 ± 0.09 , 4.12 ± 0.01 and 4.06 ± 0.12 % O₂. Neither half life after seeding, half life after medium exchange nor measured plateau levels of oxygen showed a correlation with initial seeding density.

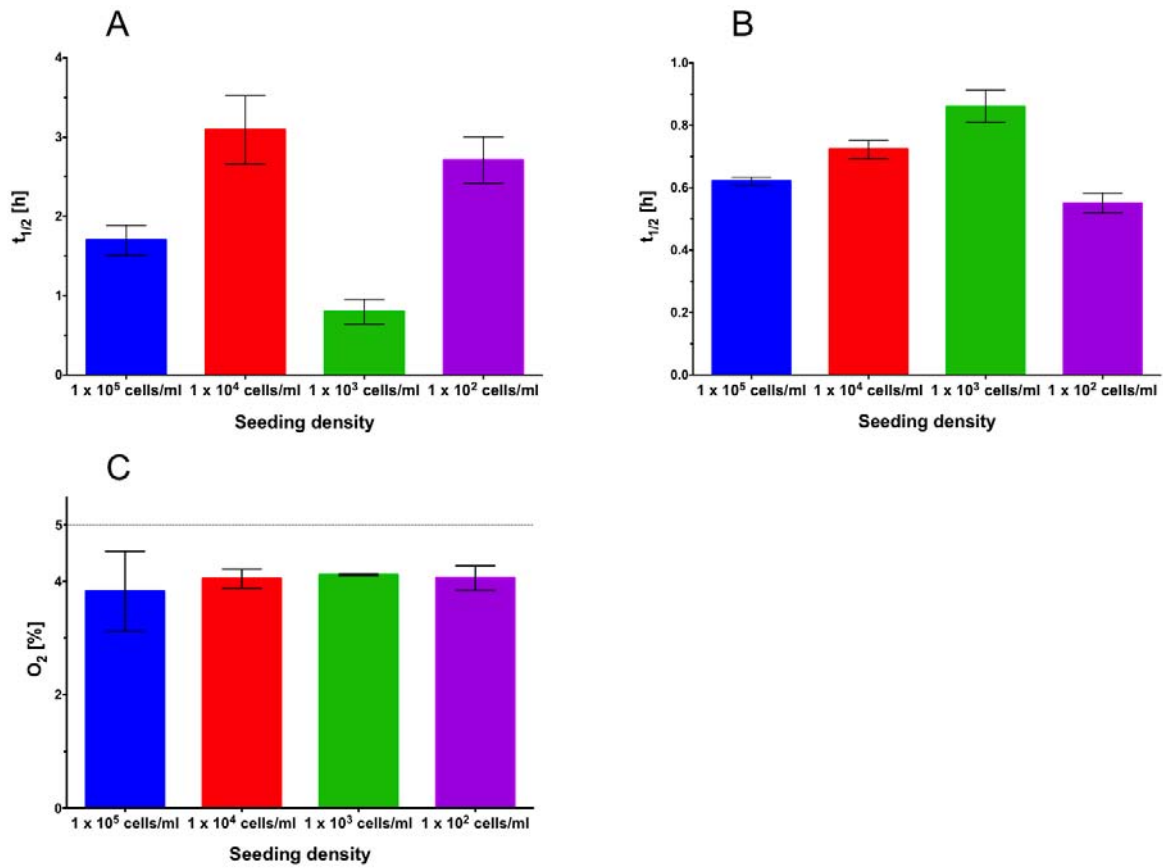


Figure 4.6: Mean half life of dissolved oxygen $t_{1/2} \pm$ SD in culture supernatant with different seeding densities under hypoxic conditions after seeding (A); after medium exchange (B) and oxygen plateau values \pm SD during cultivation period of 7 days (C).

Table 4.2: Half life of dissolved oxygen in culture supernatant with different seeding densities under hypoxic conditions after seeding, after medium exchange and oxygen plateau values during cultivation period of 7 days.

	1×10^5 cells/ml	1×10^4 cells/ml	1×10^3 cells/ml	1×10^2 cells/ml
Half life $t_{1/2}$ [h] after seeding				
Mean	1.70	3.09	0.80	2.71
SD	0.19	0.43	0.16	0.29
Std. Error of Mean	0.08	0.19	0.06	0.12
Half life $t_{1/2}$ [h] after medium exchange				
Mean	0.62	0.72	0.86	0.55
SD	0.01	0.03	0.05	0.03
Std. Error of Mean	0.01	0.02	0.04	0.02
Plateau O_2 [%]				
Mean	3.82	4.05	4.12	4.06
SD	0.71	0.16	0.01	0.21
Std. Error of Mean	0.41	0.09	0.01	0.12

4.1.2 Seeding strategies for growth on scaffolds

An optimization of cell seeding is essential for the successful *in vitro* cultivation. Seeding requirements for 3D scaffolds are spatially uniform distribution and high yield. The experimental setup is described in B.3. In order to investigate optimal seeding density, Matristypt[®] scaffolds were seeded with ucMSCs in 6 different cell concentrations on study day 0 and cultivated for 7 days. Medium change was conducted on day 4. Cell proliferation was assessed on day 1, 4 and 7 via MTT assay in 3 replicates (n=3). To investigate cell distribution on the scaffolds DAPI staining was performed at all time points respectively. Remaining glucose and lactate production were determined at each time point to indicate metabolic activity. The consumed glucose was calculated as difference between the initial glucose concentration of 1 mg/ml in the standard culture medium and the measured remaining glucose concentration.

In figure 4.7 the progress of cell proliferation of ucMSCs is shown. In all groups an increase of measured absorbance can be seen. However, cells with initial seeding concentration of 1×10^5 cells showed the highest increase over the course of cultivation. The negative extinctions resulted from the high background signal of the culture media.

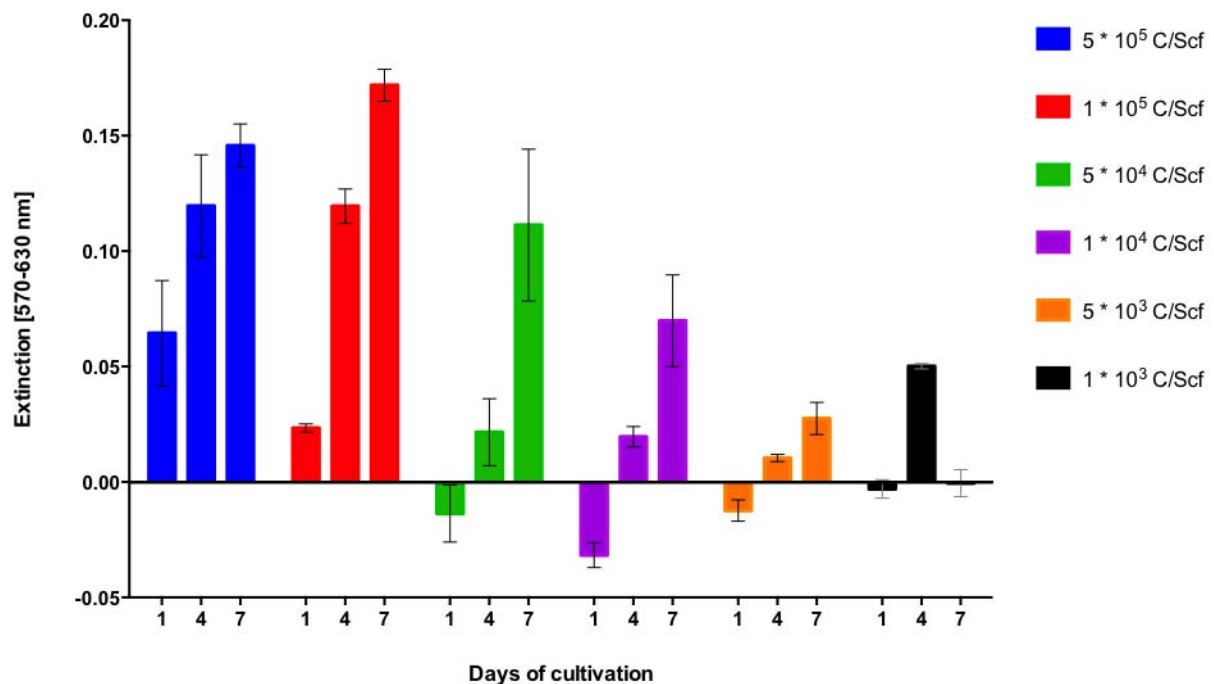


Figure 4.7: Progression of cell proliferation of ucMSCs seeded with 6 different initial cell concentrations on Matristypt[®] scaffolds. Data are the means \pm SD of sixfold measurements for each assay, three assays per each seeding density.

In figure 4.8 consumed glucose during cultivation on Matristypt[®] is shown. In the first 24 hours of incubation glucose consumption of all groups was very low except at a seeding density of 5×10^5 . At all seeding densities an increase in glucose consumption after 4 days cultivation can be seen. At a seeding density of 5×10^5 , cells consumed about 1 mg/ml, which is 100% of the glucose provided by the medium. After medium replacement on study day 4, cells were further incubated for 3 days. Reanalysis of consumed glucose on day 7 showed a lower but similar consumption rate, when compared to day 4. In the groups with a seeding density of 5×10^5 and 1×10^5 , the highest glucose consumption were determined. Drasitc lower glucose levels were measured in the other groups, indicating decreased cell growth. The results matches the

outcomes of the MTT assay. On study day 1, at seeding densities of 5×10^5 and 1×10^5 , only a small extinction was measured, correlating with a small glucose consumption and indicating a low cell proliferation rate. After 4 days of incubation a drastic increase of the measured extinction can be seen, resulting in a high glucose consumption. Both indicates a higher cell proliferation. On study day 7, a smaller increase of extinction was measured, when compared to day 4, matching the lower consumed glucose and indicating a lower cell proliferation. Lactate production is presented in figure 4.9. In the groups with a seeding density of 5×10^5 and 1×10^5 , a high concentration of lactate can be observed. Lactate levels on study day 7 are comparable to measured levels on day 4 in both groups. Very low levels of lactate were measured in the other groups. In the group with the lowest seeding density no lactate production has been found. These results match with the glucose consumption and measured extinction in the MTT assay shown above.

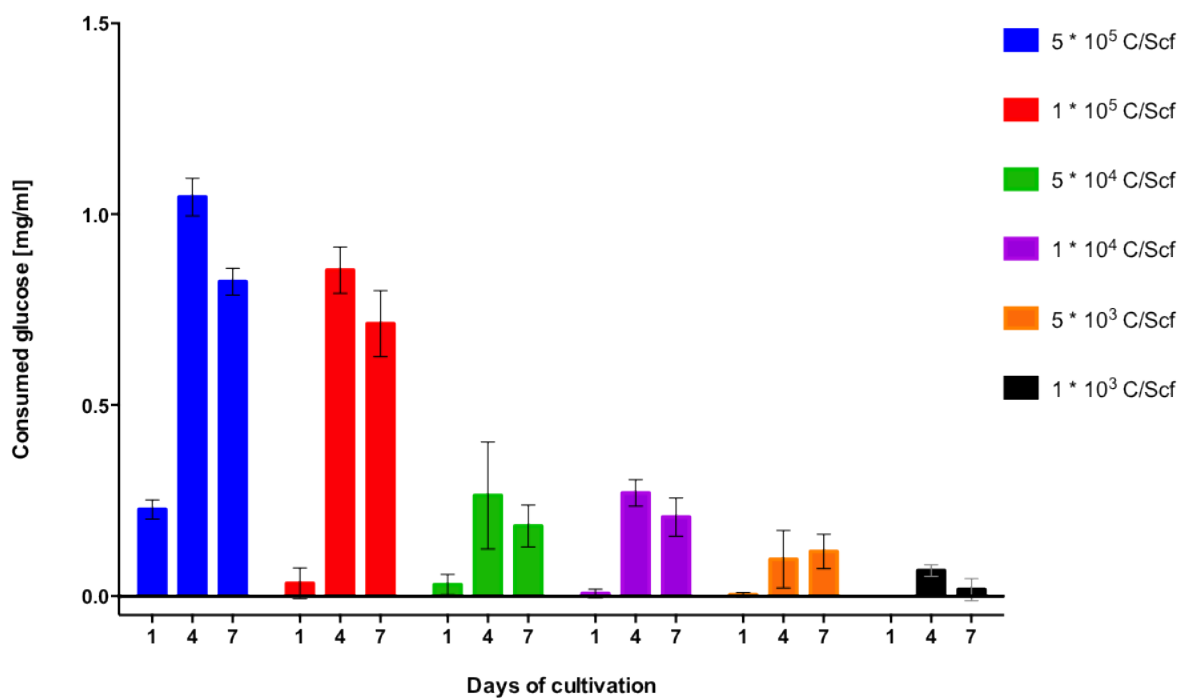


Figure 4.8: Glucose concentration of ucMSCs seeded with 6 different initial cell concentrations on Matristyp[®] scaffolds is plotted against time. Data are the means \pm SD for triplicate measurements for each seeding density.

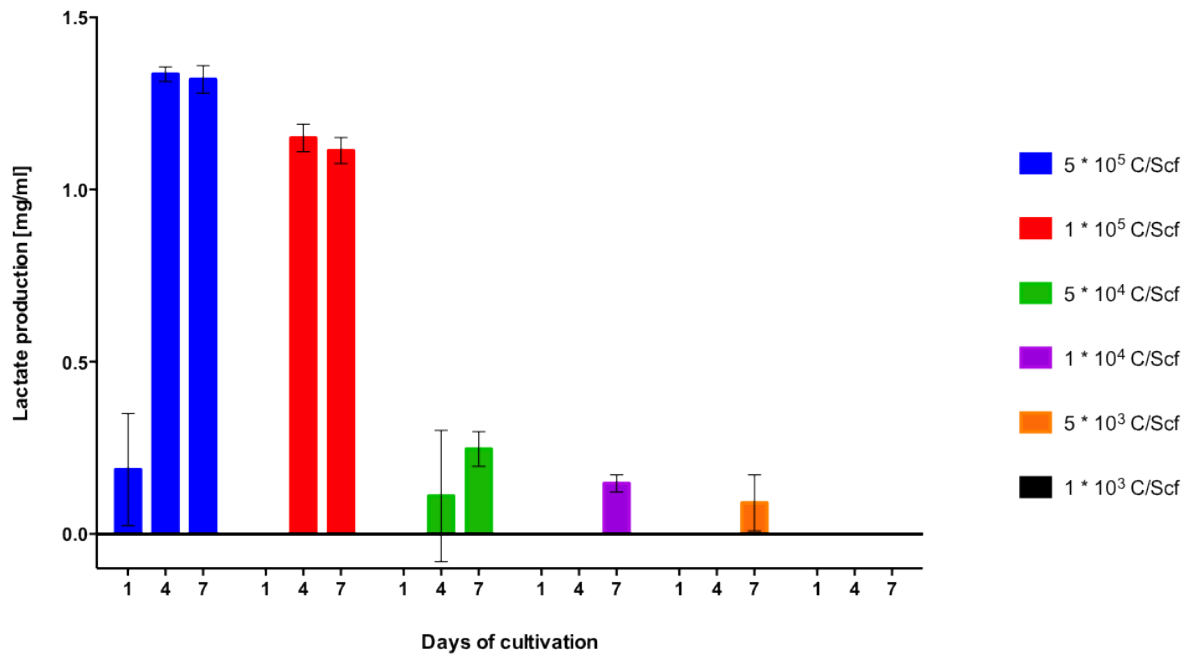


Figure 4.9: Lactate production of ucMSCs seeded with 6 different initial cell concentrations on Matristyp® scaffolds is plotted against time. Data are the means \pm SD for triplicate measurements for each seeding density.

Upper side of DAPI stained scaffolds harvested on study day 1 of all groups is presented in figure 4.10. The decreasing level of initial cell density can be observed. In Figure 4.10 the highest initial cell population is shown, indicated by the brightest color in the seeded area. Moreover, in figure 4.10 A and B a uniform cell distribution with sharp border to the unseeded area can be noticed. By contrast in the figures 4.10 C, D, E and F there are only single cells on the scaffold surface and no cell accumulation can be seen.

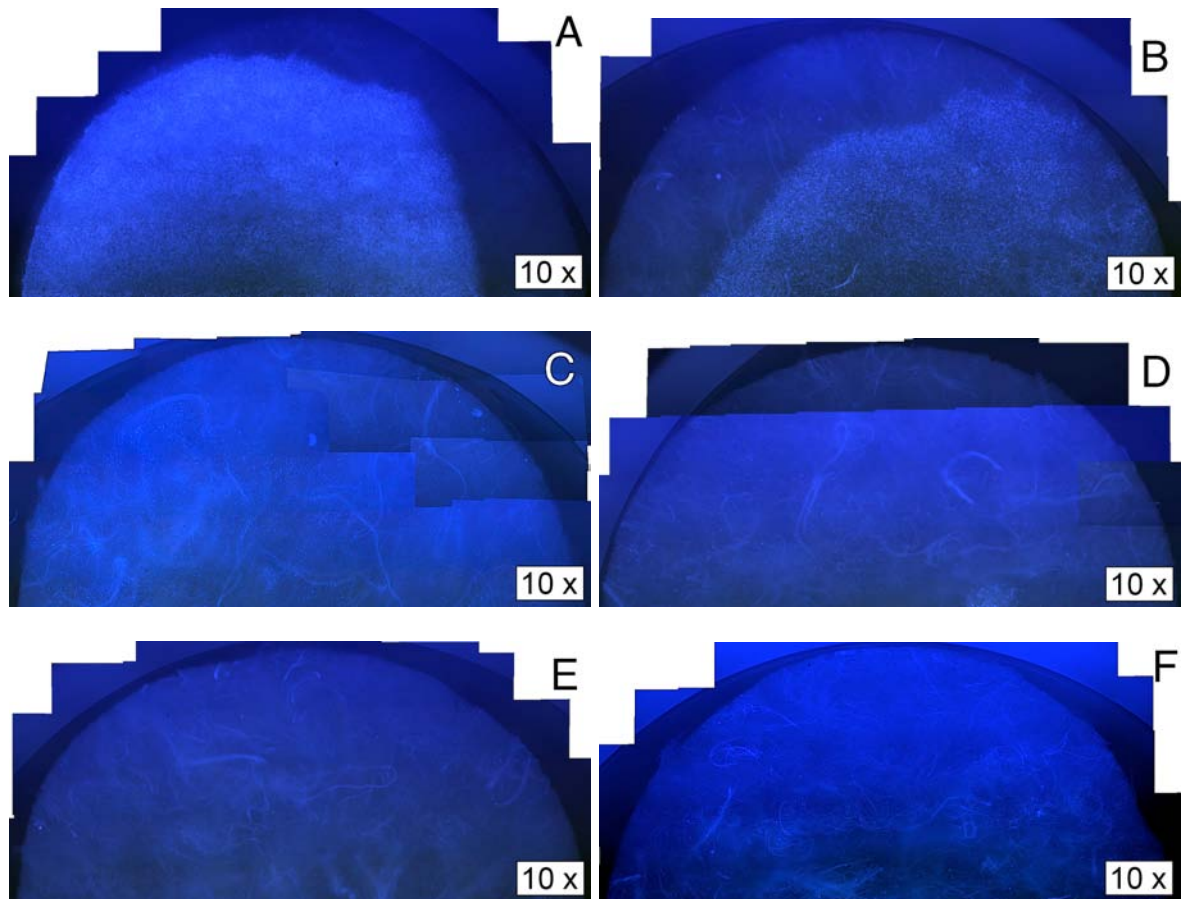


Figure 4.10: DAPI staining of harvested scaffolds on study day 1 with 6 different seeding densities: (A) 5×10^5 cells per scaffold (B) 1×10^5 cells per scaffold; (C) 5×10^4 cells per scaffold; (D) 1×10^4 cells per scaffold; (E) 5×10^3 cells per scaffold; (F) 1×10^3 cells per scaffold. Magnification 10x.

In figure 4.11 the upper side of scaffolds harvested on study day 4 is shown for all seeding densities. In the group with seeding density of 5×10^5 cells (4.11 A) a homogeneous cell distribution within the whole scaffolds can already be seen. The border to the unseeded area can still be recognized (4.11 B). An extended cell proliferation can be noticed in figures 4.11 C and D. In figure 4.11 C it can be seen that the cells already started to spread out within the scaffold surface, while in figure 4.11 D the cells stayed in a small circular area. However, in the groups with the lowest seeding density, represented in the figures 4.11 C and D, no extended cell proliferation can be determined.

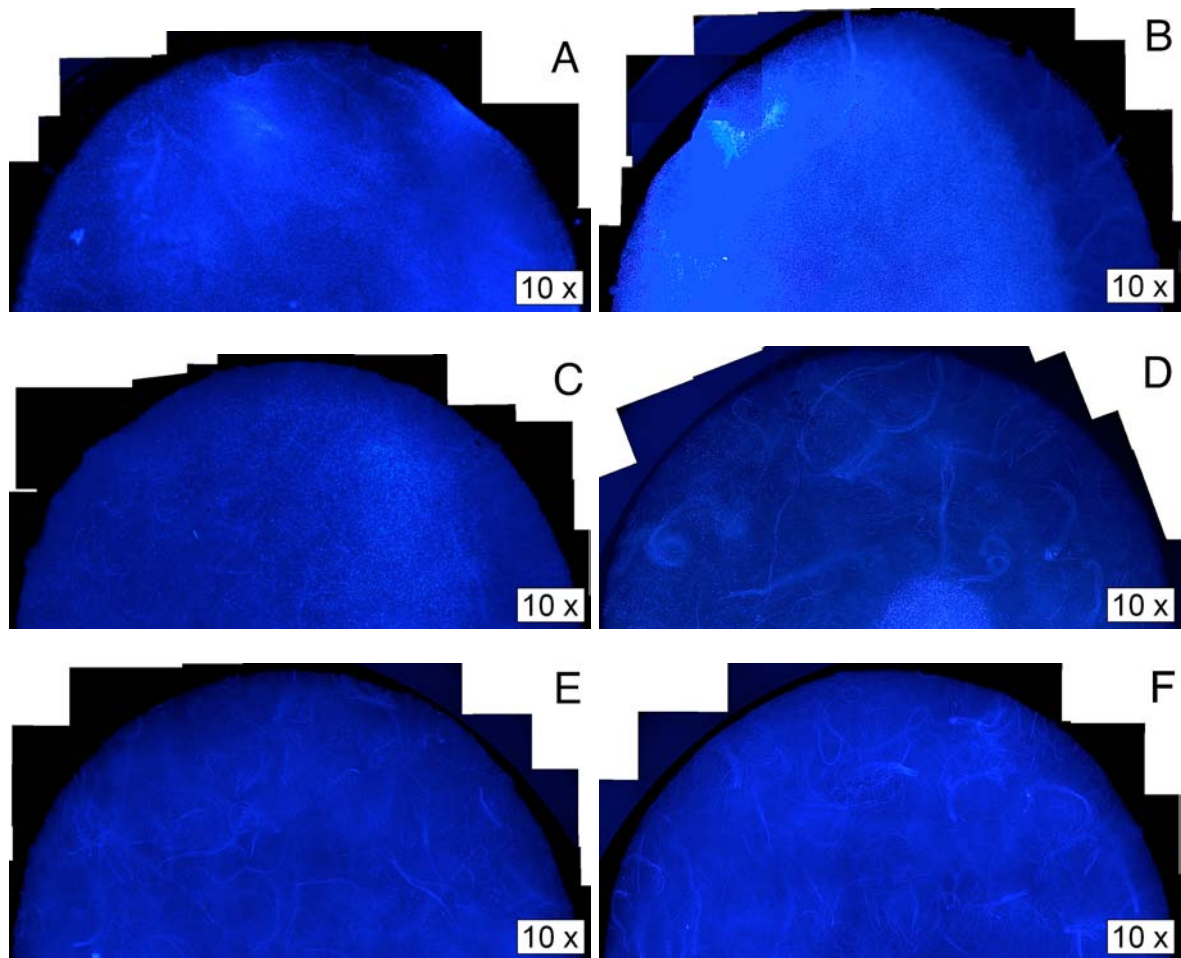


Figure 4.11: DAPI staining of harvested scaffolds on study day 4 with 6 different seeding densities: (A) 5×10^5 cells per scaffold (B) 1×10^5 cells per scaffold; (C) 5×10^4 cells per scaffold; (D) 1×10^4 cells per scaffold; (E) 5×10^3 cells per scaffold; (F) 1×10^3 cells per scaffold. Magnification 10x.

DAPI staining of scaffolds harvested on study day 7 is shown for all seeding densities in figure 4.12. In comparison with scaffolds harvested on study day 1 and 4 a highly increased cell population can be seen in most groups. In figure 4.12 A and B an uniform cell distribution over the scaffold can be recognized, with the densest population in figure 4.12 A. Furthermore, single cells spread out over the surface of scaffolds in figures 4.12 C, D and E. Only in the study group with the lowest seeding density, which is presented in figure 4.12 F no increase in cell proliferation can be found.

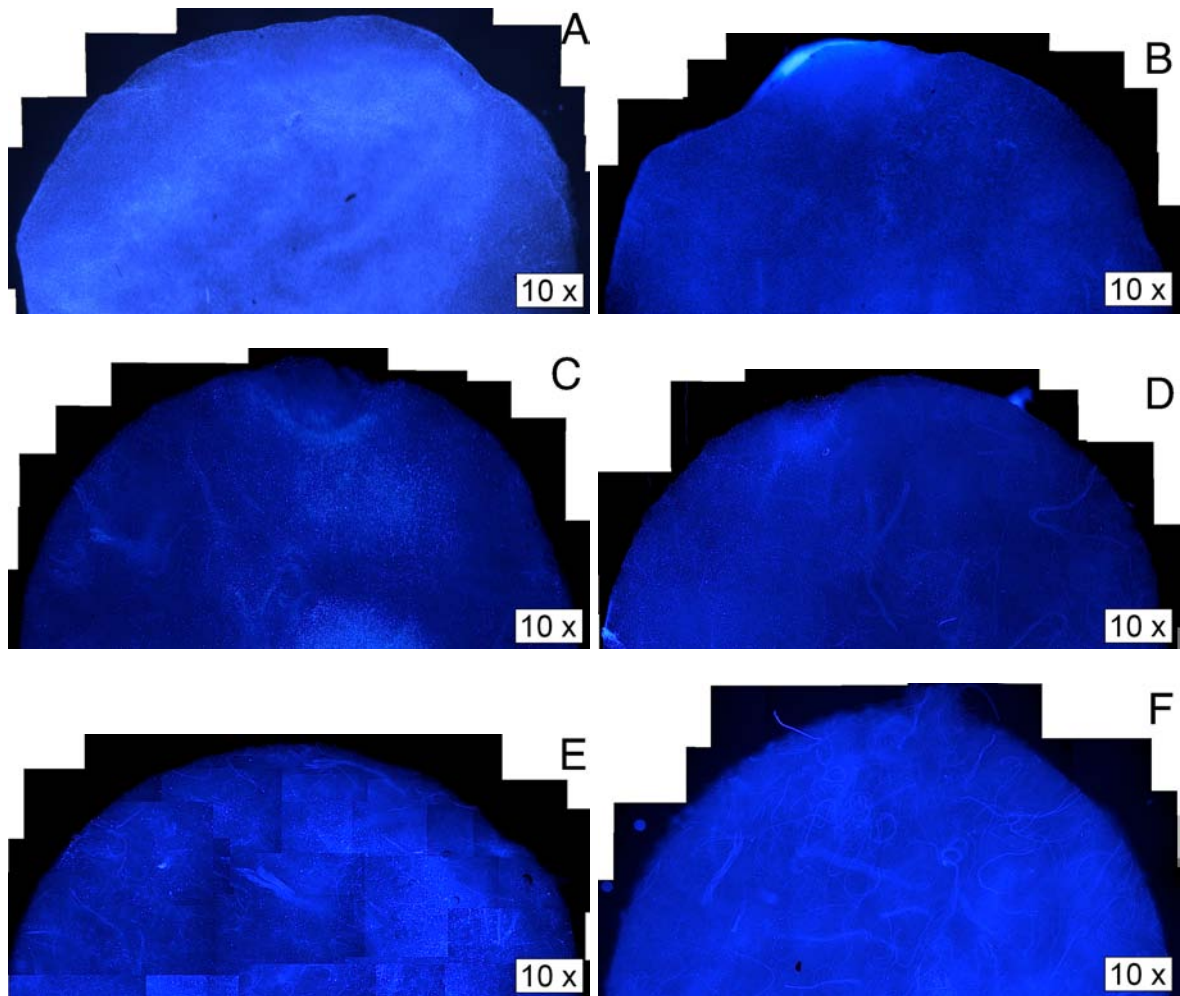


Figure 4.12: Upper side of harvested scaffolds on study day 7 with different seeding densities after DAPI staining: (A) 5×10^5 cells per scaffold (B) 1×10^5 cells per scaffold; (C) 5×10^4 cells per scaffold; (D) 1×10^4 cells per scaffold; (E) 5×10^3 cells per scaffold; (F) 1×10^3 cells per scaffold. Magnification 10x

The bottom side of the scaffolds were analyzed on study day 4 and 7. To visualize the extended cell proliferation within the whole scaffold the pictures collected on study day 7 are shown in figure 4.13. In all groups cell growth on the bottom side of the scaffolds can be observed. In figure 4.13 A a comparable cell growth as at the upper side can be seen. The growth over the scaffolds edge can be identified in figure 4.12 B and 4.13 B, which is indicated by the bright area at the edge in both figures. Indicating a successful cell invasion of the whole scaffold matrix in both groups. A circular cell growth can be seen in figure 4.13 C. By day 7 in the groups with the lowest seeding densities only single cells distributed over the scaffolds bottom side can be found (figures 4.13D, E and F). After 7 days of cultivation, sufficient cell growth was only achieved in groups with the seeding densities of 5×10^5 and 1×10^5 cells per scaffold. These findings match the results of the MTT - assay.

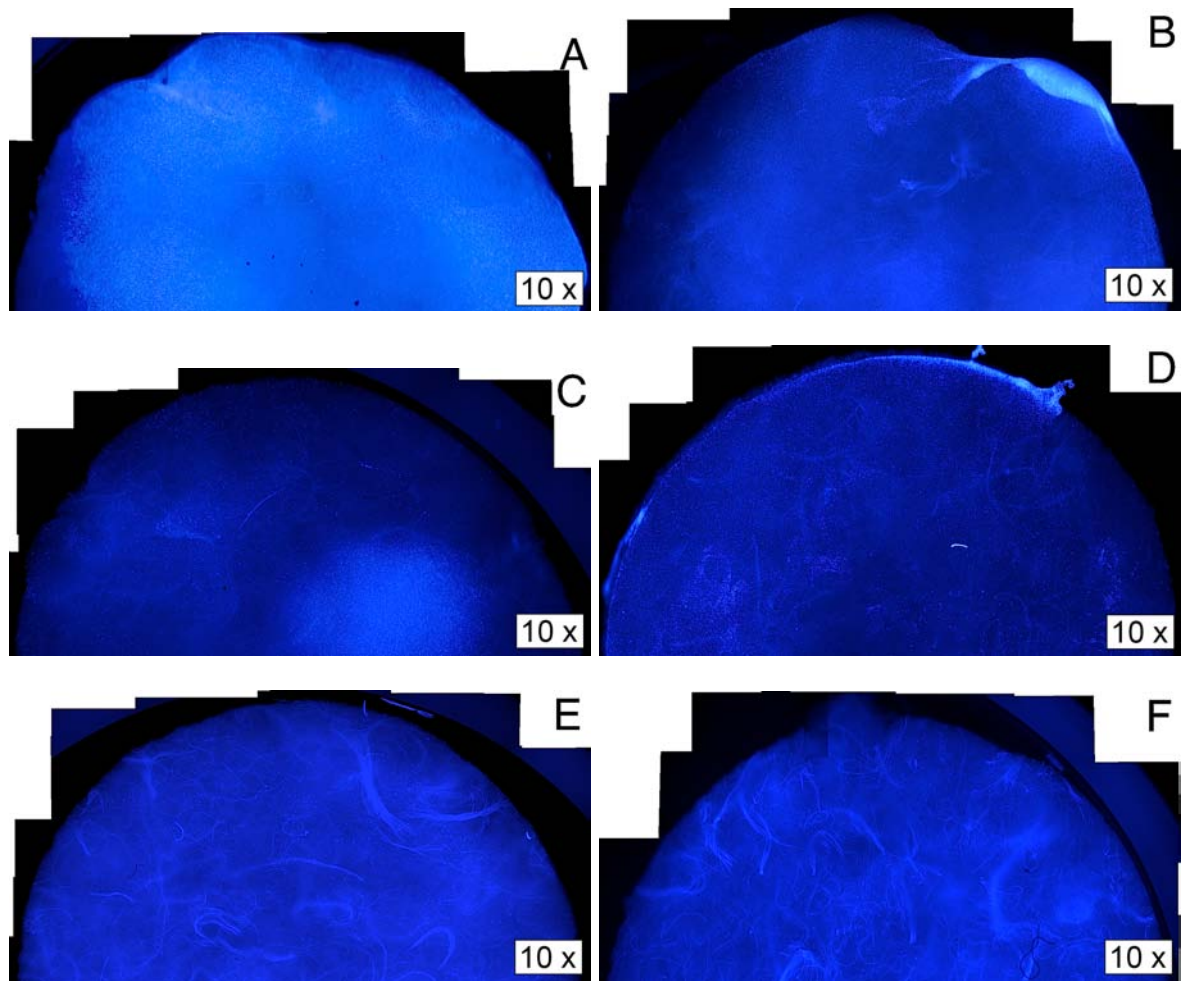


Figure 4.13: Bottom side of harvested scaffolds on study day 7 with different seeding densities after DAPI staining: (A) 5×10^5 cells per scaffold (B) 1×10^5 cells per scaffold; (C) 5×10^4 cells per scaffold; (D) 1×10^4 cells per scaffold; (E) 5×10^3 cells per scaffold; (F) 1×10^3 cells per scaffold. Magnification 10x.

4.1.3 Isolation of adMSCs from abdominoplastic surgery material

adMSCs from a female (age 82 years) and a male (age 64 years) donors, adMSCs(82f) and adMSCs(64m), were obtained by isolation out of abdominoplastic surgery tissue. The procedure is described in B.4. adMSCs(64m) and adMSCs(82f) were successfully isolated. After expansion over one passage, the cells were harvested. The obtained cell suspension was cryoconserved in aliquots (1 million viable cells per milliliter of cryconservation medium).

4.1.4 Proliferation of adMSCs(64m)

To characterize growth kinetics of freshly harvested adMSCs(64m), a proliferation study was conducted as described in B.5. In short, cells were subcultured under normoxic and hypoxic culture conditions over 14 passages every 3 to 4 days, when a confluence of approximately 80% was reached.

Over the course of cultivation, drastic changes in cell morphology were observed, as can be seen in figure 4.14. In passage 2 (figure 4.14 A and D) the typical uniform patterned flat colonies can be seen. Cells had long thin cell bodies with a large nucleus. In contrast in figure 4.14 B, D (passage 10) and E, F (passage 14) cells demonstrate an altered cell morphology: a flattened, irregular shape, bigger nuclei and a tattered rim; indicating that most of the cells became senescent.

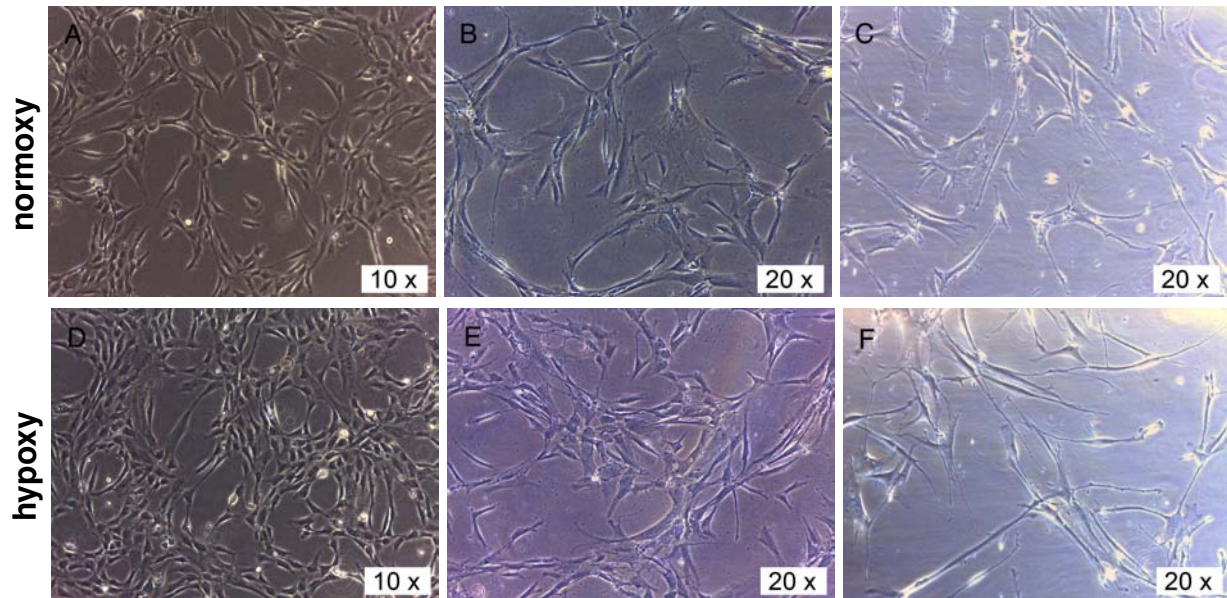


Figure 4.14: Cell proliferation of adMSCs(64m) under normoxic (A to C) and hypoxic culture conditions (D to F). A and B presents adMSCs(64m) in passage 2 (magnification 10x); C and D passage 10 (magnification 20x); E and F passage 14 (magnification 20x).

At each passage, the cells were counted using a haemocytometer and the population doublings were calculated according to the following equation:

$$PD = \frac{\ln\left(\frac{x}{x_0}\right)}{\ln 2} \quad (4.3)$$

PD population doubling during a period of time Δt

x_0 number of living cells at time point $t = 0$

x number of living cells at time point t

Cumulative cell population doublings were calculated as a sum of all population doublings from the beginning of the experiment until the time point t . Population doubling time t_{PD} was calculated with the following equation:

$$t_{PD} = \frac{\Delta t}{PD} \quad (4.4)$$

Figure 4.15 shows the results of long-term cultivation of adMSCs(64m). Cells in passage 11 to 14 of both hypoxic and normoxic cultures showed an altered behavior. After detachment

using Accutase® a cell strainer had to be used for disaggregation, which resulted in non-representative cell numbers. Cell counts of these passages had to be excluded from further evaluation and are therefore not shown in the diagrams. Hypoxic cultures revealed higher cumulative population doublings and higher cumulative cell numbers when compared to normoxic conditions. Starting with the same cell number at passage 1 of 7×10^5 cells, the yield after passage 10 (T-25 cell culture flask) was $2.60 \times 10^{18} \pm 1.12 \times 10^{18}$ cells with 5% O_2 , while it was only $3.84 \times 10^{17} \pm 1.12 \times 10^{17}$ at 21% O_2 . *In vitro*, adMSCs(64m) displayed a cell doubling time of 12 to 25 hours, depending on the passage number. The total population doublings at passage 10 were 41.64 ± 0.68 under hypoxic conditions and 38.94 ± 0.49 under normoxic conditions, which is equivalent to 6.93% more cells after 711.18 h or 10 passages. These results confirm a higher proliferation activity of adMSCs(64m) in long-term cultivation under lower oxygen tension.

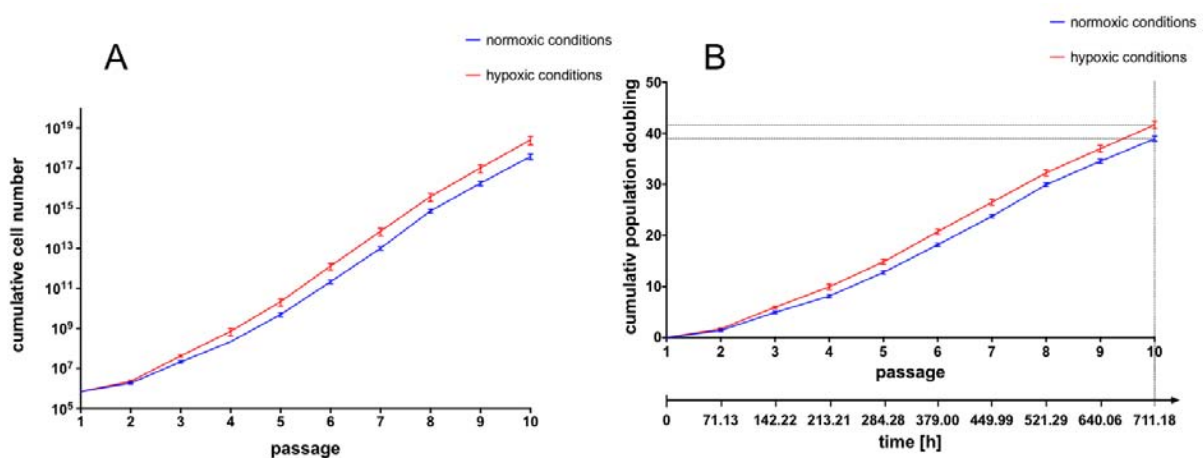


Figure 4.15: Cumulative cell number (A) and population doubling PD (B) of adMSCs(64m) over 10 passages under normoxic and hypoxic culture conditions. Data represent means \pm SD from 4 cultures

4.1.5 Differentiation of adMSCs(82f) and adMSCs(64m)

One main characteristic of adMSCs is their ability to differentiate into different tissues due to specific induction. The goal of this study was to prove the multipotent potential of freshly harvested adMSCs(82f) and adMSCs(64m) under normoxic and hypoxic culture conditions. Differentiation into adipocytes, chondrocytes and osteocytes was induced. The experimental procedure is described in B.6. In brief, cells were seeded in 12 well plates coated with human fibronectin at a density of 4,000 cells per cm^2 . Differentiation was induced after cells were grown to confluency on study day 2 to provide maximal expansion before cells enter differentiation. Medium was changed (1 ml) every first, third and fifth day of the week. 18 days after induction with adipogenic, chondrogenic and osteogenic media, lipid vacuoles, production of cartilaginous matrix and calcium deposits were detected via Oil Red-O, Alcian blue and Von Kossa staining, respectively. As control group adMSCs(64m) and adMSCs(82f) were simultaneously cultivated under identical conditions but in standard cultivation medium. Furthermore differentiation of adMSCs(64m) and adMSCs(82f) was observed under normoxic and hypoxic culture conditions. In addition, the metabolic activity during cultivation was assessed for adMSCs(64m). Glucose consumption and lactate production were measured in the culture super-

nantant. Consumed glucose was calculated by taking the blank values of the specific culture media into account.

Adipogenic differentiation

In order to investigate the adipogenic differentiation state of adMSCs(64m) and adMSCs(82f) Oil Red-O staining was performed. The lipid drops appeared identified in red under the light microscope. As a control group, both adMSCs(64m) and adMSCs(82f) were grown in standard culture medium with no change to differentiation medium. Cultivation was conducted under normoxic and hypoxic culture conditions. Negative control of Oil Red-O stained adMSCs(64m) are presented in figure 4.16 A (normoxic culture conditions) and D (hypoxic culture conditions). adMSCs(64m) and adMSCs(82f) were cultured in adipogenic media for 18 days under normoxic and hypoxic conditions and stained positively with Oil Red-O. In addition, differentiation was observed through visible changes in structure and morphology of the cells. Undifferentiated cells grew as uniform patterned flat layer (figure 4.16 A and D). Cells had long thin cell bodies with a large nucleus and lay tightly packed. By contrast, differentiated adipocytes exhibited bloated cells with a displaced nuclei and a thin compartment of cytoplasm. Regardless of 5% or 21% oxygen in the culture and donor, all cultures could be successfully differentiated into adipocytes. However, adMSCs(82f) (figure 4.16 B and E) exhibit a significantly reduced potential of differentiation capacity with respect to adMSCs(64m) (figure 4.16 C and D). Cells cultivated in hypoxic conditions exhibit a higher degree of differentiation towards adipocytes.

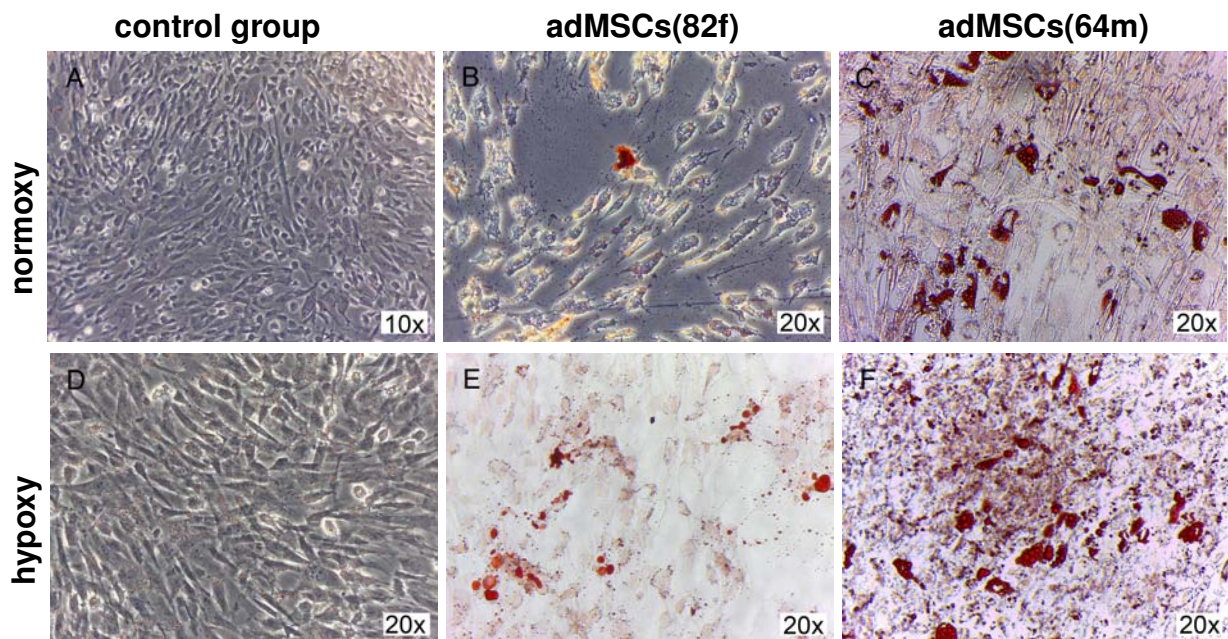


Figure 4.16: Adipogenic differentiation of adMSCs(82f) (B and E) and adMSCs(64m) (C and F) after 18 days at normoxic (A-C) and hypoxic (D-F) culture conditions. Control group (adMSCs(64m)) were expanded in standard culture medium (A and D). Magnification 10x (A), magnification 20x (B-F).

Chondrogenic differentiation

In vitro differentiation capacity was investigated using Alcian blue staining. The accumulation of chondrocyte matrix and the cartilage-specific sulfated GAG appear blue under the light microscope. As a control adMSCs(64m) and adMSCs(82f) were grown in standard culture medium. Cultivation was conducted under normoxic and hypoxic conditions and undifferentiated cells were also stained with Alcian blue. Images of undifferentiated adMSCs(64m) under normoxic culture conditions are presented in figure 4.16 A and under hypoxic culture in figure 4.16 D. Differentiation could be confirmed via prominent changes in cell morphology. Each chondrocyte is surrounded by a distinct rim of territorial matrix. adMSCs(82f) (figure 4.16 B and E) showed a lower intense staining compared to adMSCs(64m) (figure 4.16 C and F). Furthermore, Alcian Blue staining of acidic proteoglycans was more intense in cells cultivated at 5% oxygen (figure 4.17 F) than in cells cultured with 21% oxygen (figure 4.17 C). Cells cultivated in hypoxic conditions exhibit a higher degree of differentiation towards chondrocytes.

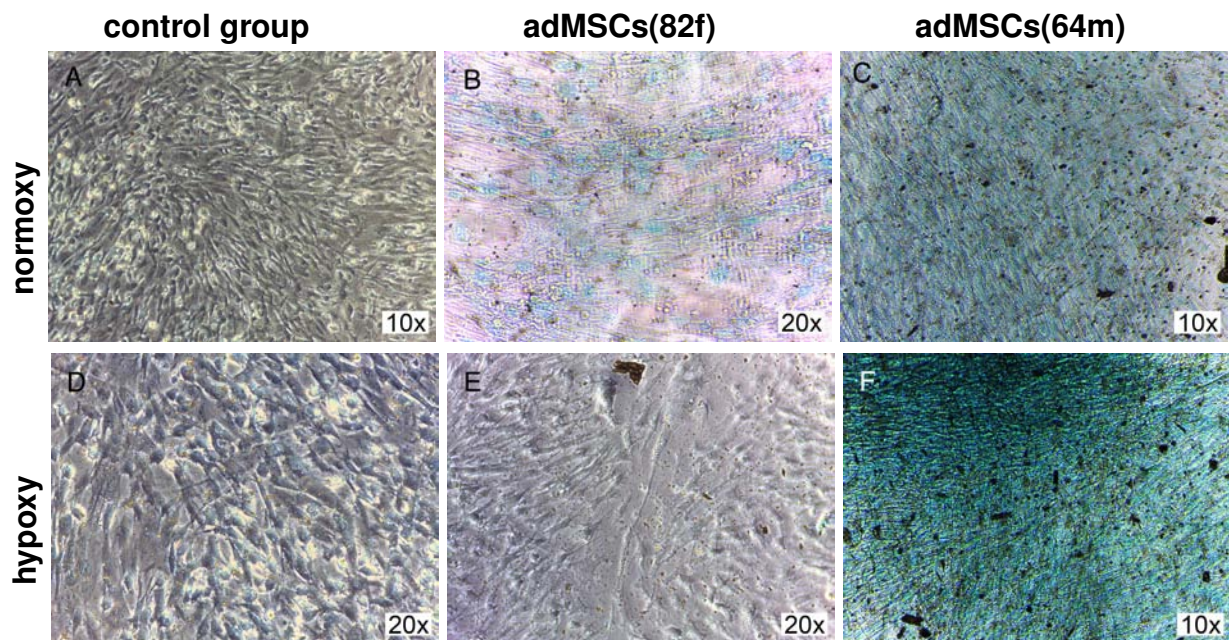


Figure 4.17: Chondrogenic differentiation of adMSCs(82f) (B and E) and adMSCs(64m) (C and F) after 18 days at normoxic (A-C) and hypoxic (D-F) culture conditions. Control group (adMSCs(64m)) were expanded in standard culture medium (A and D). Magnification 10x (A, C and F), magnification 20x (B, D and E).

Osteogenic differentiation

Osteogenic differentiation potential was analyzed via Alizarin Red and Von Kossa staining. In case of Alizarin Red calcium depositions appear red under the light microscope. Detection of calcium accumulations within the extracellular matrix via Von Kossa staining provides black stained image. Results of osteogenic differentiation are presented in figure 4.18 (Von Kossa staining) and in figure 4.19 (Alizarin Red staining). As negative control, images of stained but undifferentiated adMSCs(64m) are presented in figure 4.18 A and D (Von Kossa staining), and in figure 4.19 A and D (Alizarin Red staining). Regardless donor and oxygen tension, drastic morphological changes compared to the control group cultured with standard culture medium can be observed. In both staining assays differentiated cells exhibited an extensive connecting extracellular network. Von Kossa stained cells showed no higher degree of differentiation regarding the donor or oxygen tension. Both stainings were very intense (figure 4.18 B,E and C,F). Alizarin Red stained cells cultivated under hypoxic conditions exhibit a stronger staining. In addition, the adMSCs(62m) revealed in a slightly higher degree of differentiation compared to the adMSCs(82f).

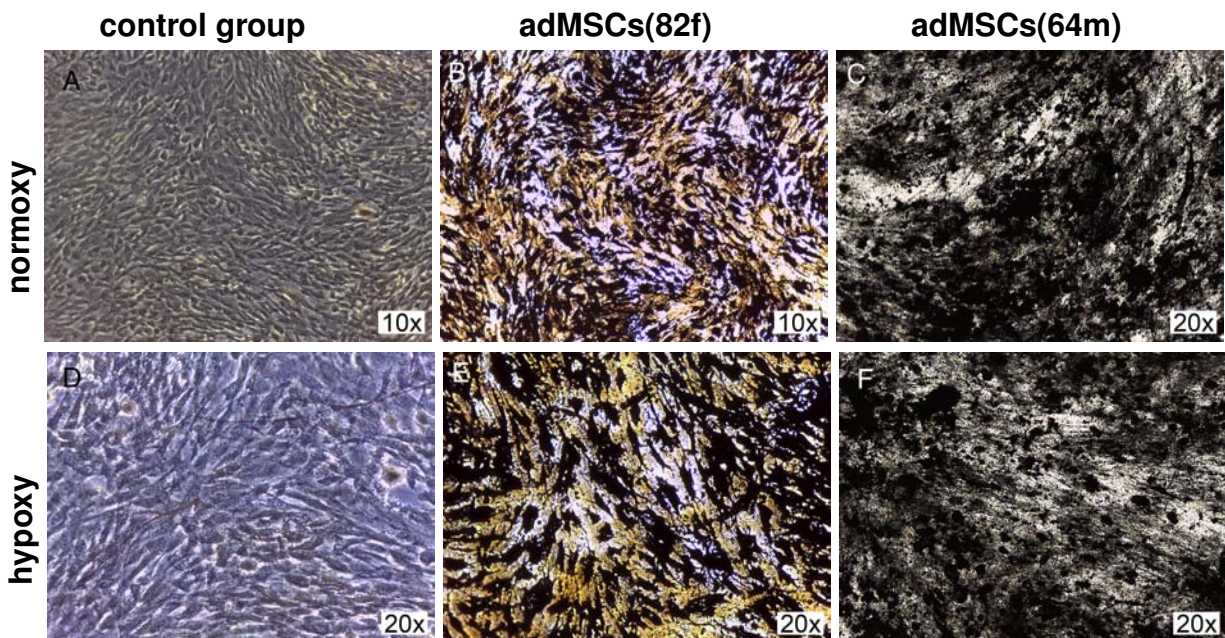


Figure 4.18: Osteogenic differentiation of adMSCs(82f) (B and E) and adMSCs(64m) (C and F) after 18 days at normoxic (A-C) and hypoxic (D-F) culture conditions stained with Von Kossa. Control group (adMSCs(64m)) were expanded in standard culture medium (A and D). Magnification 10x (A and B), magnification 20x (C-F).

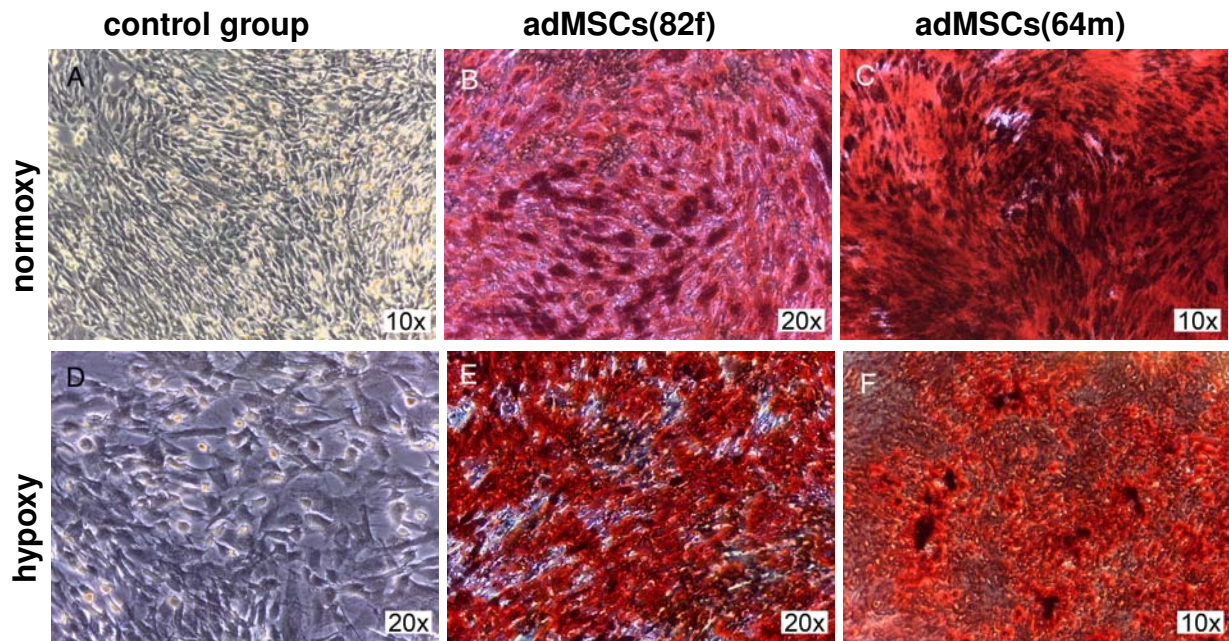


Figure 4.19: Osteogenic differentiation of adMSCs(82f) (B and E) and adMSCs(64m) (C and F) after 18 days at normoxic (A-C) and hypoxic (D-F) culture conditions stained with Alizarin Red. Control group (adMSCs(64m)) were expanded in standard culture medium (A and D). Magnification 10x (A, C and F), magnification 20x (B, E and F).

Metabolic analysis

The glucose consumption and the lactate production were measured as an indirect factor for cell survival and proliferation during cultivation and differentiation. Both are shown in figure 4.20. The initial glucose concentration of each differentiation medium is 5 mg/ml. On study day 4, 2 days after induction, cells showed a high glucose consumption of 5 mg/ml under both conditions, which is 100% of the glucose provided by the differentiation medium. During the cultivation the level dropped and showed wide variations. In the control group measured glucose concentration showed a more stable values during the course of cultivation. Moreover, the glucose consumption of adMSCs(64m) in differentiation medium is higher compared to non differentiated adMSCs(64m). These results indicate that higher glucose concentration can be correlated with differentiation activity. Under both culture conditions the adipogenically differentiated adMSCs(64m) showed the highest overall lactate production. No drastic difference in lactate production rate could be seen during cell differentiation compared to non-induced adMSCs(64m). Furthermore hypoxic and normoxic conditions had no influence in lactate production or glucose consumption of adMSCs(64m).

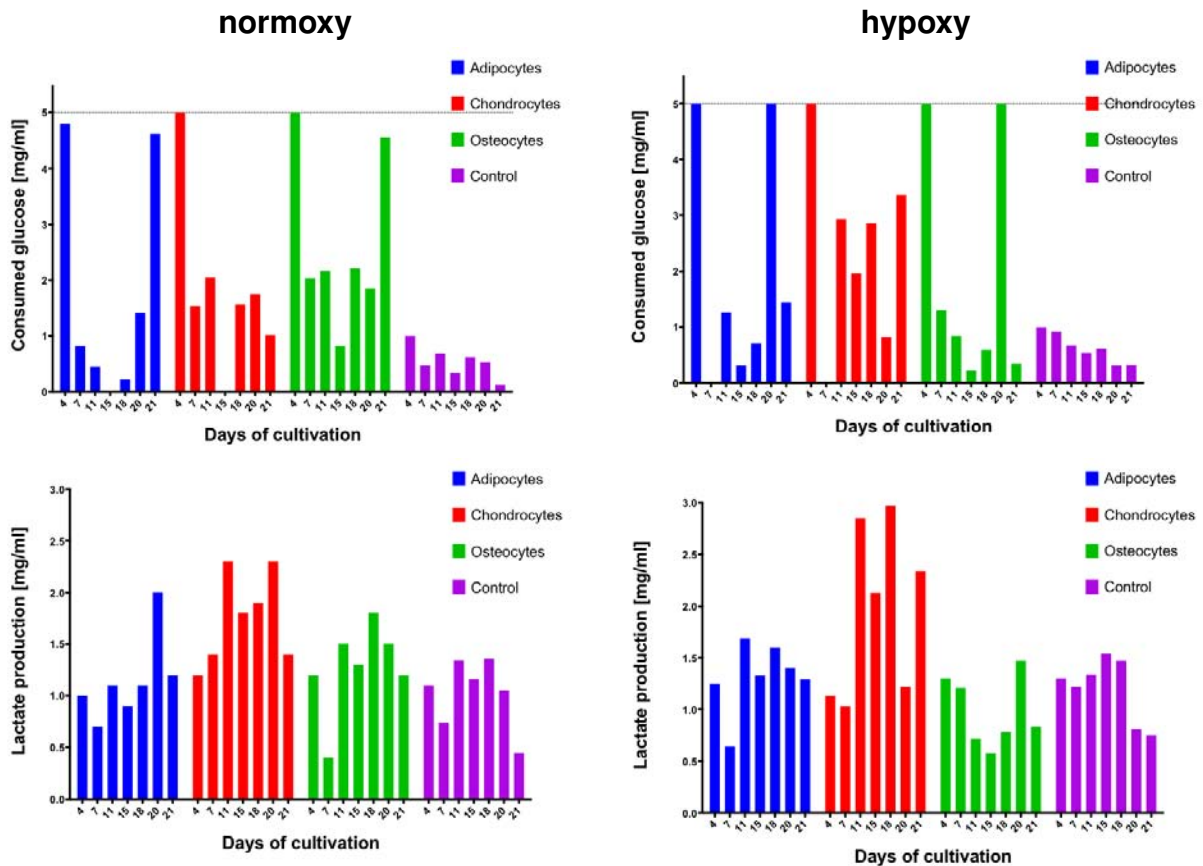


Figure 4.20: Metabolic activity of adMSCs(64m) during differentiation into adipocytes, chondrocytes and osteocytes under normoxic (A and C) and hypoxic (B and D) culture conditions.

4.1.6 Monitoring of oxygen consumption during differentiation of adMSCs(64m)

In order to evaluate oxygen kinetics of adMSCs(64m) dissolved oxygen in the culture supernatant were monitored during differentiation into adipocytes, chondrocytes and osteocytes. The experimental setup is described in subsection B.2.1 and section B.7. Briefly, adMSCs(64m) were seeded in 24 well OxoDish® plates at a density of 4,000 cells per cm². The plate was placed onto SDR SensorDish® Reader located in the incubator. To provided maximum cell expansion before cells enter differentiation, change to differentiation medium was conducted on study day two. The control group was cultivated during the whole study time in standard culture medium with no change to differentiation medium. The study was conducted for 18 days, with medium replacements every first, third and fifth day of the week.

Normoxic culture conditions

Monitored dissolved oxygen in culture supernatant during differentiation under normoxic culture conditions is shown in figure 4.21. Between the individual differentiation lineages no drastic differences in oxygen uptake can be observed. In the control group (undifferentiated cells) the oxygen uptake rate increased during cultivation due to the forming of aggregates. These results were confirmed by microscopic investigation. During the cultivation of adMSCs(64m) with adipogenic differentiation medium the oxygen value was very stable. Over the course of cultivation with chondrogenic differentiation medium, the oxygen consumption rate increased

and the dissolved oxygen in the supernatant dropped about 3% under the baseline level after every medium change. An equilibrium of oxygen diffusion into the medium and consumption rate was regained again after about 24 h. Osteogenic differentiation of adMSCs(64m) revealed a stable oxygen consumption rate over the course of cultivation. A slight increase of oxygen uptake was noticed after medium replacement.

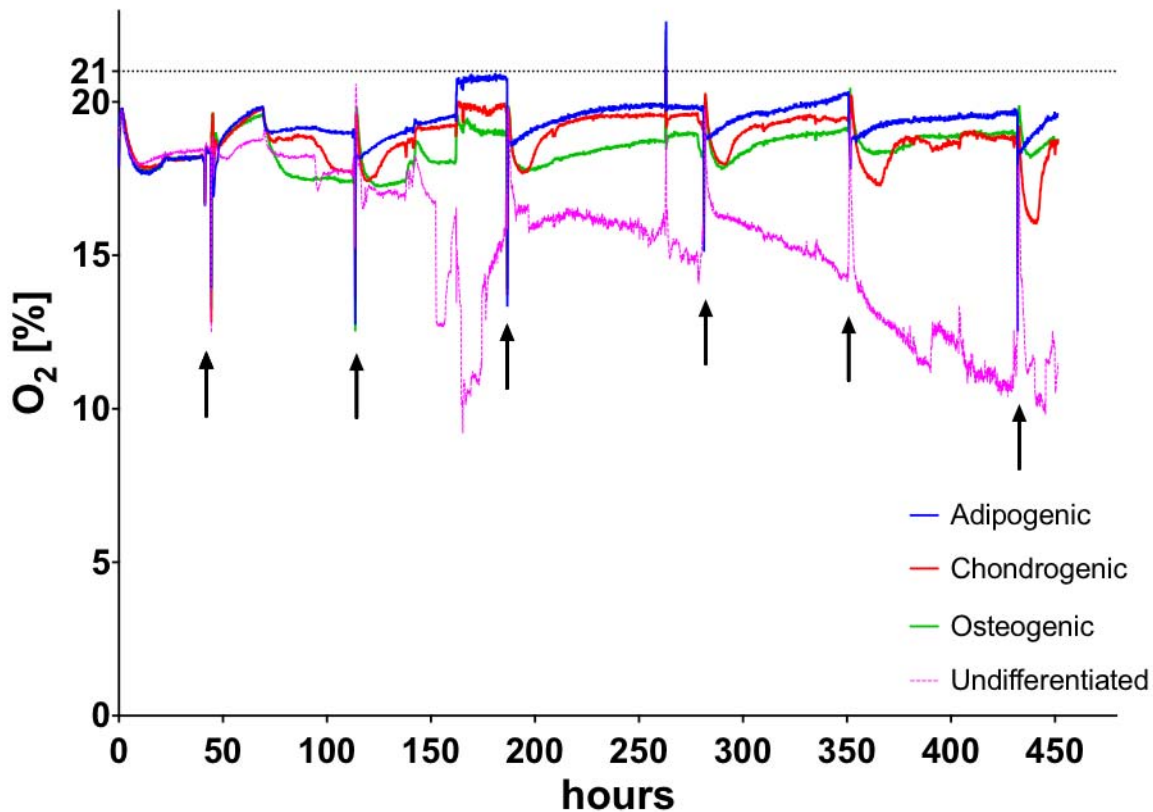


Figure 4.21: Oxygen kinetics during differentiation of adMSCs(64m) under normoxic culture conditions. Dissolved oxygen level during adipogenic, chondrogenic and osteogenic differentiation is compared to undifferentiated adMSCs(64m) expanded in standard culture medium (control group). Medium changes are indicated by arrows.

Hypoxic culture conditions

Monitored dissolved oxygen in culture supernatant during differentiation under hypoxic culture conditions is shown in figure 4.22. Between the individual differentiation lineages a difference in oxygen uptake can be observed. When compared to adipogenic differentiation, adMSCs(64m) undergoing chondrogenic differentiation metabolized 6.8% more O_2 and during osteogenic differentiation even 22.6% more O_2 . During osteogenic differentiation the cells showed a higher oxygen consumption rate compared to adipogenic and chondrogenic differentiation. After the change to differentiation medium a slight decrease in oxygen metabolism can be seen in all groups, which is indicated by the increase of oxygen in the supernatant. After the next medium replacement the final equilibrium for each differentiation lineage was established. At the end of cultivation, all study groups showed a drastic change of oxygen level in the supernatant which was caused by a higher oxygen environment in the incubator. In the control group the oxygen uptake rate increased during cultivation due to the forming of aggregates. The change in mor-

pholgy and formation of cell aggregates were confirmed by microscopic investigation. During the cultivation of adMSCs(64m) with adipogenic differentiation medium, the oxygen level was very stable. After each medium change the achieved baseline showed only minor fluctuations. The oxygen consumption had the lowest rate during the adipogenic differentiation compared to the other differentiation lineages. The achieved baseline was about 5.00% dissolved O₂ in the supernatant. Over the course of cultivation with chondrogenic differentiation medium, oxygen consumption revealed more variations in baseline level. Directly after every medium change the oxygen consumption rate increased and the dissolved oxygen in the supernatant dropped about 1% under the baseline level (about 4.66% dissolved O₂). An equilibrium of oxygen diffusion into the medium and consumption rate was regained again after about 12 h. Similar results were found under normoxic culture conditions. Osteogenic differentiation of adMSCs(64m) revealed the highest oxygen consumption rate over the course of cultivation. The baseline was about 3.87% dissolved O₂ in the supernatant. At the end of cultivation the measured dissolved oxygen values in the supernatant was significantly higher due problems with maintaining the hypoxic conditions in the incubator.

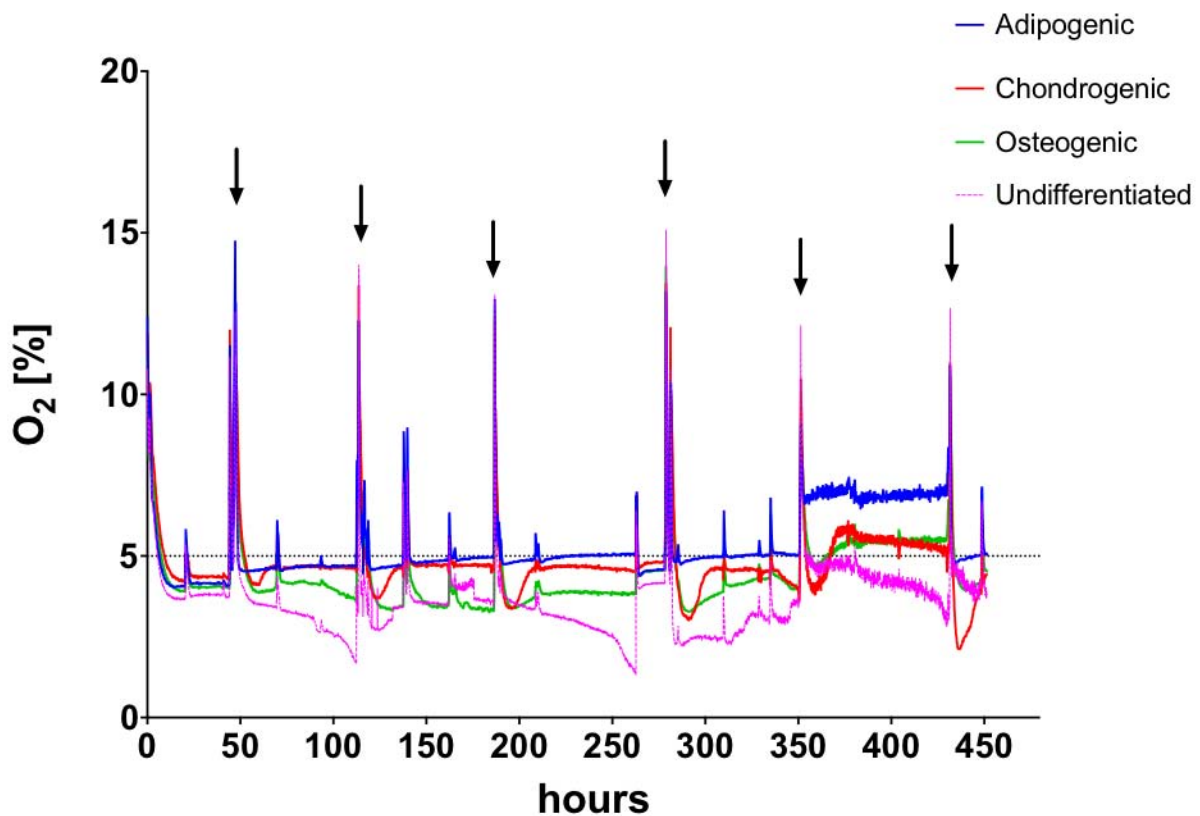


Figure 4.22: Oxygen kinetics during differentiation of adMSCs (64m) under hypoxic culture conditions (A), Dissolved oxygen level during adipogenic (B), chondrogenic (C) and osteogenic (D) differentiation compared to adMSCs(64m) expanded in standard culture medium. Medium changes are indicated by arrows.

4.2 Characterization of a specialized bioreactor system for dynamic cultivation

In order to successfully introduce a novel bioreactor system for dynamic cultivation three experiments were conducted to overcome current technical challenges.

The core of the dynamic cultivation experiments is the novel cell culture incubator IT-3a (Fraunhofer IGB), shown in figure 4.23. The design and characteristics are described in B.8.1. Briefly, the IT-3 consists of a cabinet equipped with four independent drawers. It allows normoxic and hypoxic cultivation simultaneously, while providing a stable environmental atmosphere of $37^{\circ}\text{C} \pm 0.4^{\circ}\text{C}$ and 5% CO_2 . Each drawer is equipped with an independent peristaltic pump system, which is able to accommodate up to four individual bioreactors. A single chamber can be removed without affecting remaining chambers of an experiment, which highly increases accessibility and handling for experimental analysis. Furthermore each drawer provides a reusable pressure transducer. All four drawers can be simultaneously monitored via a special supervising unit. It visualizes and logs pressure trend over time as well as current temperature, CO_2 and O_2 values.

The centerpiece of the bioreactor system is a mini perfusion reactor, which is precisely described in B.8.1. This mini perfusion reactor is integrated within the tubing circuit and provides the growth chamber. A porous scaffold lies in the chamber and is fixed with a stainless steel mesh. In all experiments Matristypt[®] (B.8.4) scaffolds are used. Medium was pumped using the peristaltic pump in a circular manner. Various flow rates were used to introduce different shear stress levels and direct mechanical stimuli over scaffolds.



Figure 4.23: IT-3a cell culture incubator table (Fraunhofer IGB)

4.2.1 Medium evaporation behavior of a bioreactor setup

In order to determine the effect of medium evaporation on the bioreactor setup and define a feeding regime for dynamic cultivation, an experiment was performed as described in B.8.2.1. Bioreactor systems containing different volumes of PBS were run for 10 days and the mass loss in defined time intervals (24 h) was measured.

Percentual weight loss of bioreactor systems during the study is shown in figure 4.24. It can be seen, that although bioreactors were free from leakages, particular volume loss occurred. Exact weight of evaporated PBS per day is given in table 4.3. On study day 4 the bioreactor system loaded with 5 ml reached a PBS level below the minimum threshold and had to be terminated. The PBS level of the bioreactor system loaded with 10 ml also decreased below the minimum threshold and had to be excluded from further tests.

Average daily weight loss in percent for 5 ml 12.33 ± 10.22 %, for 10 ml 7.06 ± 4.28 %, for 15 ml 4.39 ± 1.76 % and for 20 ml PBS loaded 3.12 ± 1.97 %. Daily medium evaporation varied between a maximum of 0.90 g and minimum of 0.12 g with an average medium loss between 0.62 ± 0.29 g and 0.71 ± 0.16 g a day. The overall average of daily evaporation was 0.65 ± 0.02 g.

Table 4.3: Weight loss of bioreactors systems in g per day.

Bioreactor systems	Study days										Mean $\Delta m[g]/d \pm SEM$	
	d1	d2	d3	d4	d5	d6	d7	d8	d9	d10		
5 ml	0.09	0.65	1.11									0.62 ± 0.29
10 ml	1.42	0.90	0.57	0.68	0.12	0.92	0.33					0.71 ± 0.16
15 ml	1.16	1.07	0.51	0.70	0.38	0.50	0.61	0.45	0.73	0.48		0.66 ± 0.08
20 ml	0.62	1.56	0.42	0.90	0.46	0.71	0.13	0.35	0.42	0.68		0.63 ± 0.12
Overall average											0.65 ± 0.02	

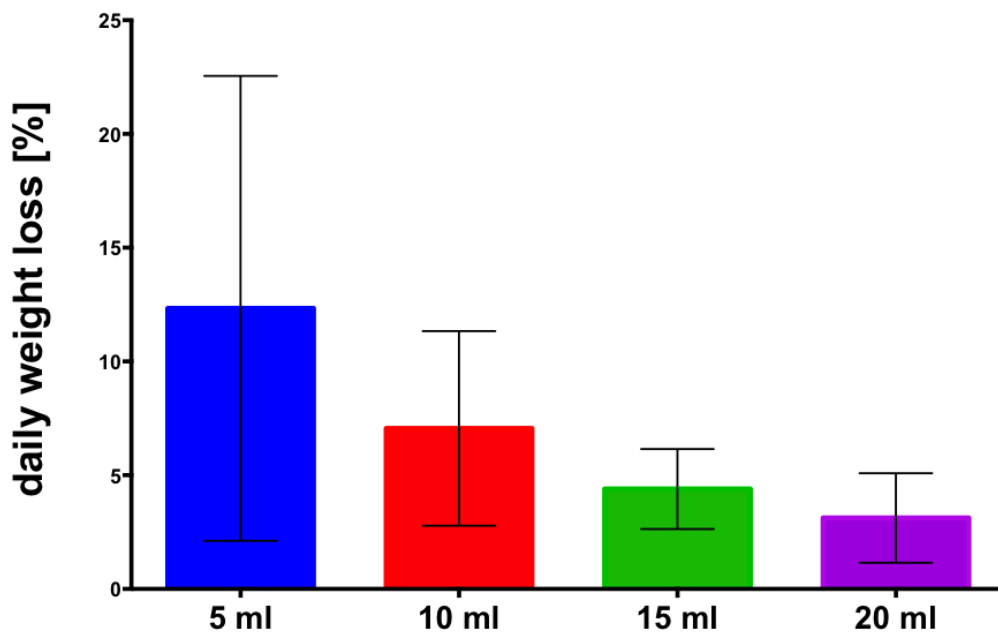


Figure 4.24: Percentual weight loss of bioreactor systems containing 5, 10, 15 and 20 ml of PBS.

4.2.2 Fluid flow, back pressure and shear stress correlation for a bioreactor system

In order to prove the functionality of the bioreactor system two experimental trials were performed. The aim of this study was to evaluate several outcomes: (I) leak tightness, (II) media distribution within scaffolds and (III) the resulting back pressure due to various fluid flows.

Leak tightness of the bioreactor system and medium distribution within scaffolds

This study was performed to assure leak tightness of the assembled bioreactor system and to visualize medium distribution on the scaffold during dynamic cultivation. Briefly, one bioreactor system was fully assembled and loaded with 10 ml working solution, which was stained with methylene blue. Back pressure was monitored for 25 h at a constant fluid flow of 1.5 ml/min. After perfusion the scaffold was investigated for medium distribution habit and texture.

The received data from back pressure monitoring are shown in figure 4.25. A large oscillation range of measurement data can be seen. The maximum value determined was 38.00 mbar. During the first hour of the study the back pressure fell below zero several times. Total variation was calculated to be 30.93 mbar. The slope of the linear regression line showed a slight increase of 0.17 mbar, which indicates a back pressure increase within the experiment. Further, the average back pressure for a fluid flow of 1.5 ml/min was 8.73 mbar. Medium distribution in the harvested scaffold was homogeneous throughout the matrix, which indicates a sufficient medium nutrition supply for all seeded cells within scaffolds. Its texture was smooth and was not harmed by the stainless steel mesh.

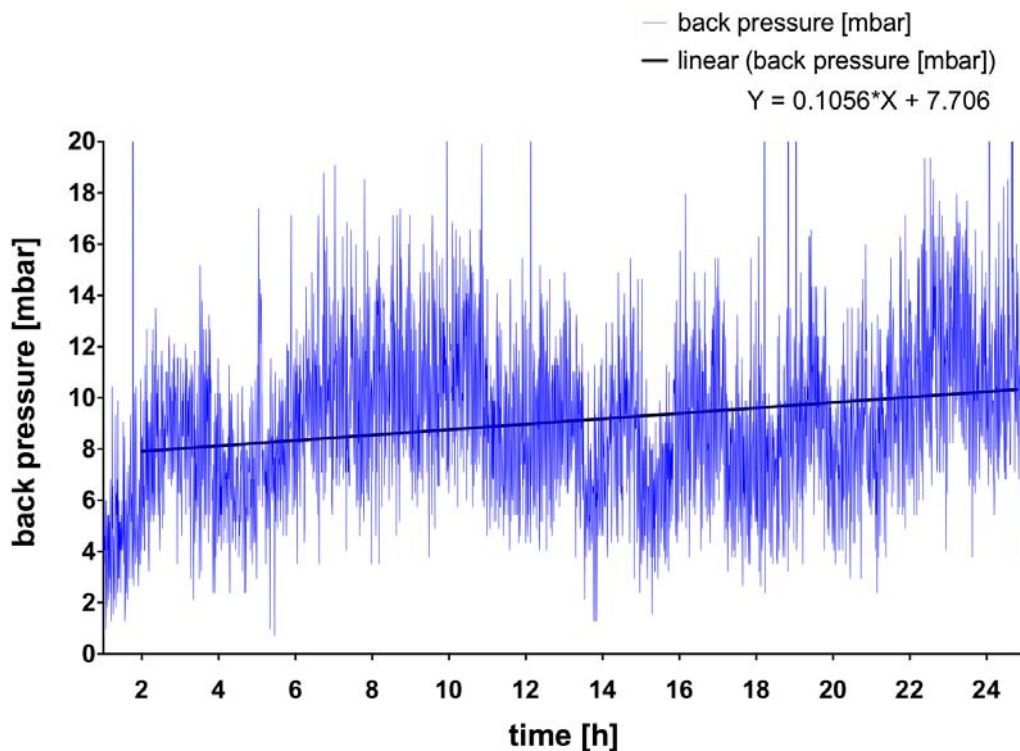


Figure 4.25: Short term pressure regime for a bioreactor system at a constant fluid flow of 1.5 ml/min for 25 h. Back pressure is sketched against time and interpolated by linear regression.

Influence of fluid flow on back pressure and shear stress

This experiment was performed to evaluate a calibration curve for the back pressure and resulting shear stress habit of the bioreactor system. One bioreactor was assembled and loaded with 10 ml stained working solution as mentioned before in 4.2.2.1. The working solution was stained in order to visualize any leakage and medium distribution in the scaffold. Perfusion was started with a flow rate of 0.3 ml/min and stepwise increased in 0.1 ml/min steps until the final flow rate of 1.5 ml/min was reached. Back pressure was monitored during the study. The recorded back pressure increases exponentially and the resulting shear stress was calculated following the equation 4.5.

$$\tau_{max} = \frac{r \cdot \Delta p}{2 \cdot L} \quad (4.5)$$

Used parameters:

k intrinsic permeability [m²]

r Radius of the scaffold = 0.0005 m

L Thickness of the scaffold = 0.002 m

μ Dynamic viscosity = 0.001 Pas

p Measured back pressure [Pa]

τ Shear stress [N/m²]

In figure 4.26 received shear stress values averaged over the flow rate are plotted. In order to develop a calibration curve of the experimental shear stress habit, an exponential trend line is calculated. It can be recognized that until a flow rate of 0.7 ml/min is reached, only small changes of the shear stress levels occurred. After 0.7 ml/min the resulting shear stress increases drastically. The exponential trend line of this figure points out the exponential relationship of shear stress to fluid flow more clearly. The equation 4.5 and its derivation assume that shear stress is directly proportional to the fluid flow. This assumption could not be confirmed in the experiment.

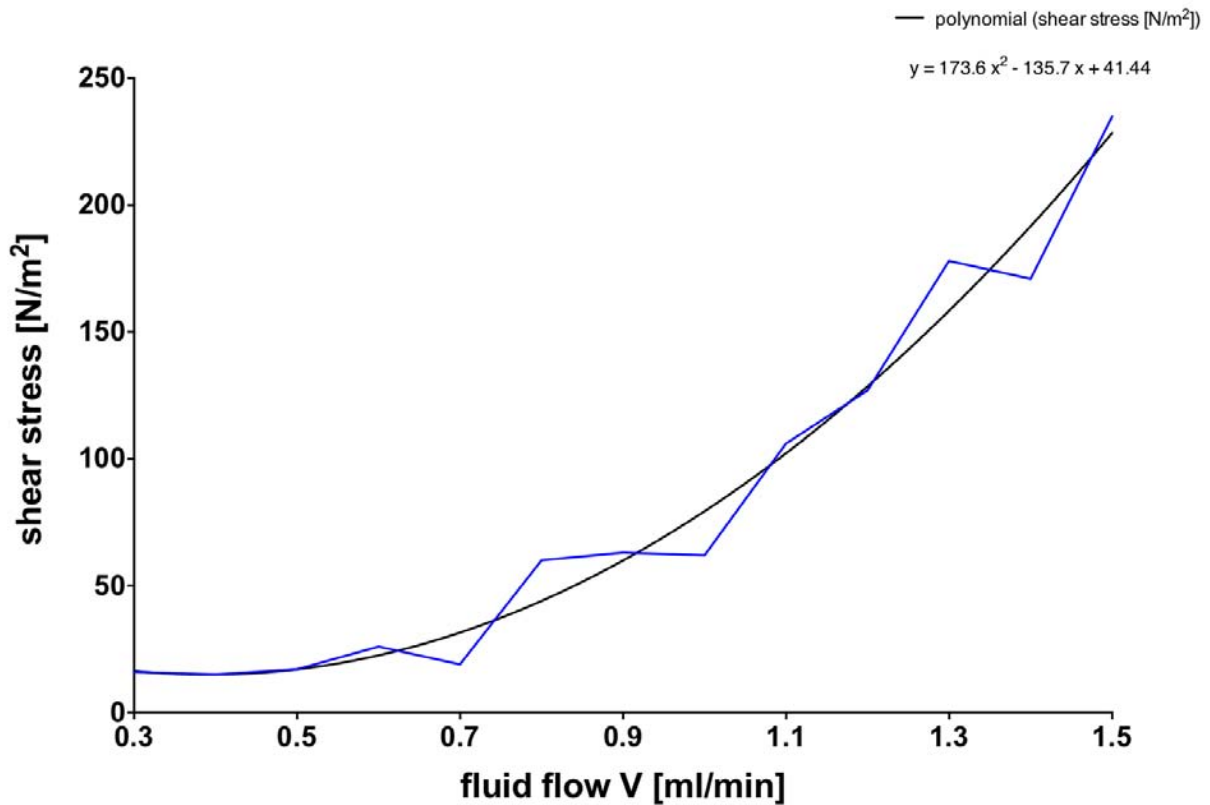


Figure 4.26: Back pressure [mbar] and shear stress [N/m²] trend plotted against fluid flow.

Furthermore, shear stress values are calculated according to the derivation shown in B.8.3.2 equation B.14. To provide comparable data, the mean shear stress values in N/m² were converted to dyn/cm² and are shown in table 4.4. The shear stress unit dyn/cm² is a small pressure unit widely used in the field of medical research and is equal to 0.1 N/m². Very high shear stress levels can be observed from the beginning of the experiment.

Table 4.4: Resulting shear stress at various fluid flow levels

Fluid flow [ml/min]	Shear stress [N/m ²]	Shear stress [dyn/cm ²]
0.3	16	161
0.4	15	153
0.5	17	173
0.6	26	257
0.7	19	190
0.8	60	598
0.9	63	627
1.0	62	618
1.1	106	1061
1.2	127	1271
1.3	178	1780
1.4	171	1713
1.5	235	2353

The intrinsic permeability k of Matristypt[®] was calculated according to Darcy's law (equation 4.6), which is a measure to determine the ability of a porous material to allow fluids to pass through it

$$k = \frac{\dot{V} \cdot \mu}{A} \cdot \frac{L}{\Delta p} \quad (4.6)$$

Used parameters:

k intrinsic permeability [m^2]

\dot{V} Flow rate [m^3/s]

p Measured back pressure [Pa]

μ Dynamic viscosity = 0.001 Pas

A Cross-sectional area = $7.85 \times 10^{-7} \text{ m}^2$

L Thickness of the scaffold = 0.002 m

The received data are presented in figure 4.27. The mean permeability was revealed to be 9×10^{-12} . The calculation data however, show a wide scatter. The maximum value was 1.9×10^{-11} and the minimum value was 3.4×10^{-12} , which result in an range of 1.6×10^{-11} . The low of permeability values fit well with the high shear stress values and reaffirm the previously made assumption.

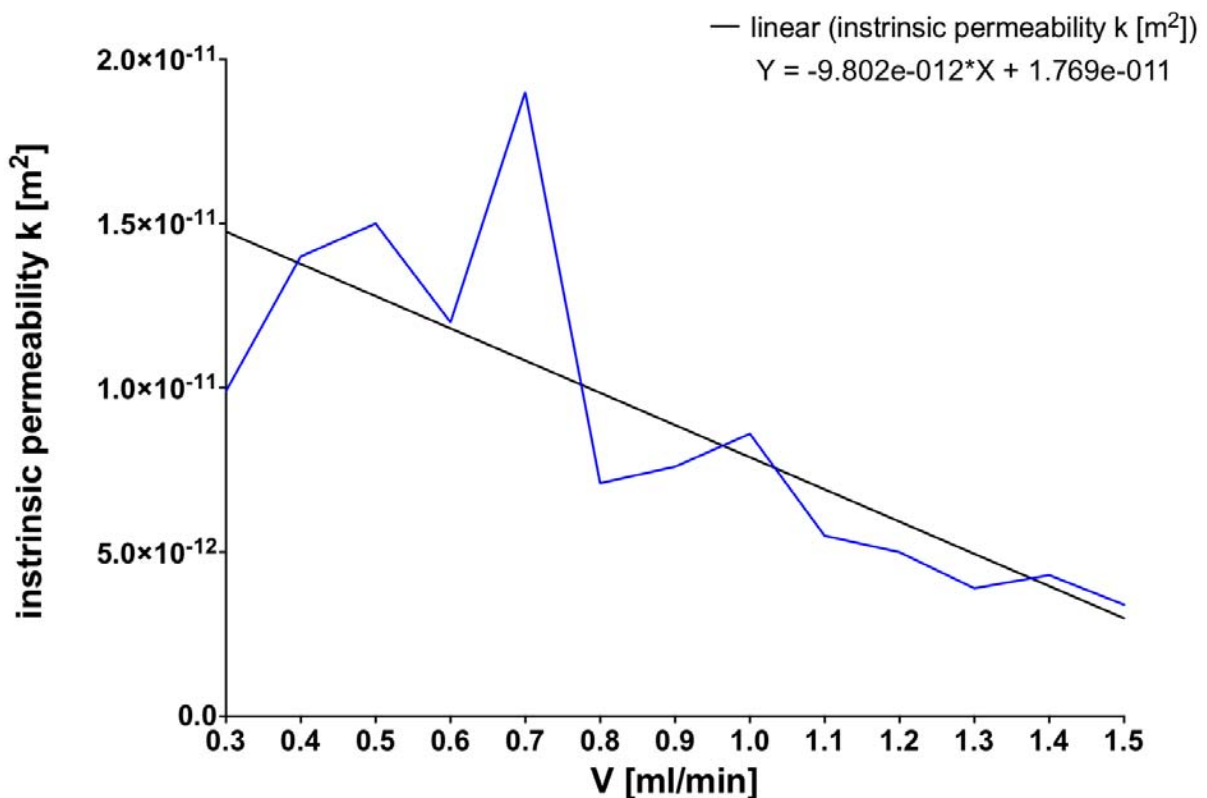


Figure 4.27: Calculated intrinsic permeability of Matristypt[®] plottet against fluid flow.

5 Discussion and Outlook

5.1 Experiments under static culture conditions

To evaluate multipotent character and proliferation of freshly harvested adMSCs under normoxic and hypoxic culture conditions, 2D cell culture experiments were performed. First, the need of preconditioned medium for cultivation under hypoxic culture conditions was tested using ucMSCs. Further to optimize growth on 3D Matristypt® scaffolds, a seeding strategy experiment with ucMSCs was conducted. Proliferation kinetic for adMSCs(64m) and differentiation capability of adMSCs(64m) and adMSCs(82f) were investigated under normoxic and hypoxic culture conditions. In addition, the effect of the reduced oxygen tension on oxygen consumption during differentiation was evaluated for adMSCs(64m).

In vivo physiological tissue oxygen concentration is maintained in a range of 1 to 7%. To better mimic this specific physiological microenvironment *in vitro*, experiments must be conducted with adapted oxygen tensions. As a consequence the use and need of preconditioned medium must be considered and evaluated. Especially, the duration until an equilibrium of dissolved oxygen in the culture medium is achieved, after exposure to hypoxic environment, must be investigated. An experiment was conducted in normoxic and hypoxic culture conditions. For both conditions non-preconditioned standard culture medium was used. Oxygen concentration in the culture supernatant was non-invasively monitored. To investigate the specific oxygen kinetic, the half life of oxygen ($t_{1/2}$) was determined in the culture supernatant after seeding and medium replacements. Additionally, the correlation of the dissolved oxygen in the standard culture medium in comparison to different seeding densities was evaluated. Over the course of cultivation under normoxic conditions, continuously decreasing oxygen values in parallel to enhanced cell proliferation were observed. This indicates that the oxygen consumption rate of the cells is higher than the diffusion rate of oxygen into the standard culture medium. Oxygen kinetic correlated well with the initial start concentration of ucMSCs. Wells with the lowest cell concentration did not show any decrease in dissolved oxygen due to the lack of sufficient cell growth. This experiment suggests that oxygen consumption depends directly on cell concentration. During cultivation under hypoxic conditions the oxygen concentration in the medium increased up to a maximum of 14% after medium replacement and seeding in the normoxic laboratory environment. Calculation of half life of oxygen decrease, leads to the result that it takes about 1 h to fully reestablish hypoxic culture conditions. Half life values were between 0.86 ± 0.4 h to 0.55 ± 0.02 h. These outcomes confirm that cultivation under hypoxic conditions can be conducted with standard culture medium without precondition the medium in an environment with 5% oxygen tension. However, no correlation between initial seeding concentration and half life of oxygen could be observed. In addition, it could be observed that baseline levels of dissolved oxygen in the supernatant never reached the maximum of 21% or 5% O₂ during cultivation. Oxygen solubility in medium is mainly influenced by temperature, partial pressure and salt concentration. To guarantee successful cultivation, oxygenation of the medium and oxygen consumption must be in balance. Further experiments should be conducted to evaluate specific oxygen dissolubility in the standard culture medium. Moreover, specific oxygen consumption could be calculated as the difference of dissolved oxygen concentration during cultivation and standard medium without cells.

Important for successful cartilage tissue engineering is a uniform distribution and cell growth

within in the whole scaffold or matrix. Cell seeding on 3D scaffolds is the first step of further cultivation in bioreactors. Seeding requirements are high yield and spatial uniformity in the distribution of cells. The optimal seeding density for growth on Matristypt® 3D collagen scaffolds were investigated. Especially ucMSCs seeded at a density of 1×10^5 cells per scaffold showed the best proliferation assessed by MTT assay. Distribution imaging via DAPI staining confirmed these results. Nevertheless, directly after seeding adhering cells showed a inhomogeneous distribution on the scaffold surface due to the static seeding procedure. After 7 days of cultivation DAPI staining showed, that a uniform distribution within and on the surface was reached. Moreover, cell growth on the bottom side was observed, indicating a successful cell invasion of the whole scaffold. In addition, glucose consumption and lactate production measurement implied a high metabolic activity. At the highest seeding density (5×10^5 cells per scaffold) a very dense cell layer could be observed in DAPI images. Results of metabolic activity measurements and MTT - assay confirmed this finding. Lower seeding (5×10^4 , 1×10^4 , 5×10^3 and 1×10^3) densities showed significantly decreased cell proliferation and metabolic activity, suggesting a minimal seeding density higher than 5×10^4 cells per scaffolds.

To accomplish the high yield of cells required for the manufacture of engineered cartilage tissue, isolated adMSCs need to be expanded in passages. In addition, it must be assured that adMSCs don't loose their specific cell morphology as well as their capability of differentiation. In order to investigate the growth kinetics of adMSCs(64m), a proliferation study was conducted. The results showed that adMSCs(64m) can be subcultivated *in vitro* for a period of 10 passages without losing their proliferative activity. It can be seen that hypoxic cultures resulted in increased cumulative population doubling (41.64 ± 0.68 at 5% O₂ versus 38.94 ± 0.49 at 21% O₂) and higher total cell numbers ($2.60 \times 10^{18} \pm 12 \times 10^{18}$ cells at 5% O₂ versus $3.84 \times 10^{17} \pm 1.12 \times 10^{17}$ at 21% O₂) compared to normoxic conditions. This is equivalent to 6.93% more cells after 711.18 h or 10 passages. These outcomes demonstrate that under cultivation with a lower oxygen tension, a higher cell yield can be achieved in a shorter period of time. Furthermore, it was proven that adMSCs(64m) can be expanded until passage 10 without losing their characteristic cell morphology. These results indicate, that adMSCs are a secure and attractive cell source for cartilage tissue engineering. To prove their capability of differentiation in advanced passages, follow up differentiation studies must be conducted with adMSCs in passage stages between 3 and 10.

The main characteristic of adMSCs is their capability to differentiate into adipocytes, chondrocytes and osteocytes after specific induction. To prove the multipotent character of harvested adMSCs from 2 donors, adMSCs(64m) and adMSCs(82f), a differentiation experiment was performed. Metabolic analysis during the differentiation of adMSCs(64m) showed an increased glucose consumption. This effect implies that adMSCs(64m) need higher amounts of glucose to maintain their metabolic activity or to perform differentiation. The main histological characteristic of adipocytes is the formation of intracellular triglyceride droplets. Oil Red-O staining was used to confirm positive differentiation of adMSCs(64m) and adMSCs(82f). It intercalates with the neutral lipids, which then appear red under the light microscope. Both adMSCs(64m) and adMSCs(82f) were successfully differentiated into adipocytes, indicated by stained lipid droplets and prominent changes in the cell morphology. Moreover, cells cultivated under hypoxic conditions revealed a higher number of lipid droplets suggesting that lower oxygen stress enhances adipogenic differentiation. Chondrogenic differentiation was assessed by Alcian blue staining. Chondrocytes exhibit a specific extracellular proteoglycan matrix. These sulfated GAG can be visualized by staining with Alcian blue. This is a copper phthalocyanin dye and contains positively charged groups, which form a salt linkage with the sulfated GAG. Chondrogenic differentiation

potential was confirmed for adMSCs(64m) and adMSCs(82f). Both showed intense production of the extracellular proteoglycan matrix under normoxic and hypoxic culture conditions, but under hypoxic conditions a more dense cell layer and a higher degree of staining was observed. These findings support the previous made assumption, that lower oxygen tension promotes cell differentiation. Osteogenic differentiation was analyzed by two histological stainings: Von Kossa and Alizarin Red. Osteocytes form an extensive extracellular network consisting of calcium. In case of Von Kossa staining the calcium ions are substituted with silver ions and a precipitation reaction with phosphate visualize them as black spots. Whereas, Alizarin Red forms a red chelate complex with calcium ions. adMSCs(64m) and adMSCs(82f) showed prominent changes in their cell morphology and an intense Von Kossa and Alizarin Red staining. No significant differences regarding oxygen tension or donor could be observed. This might be due to the high degree of differentiation. To sum up, histological stainings confirmed successful differentiation of adMSCs(64m) and adMSCs(82f) towards adipocytes, chondrocytes and osteocytes. Moreover, differentiation could be verified by the cell morphology via light microscopy. Under hypoxic conditions a more dense cell layer and an enhanced differentiation capacity was observed. Furthermore, adMSCs(82f) showed a lower grade of differentiation, this might due to the age of the donor. Nevertheless, the results demonstrate that lower oxygen tensions seem to be beneficial for adMSCs to differentiate into adipocytes and chondrocytes.

In addition, oxygen consumption of adMSCS(64m) was monitored during differentiation under normoxic and hypoxic culture conditions. Non-invasive insitu monitoring of oxygen consumption could be an indirect parameter for metabolic activity during differentiation. Further knowledge of differentiation lineage specific oxygen requirement could also be a promising tool to control and and guide cell differentiation. Under both culture conditions in the control group, adMSCS(64m) cultured in standard culture medium, continuously decreasing oxygen values in parallel to enhanced cell proliferation was observed. The non-differentiated adMSCs(64m) formed cell aggregates over longer cultivation times. This may effect the oxygen kinetics in two ways. First, cell aggregates could be accidentally removed during media change and second, aggregate structures may influence cellular metabolism, which might be the reason for the oxygen decrease during cultivation. During differentiation under normoxic conditions no significant difference of the oxygen consumption between the differentiation lineage could be observed. However, a continuously decreasing oxygen value directly after seeding was noticed, indicating that the oxygen consumption rate of the viable cells might be higher than the diffusion rate of oxygen into the culture medium. In particular, adMSCs(64m) during chondrogenic differentiation under both culture conditions showed this increased oxygen uptake. Under hypoxic culture conditions, a differentiation lineage specific oxygen consumption was noticed. Cells cultivated in osteogenic differentiation medium revealed the highest oxygen consumption rate, 22.6 % higher than adMSCs(64m) in adipogenic differentiation, which had the lowest uptake of oxygen. During chondrogenic differentiation, adMSCs(64m) metabolized about 6.8% more oxygen compared to cells undergoing adipogenic differentiation. Further experiments should be conducted to determine the specific oxygen dissolubility in each differentiation media. Moreover, differentiation characteristic oxygen consumption could be calculated as the difference of dissolved oxygen concentration during differentiation in the medium and corresponding differentiation in medium without cells. In future, exactly defined oxygen content during *in vitro* cultivation could be monitored precisely and, if necessary, regulated. Hence, controlled cell differentiation under hypoxic conditions could be performed at a higher security level. Non-invasive characterization and control of the optimal culture conditions is crucial for process development.

5.2 Characterization of a specialized bioreactor system for dynamic cultivation

To develop a hydrodynamic environment, which is known to enhance chondrogenic differentiation, a perfusion bioreactor system was tested. To characterize this system 3 experiments were conducted.

Initially, its medium evaporation behavior was evaluated. It was shown that drastic fluid loss occurred in all assessed bioreactor systems. This phenomenon seems to be independent of the initial volume of PBS loaded and is indicated by similar daily mean weight loss. However, the higher the initial loaded volume the lower the daily weight loss in percent, resulting in better conditions during the experiment. In the daily measured weight, a wide variation was recorded. The high dead weight of a bioreactor system respective to the relatively small weight changes may have caused these measurement variations. In general, fluid evaporation is influenced by following factors: air saturation, intermolecular forces, pressure, surface area, temperature and density of the substance. These factors were constant in this experiment. All four bioreactor systems had exactly the same setup except for minor divergences in tubing length (millimeter range). A more suitable tracking system of bioreactor weight must be implicated to overcome the measurement errors and generate more comparable data. Nevertheless, this experiment suggests that medium evaporation is an important factor in developing a feeding regime.

Then leak tightness and medium distribution within a loaded scaffold was tested. A short term perfusion experiment applying a high flow rate (1.5 ml/min) for 25 h was performed. The recorded back pressure showed a large oscillation range and a slight increase over time. Further studies must be conducted to prove and investigate this behavior. The measured oscillation range might be due to peristaltic pump movement and could be overcome by repeating the experiment with a higher number of bioreactor systems and operating the peristaltic pumps in a shifted manner. The investigated scaffold showed a homogeneous medium distribution. Moreover, its texture was smooth and was not harmed by the stainless steel mesh. It can be assumed that sufficient medium nutrition supply within the scaffold matrix can be ensured.

Furthermore, the influence of the fluid flow on shear stress and permeability of the scaffold was investigated. Calculations assumed that shear stress increases direct proportional to the fluid flow. The received curve showed a second polynomial characteristic course for the shear stress and the previously made assumption could not be confirmed. Based on equation B.11 a linear correlation was expected. However, very high shear stress levels occurred already at 0.3 ml/min and an exponential trend could be observed. The received data indicates a low intrinsic permeability of Matristypt[®]. Additional calculations according to Darcy's law confirmed this assumption. Though, these results showed vast deviations. The high variation of the measured back pressure values may have been the cause of the wide range of calculated values. Further experiments need to be carry out to evaluate the exact intrinsic permeability of Matristypt[®].

Based on these results it could be shown that this bioreactor system combines mechanical forces of perfusion and compression. Bioreactors can be used to accelerate and enhance the growth of cartilage tissue *in vitro*. They improve nutrient transport and are able provide a fluid flow induced shear stress to promote the synthesis of cartilage-specific matrix proteins. Moreover, it can be concluded that Matristypt[®] is a non-suitable matrix for dynamic cultivation in this particular perfusion system. Further investigations must be conducted with special focus

to find a scaffold which provides the same biological compatibility with a more porous matrix.

Bibliography

- Archer, Charles W and Philippa Francis-West (Apr. 2003). "The chondrocyte". In: *Int J Biochem Cell Biol* 35.4, pp. 401–4.
- Awad, Hani A et al. (July 2004). "Chondrogenic differentiation of adipose-derived adult stem cells in agarose, alginate, and gelatin scaffolds". In: *Biomaterials* 25.16, pp. 3211–22. DOI: 10.1016/j.biomaterials.2003.10.045.
- Baer, Patrick C and Helmut Geiger (2012). "Adipose-derived mesenchymal stromal/stem cells: tissue localization, characterization, and heterogeneity". In: *Stem Cells Int* 2012, p. 812693. DOI: 10.1155/2012/812693.
- Baumgartner, Laura et al. (June 2010). "Human mesenchymal stem cells: Influence of oxygen pressure on proliferation and chondrogenic differentiation in fibrin glue in vitro". In: *J Biomed Mater Res A* 93.3, pp. 930–40. DOI: 10.1002/jbm.a.32577.
- Bjerre, Lea et al. (June 2008). "Flow perfusion culture of human mesenchymal stem cells on silicate-substituted tricalcium phosphate scaffolds". In: *Biomaterials* 29.17, pp. 2616–27. DOI: 10.1016/j.biomaterials.2008.03.003.
- Boschetti, Federica et al. (2006). "Prediction of the micro-fluid dynamic environment imposed to three-dimensional engineered cell systems in bioreactors". In: *J Biomech* 39.3, pp. 418–25. DOI: 10.1016/j.jbiomech.2004.12.022.
- Brittberg, M et al. (Oct. 1994). "Treatment of deep cartilage defects in the knee with autologous chondrocyte transplantation". In: *The New England journal of medicine* 331.14, pp. 889 –895.
- Buckwalter, JA and HJ Mankin (Apr. 1999). "Articular cartilage .2. Degeneration and osteoarthritis, repair, regeneration, and transplantation". In: *Journal bone joint surgery - American Volume* 79A, pp. 612 –632.
- Bunnell, Bruce A et al. (June 2008). "Adipose-derived stem cells: isolation, expansion and differentiation". In: *Methods* 45.2, pp. 115–20. DOI: 10.1016/j.ymeth.2008.03.006.
- Carey-Beth, James and Timothy L. Uhl (2001). "A Review of Articular Cartilage Pathology and the Use of Glucosamine Sulfate". In: *Journal of Athletic Training* 36, pp. 413–419.
- Carter, Dennis R and Marcy Wong (Sept. 2003). "Modelling cartilage mechanobiology". In: *Philos Trans R Soc Lond B Biol Sci* 358.1437, pp. 1461–71. DOI: 10.1098/rstb.2003.1346.
- Chung, Cindy and Jason A Burdick (Jan. 2008). "Engineering cartilage tissue". In: *Adv Drug Deliv Rev* 60.2, pp. 243–62. DOI: 10.1016/j.addr.2007.08.027.
- Csaki, C, P R A Schneider, and M Shakibaei (Nov. 2008). "Mesenchymal stem cells as a potential pool for cartilage tissue engineering". In: *Ann Anat* 190.5, pp. 395–412. DOI: 10.1016/j.aanat.2008.07.007.
- Fehrer, Christine et al. (Dec. 2007). "Reduced oxygen tension attenuates differentiation capacity of human mesenchymal stem cells and prolongs their lifespan". In: *Aging Cell* 6.6, pp. 745–57. DOI: 10.1111/j.1474-9726.2007.00336.x.

- Flynn, Lauren E et al. (Apr. 2008). "Proliferation and differentiation of adipose-derived stem cells on naturally derived scaffolds". In: *Biomaterials* 29.12, pp. 1862–71. DOI: 10.1016/j.biomaterials.2007.12.028.
- Frenkel, Sally R. and Paul E. di Cesare (Jan. 2004). "Scaffolds for Articular Cartilage Repair". In: *Annals of Biomedical Engineering* 32.1, pp. 26–34.
- Gimble, Jeffrey M. et al. (2008). "In vitro Differentiation Potential of Mesenchymal Stem Cells". In: *Transfus Med Hemother* 35, pp. 228–238.
- Goldring, Mary B (Oct. 2006). "Update on the biology of the chondrocyte and new approaches to treating cartilage diseases". In: *Best Pract Res Clin Rheumatol* 20.5, pp. 1003–25. DOI: 10.1016/j.berh.2006.06.003.
- Grad, Sibylle et al. (Oct. 2011). "Physical stimulation of chondrogenic cells in vitro: a review". In: *Clin Orthop Relat Res* 469.10, pp. 2764–72. DOI: 10.1007/s11999-011-1819-9.
- Grayson, Warren L et al. (May 2006). "Effects of hypoxia on human mesenchymal stem cell expansion and plasticity in 3D constructs". In: *J Cell Physiol* 207.2, pp. 331–9. DOI: 10.1002/jcp.20571.
- Hansen, U et al. (July 2001). "Combination of reduced oxygen tension and intermittent hydrostatic pressure: a useful tool in articular cartilage tissue engineering". In: *J Biomech* 34.7, pp. 941–9.
- Huang, Alice H, Megan J Farrell, and Robert L Mauck (Jan. 2010). "Mechanics and mechanobiology of mesenchymal stem cell-based engineered cartilage". In: *J Biomech* 43.1, pp. 128–36. DOI: 10.1016/j.jbiomech.2009.09.018.
- Hunziker, E B (June 2002). "Articular cartilage repair: basic science and clinical progress. A review of the current status and prospects". In: *Osteoarthritis Cartilage* 10.6, pp. 432–63. DOI: 10.1053/joca.2002.0801.
- Ivanovic, Zoran (May 2009). "Hypoxia or in situ normoxia: The stem cell paradigm". In: *J Cell Physiol* 219.2, pp. 271–5. DOI: 10.1002/jcp.21690.
- Jackson, DW et al. (Jan. 2001). "pontaneous repair of full-thickness defects of articular cartilage in a goat model - A preliminary study." In: *Journal bone joint surgery - American Volume* 83A, pp. 53–64.
- Jones, D et al. (Apr. 2007). *Adult mesenchymal stem cells: Differentiation potential and therapeutic applications*. 10.4103/0022-3859.32215. URL: <http://www.jpgmonline.com/article.asp?issn=0022-3859;year=2007;volume=53;issue=2;epage=121;epage=127;aulast=Jackson>.
- Kock, Linda, Corrinus C. van Donkelaar, and Keita Ito (2012). "Tissue engineering of functional articular cartilage: the current status". In: *Cell Tissue Res* 347, pp. 613–627.
- Kode, Jyoti A. et al. (2009). "Mesenchymal stem cells: immunobiology and role in immunomodulation and tissue regeneration". In: *Cytotherapy* 11.4, pp. 377–391.
- Krinner, A et al. (Aug. 2009). "Impact of oxygen environment on mesenchymal stem cell expansion and chondrogenic differentiation". In: *Cell Prolif* 42.4, pp. 471–84. DOI: 10.1111/j.1365-2184.2009.00621.x.
- Leavitt M Gerberding J, Sondik E (2005). "Health, United States". In: *National Center for Health Statistics* MD, pp 550.

- Lindroos, Bettina, Riitta Suuronen, and Susanna Miettinen (June 2011). "The potential of adipose stem cells in regenerative medicine". In: *Stem Cell Rev* 7.2, pp. 269–91. DOI: 10.1007/s12015-010-9193-7.
- Liu, Liyue, Wenji Yuan, and Jinfu Wang (Dec. 2010). "Mechanisms for osteogenic differentiation of human mesenchymal stem cells induced by fluid shear stress". In: *Biomech Model Mechanobiol* 9.6, pp. 659–70. DOI: 10.1007/s10237-010-0206-x.
- Liu, Zhao-Jun, Ying Zhuge, and Omaid C Velazquez (Apr. 2009). "Trafficking and differentiation of mesenchymal stem cells". In: *J Cell Biochem* 106.6, pp. 984–91. DOI: 10.1002/jcb.22091.
- Mahmoudifar, Nastaran and Pauline M Doran (Mar. 2012). "Chondrogenesis and cartilage tissue engineering: the longer road to technology development". In: *Trends Biotechnol* 30.3, pp. 166–76. DOI: 10.1016/j.tibtech.2011.09.002.
- Malladi, Preeti et al. (Apr. 2006). "Effect of reduced oxygen tension on chondrogenesis and osteogenesis in adipose-derived mesenchymal cells". In: *Am J Physiol Cell Physiol* 290.4, pp. C1139–46. DOI: 10.1152/ajpcell.00415.2005.
- Manual. *SDR Getting started v6*. PreSens Precision Sensing GmbH. URL: www.presens.at (visited on 03/09/2013).
- Martin, I., D. Wendt, and M. Heberer (2004). "The role of bioreactors in tissue engineering". In: *Trends in Biotechnology* 22.2, pp. 80–86.
- Mauk, Robert L. and Jason A. Burdick (2011). "Engineering Cartilage Tissue". In: *Tissue Engineering*, pp. 493–520.
- Mawatari, Taro et al. (July 2010). "Effects of tensile strain and fluid flow on osteoarthritic human chondrocyte metabolism in vitro". In: *J Orthop Res* 28.7, pp. 907–13. DOI: 10.1002/jor.21085.
- Maxson, Scott, David Orr, and Karen J.L. Burg (2011). "Bioreactors for Tissue Engineering". In: *Tissue Engineering*, pp. 179–197.
- Melero-Martin, J. M. and M. Al-Rubeai (2007). "In Vitro Expansion of Chondrocytes". In: *Topics in Tissue Engineering* 3.
- Meyer, Eric G et al. (Sept. 2010). "Low oxygen tension is a more potent promoter of chondrogenic differentiation than dynamic compression". In: *J Biomech* 43.13, pp. 2516–23. DOI: 10.1016/j.jbiomech.2010.05.020.
- Mohyeldin, Ahmed, Tomás Garzón-Muvdi, and Alfredo Quiñones-Hinojosa (Aug. 2010). "Oxygen in stem cell biology: a critical component of the stem cell niche". In: *Cell Stem Cell* 7.2, pp. 150–61. DOI: 10.1016/j.stem.2010.07.007.
- O’Conor, Christopher J, Natasha Case, and Farshid Guilak (2013). "Mechanical regulation of chondrogenesis". In: *Stem Cell Research and Therapy* 4.61.
- Pearle, Andrew D, Russell F Warren, and Scott A Rodeo (Jan. 2005). "Basic science of articular cartilage and osteoarthritis". In: *Clin Sports Med* 24.1, pp. 1–12. DOI: 10.1016/j.csm.2004.08.007.
- Pelttari, Karoliina, Eric Steck, and Wiltrud Richter (Apr. 2008). "The use of mesenchymal stem cells for chondrogenesis". In: *Injury* 39 Suppl 1, S58–65. DOI: 10.1016/j.injury.2008.01.038.
- Porter, Blaise et al. (Mar. 2005). "3-D computational modeling of media flow through scaffolds in a perfusion bioreactor". In: *J Biomech* 38.3, pp. 543–9. DOI: 10.1016/j.jbiomech.2004.04.011.

- Rodriguez, A-M et al. (Jan. 2005). "The human adipose tissue is a source of multipotent stem cells". In: *Biochimie* 87.1, pp. 125–8. DOI: 10.1016/j.biochi.2004.11.007.
- Schmidt, C E and J M Baier (Nov. 2000). "Acellular vascular tissues: natural biomaterials for tissue repair and tissue engineering". In: *Biomaterials* 21.22, pp. 2215–31.
- Schulz, Ronny Maik and Augustinus Bader (Apr. 2007). "Cartilage tissue engineering and bioreactor systems for the cultivation and stimulation of chondrocytes". In: *Eur Biophys J* 36.4-5, pp. 539–68. DOI: 10.1007/s00249-007-0139-1.
- Stillaert, F B et al. (Oct. 2008). "Human clinical experience with adipose precursor cells seeded on hyaluronic acid-based spongy scaffolds". In: *Biomaterials* 29.29, pp. 3953–9. DOI: 10.1016/j.biomaterials.2008.06.005.
- Swieszkowski, Wojciech et al. (2007). "Repair and regeneration of osteochondral defects in the articular joints". In: *Biomol Eng* 24.5, pp. 489–95. DOI: 10.1016/j.bioeng.2007.07.014.
- Symonds, Michael E., ed. (2012). *Adipose Tissue Biology*. Springer New York Dordrecht Heidelberg London.
- Temenoff, Johnna S. and Antonios G. Mikos (2000). "Review: tissue engineering for regeneration of articular cartilage". In: *Biomaterials* 21, pp. 431–440.
- Tremp, M et al. (2011). "Adipose-derived stem cells for tissue engineering applications". In: *Regenerative Medicine and Tissue Engineering. Cells and Biomaterials*, pp. 179–194.
- Valorani, M G et al. (June 2012). "Pre-culturing human adipose tissue mesenchymal stem cells under hypoxia increases their adipogenic and osteogenic differentiation potentials". In: *Cell Prolif* 45.3, pp. 225–38. DOI: 10.1111/j.1365-2184.2012.00817.x.
- Wang, Yongzhong et al. (Dec. 2005). "In vitro cartilage tissue engineering with 3D porous aqueous-derived silk scaffolds and mesenchymal stem cells". In: *Biomaterials* 26.34, pp. 7082–94. DOI: 10.1016/j.biomaterials.2005.05.022.
- Wescoe, Kristin E et al. (2008). "The role of the biochemical and biophysical environment in chondrogenic stem cell differentiation assays and cartilage tissue engineering". In: *Cell Biochem Biophys* 52.2, pp. 85–102. DOI: 10.1007/s12013-008-9029-0.
- Wu, F. et al. (Feb. 1999). "Bioreactor Development for Tissue-Engineered Cartilage". In: *Annals of the New York Academy of Sciences* 875, pp. 405–411.
- Wu, Ling et al. (May 2013). "Regeneration of articular cartilage by adipose tissue derived mesenchymal stem cells: perspectives from stem cell biology and molecular medicine". In: *J Cell Physiol* 228.5, pp. 938–44. DOI: 10.1002/jcp.24255.
- Yamamoto, Yoritsuna et al. (June 2013). "Low oxygen tension enhances proliferation and maintains stemness of adipose tissue-derived stromal cells". In: *Biores Open Access* 2.3, pp. 199–205. DOI: 10.1089/biores.2013.0004.
- Yeatts, Andrew B, Daniel T Choquette, and John P Fisher (Feb. 2013). "Bioreactors to influence stem cell fate: augmentation of mesenchymal stem cell signaling pathways via dynamic culture systems". In: *Biochim Biophys Acta* 1830.2, pp. 2470–80. DOI: 10.1016/j.bbagen.2012.06.007.

- Yeatts, Andrew B and John P Fisher (Feb. 2011). "Bone tissue engineering bioreactors: dynamic culture and the influence of shear stress". In: *Bone* 48.2, pp. 171–81. DOI: 10.1016/j.bone.2010.09.138.
- Yeatts, Andrew B et al. (Sept. 2012). "Human mesenchymal stem cell position within scaffolds influences cell fate during dynamic culture". In: *Biotechnol Bioeng* 109.9, pp. 2381–91. DOI: 10.1002/bit.24497.
- Zhang, L., J. Hu, and K. A. Athanasiou (2009). "The Role of Tissue Engineering in Articular Cartilage Repair and Regeneration". In: *Crit Rev Biomed Eng.* 37, pp. 1–57.
- Zuk, Patricia A. et al. (Oct. 2002). "Human Adipose Tissue Is a Source of Multipotent Stem Cells". In: *Molecular Biology of the Cell* 13, pp. 4279–4295.

A Material

A.1 Cells

Name	Type
adMSCs(64m)	MSCs isolated from adipose tissue of a 64 year old male
adMSCs(82f)	MSCs isolated from adipose tissue of a 82 year old female
ucMSCs	MSCs isolated from umbilical cord tissue

A.2 Disposables

Material	Manufacturer
Biocoat™ cell environments	
human fibronectin cellware 12-well plate	BD Bioscience GmbH, Heidelberg, Germany
Cell culture flasks (T-25, T-75, T-175)	Sarstedt AG & Co, Nümbrecht, Germany
Cell culture plates (12-, 24-, 96-wells)	Sarstedt AG & Co, Nümbrecht, Germany
Conical falcon™ tubes (15 ml, 50 ml)	Sarstedt AG & Co, Nümbrecht, Germany
Cryo Pure Tubes	Sarstedt AG & Co, Nümbrecht, Germany
Falcon™ cell strainer, 40 μm nylon	BD Bioscience GmbH, Heidelberg, Germany
Latex gloves	VWR International GmbH, Darmstadt, Germany
Nitril gloves	VWR International GmbH, Darmstadt, Germany
Matristypt®	Dr. Suwelack Skin and Healthcare GmbH
OxoDish® 24-well plate	PreSens GmbH, Regensburg, Germany
Peristaltic pump tubing, PharMed® BPT	VWR International GmbH, Darmstadt, Germany
Pipette tips (20, 200, 1000 μl)	Greiner Bio-One GmbH, Frickenhausen, Germany
Serologic pipetts (2, 5, 10, 25, 50 ml)	Sarstedt AG & Co, Nümbrecht, Germany
Sterile disposable dome 844-28	Memscap SA, Crolles Cedex, France
Sterile filter, Filtropur 0,2 μm	Sarstedt AG & Co, Nümbrecht, Germany
Syringe filter, Minisart NY25, 0.25 μl	Sartorius AG, Göttingen, Germany
Syringes, 5 ml	B. Braun Austria GmbH, Maria Enzersdorf, Austria
Tube connectors	Carl Roth GmbH & Co KG, Karlsruhe, Germany
Tubes	VWR International GmbH, Darmstadt, Germany

A.3 Laboratory equipment and devices

Device	Model	Manufacturer
Analytical balance		Sartorius AG, Göttingen, Germany
Centrifuge for conical tubes	Centrifuge 5702	Eppendorf AG, Hamburg, Germany
Fluorescence microscope		Leica Microsystems GmbH, Wetzlar, Germany
Freezing container	Mr. Frosty	Thermo Scientific GmbH, Langenselbold, Germany
Glass bottles		Duran Group, Wertheim, Germany
Glucose/Lactate analysis	BioProfile 100 Plus	Nova Biomedical GmbH, Rödermark, Germany
Haematocytometer	Neubauer improved	Carl Roth GmbH & Co KG, Karlsruhe, Germany
Incubator	Heracell 240i	Thermo Scientific GmbH, Langenselbold, Germany
Incubator table	IT-3a	Fraunhofer Gessellschaft, München, Germany
Laminar flow cabinet	HeraSafe KS 18	Thermo Scientific GmbH, Langenselbold, Germany
Magnetic stirrer		
Magnetic stir bar		
Microplate Photometer	Multiskan [®] FC	Thermo Scientific GmbH, Langenselbold, Germany
Microscope		Leica Microsystems GmbH, Wetzlar, Germany
Microscope Camera	ICC50 HD	Leica Microsystems GmbH, Wetzlar, Germany
Perfusion bioreactor	Mini Reactor	Leibnitz Universität Hannover, Hannover Germany
Peristaltic pump	IPC-4	Ismatec, Wertheim-Mondfeld, Germany
Pipetting aid	Easypet	Eppendorf AG, Hamburg, Germany
SDR SensorDish Reader		PreSens GmbH, Regensburg, Germany
Ultra pure water system		
Vortex mixer		VWR International GmbH, Darmstadt, Germany
Water bath		GFL GmbH, Burgwedel, Germany

A.4 Chemicals

Chemical/Reagent	Manufacturer
Accutase®	PAA Laboratories GmbH, Pasching, Austria
Acetic acid	PAA Laboratories GmbH, Pasching, Austria
Alizarin Red S	Carl Roth GmbH & Co KG, Karlsruhe, Germany
Alcian blue	Sigma Aldrich Chemie GmbH, Munich, Germany
Calcein	Sigma Aldrich Chemie GmbH, Munich, Germany
Calcium chloride	Sigma Aldrich Chemie GmbH, Munich, Germany
Collagenase type I, crude from <i>Clostridium histolyticum</i>	Sigma Aldrich Chemie GmbH, Munich, Germany
DAPI	Sigma Aldrich Chemie GmbH, Munich, Germany
Ethanol 96%	Merck KGaA, Darmstadt, Germany
Gentamicin (10 mg/ml)	PAA Laboratories GmbH, Pasching, Austria
Hanks buffer I	Sigma Aldrich Chemie GmbH, Munich, Germany
Human Serum	Blutbank Linz, Austria
Hypochloric acid 36.5%	Sigma Aldrich Chemie GmbH, Munich, Germany
Isopropanole	Merck KGaA, Darmstadt, Germany
Magnesium chloride	Sigma Aldrich Chemie GmbH, Munich, Germany
MTT	Sigma Aldrich Chemie GmbH, Munich, Germany
NH AdipoDiff Medium	Miltenyi Biotec GmbH, Bergisch Gladbach, Germany
NH ChondroDiff Medium	Miltenyi Biotec GmbH, Bergisch Gladbach, Germany
NH OsteoDiff Medium	Miltenyi Biotec GmbH, Bergisch Gladbach, Germany
Nonidet-P 40	Sigma Aldrich Chemie GmbH, Munich, Germany
Oil Red O Solution	Sigma Aldrich Chemie GmbH, Munich, Germany
<i>para</i> -Formaldehyde	Sigma Aldrich Chemie GmbH, Munich, Germany
Phosphate buffered saline	Sigma Aldrich Chemie GmbH, Munich, Germany
SDS	Sigma Aldrich Chemie GmbH, Munich, Germany
Sodium chloride	Sigma Aldrich Chemie GmbH, Munich, Germany
Sodium carbonate	Sigma Aldrich Chemie GmbH, Munich, Germany
Sodium hydrogen carbonate	Sigma Aldrich Chemie GmbH, Munich, Germany
Silver nitrate solution	Carl Roth GmbH & Co KG, Karlsruhe, Germany
Tris-base	Sigma Aldrich Chemie GmbH, Munich, Germany
Trypan blue solution (0.4%)	Sigma Aldrich Chemie GmbH, Munich, Germany
α -Minimum Essential Medium (MEM)	GIBCO Invitrogen GmbH, Darmstadt, Germany

A.5 Culture media and solutions

Culture media/Solution	Formation
Adipogenic differentiation medium	NH AdipoDiff Medium + 0.5% gentamycin
Alcian blue staining solution	1% alcian blue (w/v) in 3% acetic acid
Chondrogenic differentiation medium	NH ChondroDiff Medium + 0.5% gentamycin
Cryomedium	70% human serum + 20% α MEM + 10% DMSO
DAPI stock solution	0.5 mg/ml DAPI in ddH ₂ O
DAPI buffer	100 mM Tris pH 7, 150 mM NaCl, 1 mM CaCl ₂ , 0.5 MgCl ₂ , 0.1% Nonidet
DAPI working solution	0.1% DAPI stock solution in DAPI buffer
Fixer solution	4% <i>para</i> -formaldehyde w/v in PBS
Hanks buffer II	Hanks buffer I + 10% human serum
MTT solution	5 mg/ml MTT in PBS
Osteogenic differentiation medium	NH OsteoDiff Medium + 0.5% gentamycin
SDS solution	10% in 0.01 M HCl
Standard culture medium	α MEM + 10% human serum + 0.5% gentamycin
Von Kossa AgNO ₃ solution	5% AgNO ₃ in ddH ₂ O
Von Kossa formaldehyde solution	5% Na ₂ CO ₃ + 0.2% formaldehyde in ddH ₂ O
α MEM	10.8 g/l α MEM powder + 2.2 g/l NaHCO ₃ in steam sterilized ddH ₂ O

B Methods

B.1 Culture conditions

Both standard normoxic conditions (21% O₂) and hypoxic conditions (5% O₂) in the presence of 5% CO₂ at 37°C in a humidified atmosphere were used for culturing cells to emulate the typical bradytrophe environment of cartilage tissue. O₂ tension was reduced in a standard humidified incubator using supplemental N₂.

B.2 Non invasive in situ monitoring of dissolved oxygen in culture media during cultivation

Dissolved oxygen in the cell culture supernatant was recorded online during the complete study time. Cells were seeded in 24 well plates with an integrated O₂ sensor spot in the base of each well (OxoDish[®], Presens GmbH). Dissolved oxygen was monitored every 2 to 5 min by using a SDR SensorDish[®] Reader (Presens GmbH). The SDR - Sensor Dish Reader is a 24 channel reader with optical sensors integrated and precalibrated by Presens GmbH. The sensor spot contains a luminescent dye. The measurements are based on the luminescence lifetime of the sensor dye. It is excited by the SensorDish[®] Reader and its luminescence lifetime is detected through the transparent well bottom.

B.2.1 Experimental setup

Cells were seeded in 24 well OxoDish[®] plates and incubated under normoxic and hypoxic culture conditions. Each OxoDish[®] was placed on a SDR SensorDish[®] Reader, these were then joined in series by RJ-45 cable and placed in an incubator with either normoxic or hypoxic environment. A splitter was connected to the first SDR SensorDish[®] Reader via an RJ-45 cable, to the PC via an RS-232 interface cable (male), and via the power adapter 24 V to a power supply. An end-cap for closing the second connector of the last SensorDish[®] Reader in the row was plugged in.

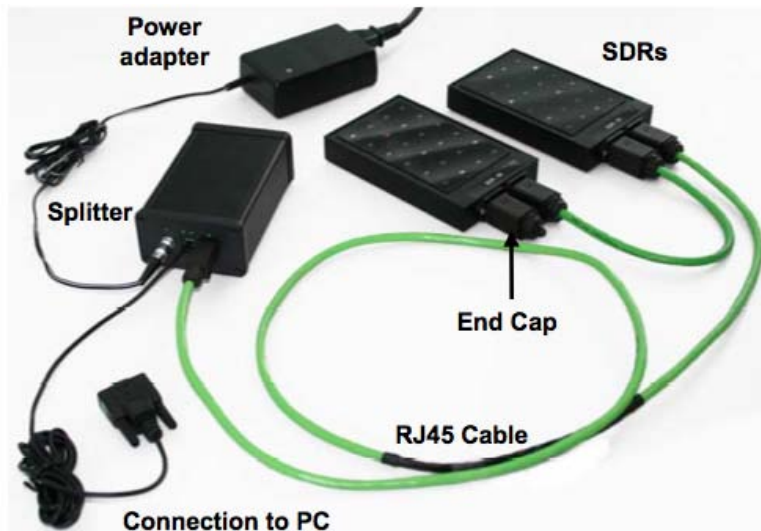


Figure B.1: Setup of the oxygen monitoring system (*SDR Getting started v6*)

B.2.2 Non invasive in situ monitoring of oxygen partial pressure distribution

Cryoconserved ucMSCs in passage 5 were removed from the liquid nitrogen container. The sample vial was swirled in a 37°C water bath for approximately 2 min. Following thawing, the sample was topped up with 1 ml cold α MEM and incubated for 2 min. Afterwards the sample was transferred into a 50 ml tube. 2 ml α MEM were added and the sample was incubated for 2 min. Subsequently, the sample was topped up to 10 ml with α MEM and was centrifuged for 5 min at 300 g. The pellet was resuspended in standard culture medium and the cells were plated in a cell culture flask. After incubation over night, standard culture medium was replaced and cells were cultivated until the cultures became 80% confluent. The cell layer was washed once with PBS and thereafter cells were harvested by trypsinization with Accutase®. The detachment treatment was stopped after 5 min incubation at 37°C by adding standard culture medium. After sedimentation by centrifugation for 5 min with 300 g the supernatant was discarded. In the next step the pellet was resolved in 1 ml standard culture medium, an aliquot of 20 μ l was mixed with 20 μ l trypan blue. Cells were introduced to a haematocytometer and counted. Then cells were re-plated at a density of 4,000 cm^2 in culture flasks. After the first subconfluent passage, cells were harvested for the experiment. On study day 0, ucMSCs (passage 7) were plated with 4 different cell concentrations shown in table B.1 in 6 replicates ($n=6$). Cultivation was conducted in 1 ml standard medium. Dissolved oxygen was monitored every 2 min during the complete study time. The study was conducted for 7 days with medium changes on day 2 and 5. After each medium replacement, half life of oxygen decrease and the equilibrium value was calculated. All data are represented as mean \pm standard deviation of the mean for sixfold measurements.

Table B.1: Cell concentrations

Cell concentration in suspension (cells/ml)	Cells per well area (cells/cm ²)
1×10^5	5.3×10^5
1×10^4	5.3×10^4
1×10^3	5.3×10^2
1×10^2	5.3×10

B.3 Seeding Strategies for growth on scaffolds

Cryoconserved ucMSCs in passage 5 were thawed and prepared for the experiment as explained in B.2.2. Scaffolds (described in B.8.4) were seeded with ucMSCs in 6 different cell concentrations as shown in table B.2. On study day 0, sterilized scaffolds were prewetted with 100 μ l PBS for 5 min. Then 100 μ l freshly harvested cell suspension were added centrally. To enhance cell infiltration, cells were incubated for 1.5 h at 37°C. Afterwards 1 ml medium was added and finally the seeded scaffolds incubated at 37°C over night. Acellular blank scaffolds were also prepared and incubated in identical conditions. The study was conducted for 7 days with time points on day 1, 4, and 7. All scaffolds were cultured in 24 well plates. Medium was replaced on day 4. Proliferation of each cell concentration was analyzed via MTT assay on all time points in 3 replicates. For imaging of cell distribution one sample of each concentration was taken on all time points respectively. To evaluate the general metabolic activity and cell growth, glucose and lactate were measured at all time points in the supernatant of the cultures. These factors can be used as an indicator for cell survival and proliferation. Standard culture medium was used as blank value. The concentrations in the supernatant were measured using Bioprofile 100 Plus analyzer. Consumed glucose was calculated by taking the blank values into account. All data are represented as mean \pm standard deviation of the mean for triplicate measurements.

Table B.2: Cell concentrations

Initial cell concentration in suspension (cells/ml)	Cells per scaffold (cells/scf)	Cells per scaffold volume (cells/cm ³)
5×10^6	5×10^5	6.37×10^6
1×10^6	1×10^5	1.27×10^6
5×10^5	5×10^4	6.37×10^5
1×10^5	1×10^4	1.27×10^5
5×10^4	5×10^3	6.37×10^4
1×10^4	1×10^3	1.27×10^4

B.3.1 MTT assay

Cell proliferation and metabolic activity of seeded ucMSCs was determined by MTT viability assay. The yellow MTT is metabolized to violet formazan by dehydrogenases in the mitochondria of living cells. The concentration of the formazan (measured by its absorption of yellow

light) is used as an indicator of the viability and proliferation respectively. Scaffolds were harvested at indicated time points and transferred in a new 24 well plate. Each scaffold was washed with 1 ml PBS and 660 μ l of MTT solution (60 μ l MTT in 600 μ l α MEM) was added. Incubation for 4 h at 37°C allowed the formation of MTT formazan crystals. Resulting crystals were solubilized with 600 μ l SDS solution (in 10% 0.01 M HCl). Then the plates were scanned in 800 dpi using a common scanner. Afterwards the plate gets further incubated for at least 24 hours at 37°C. Finally, six aliquots of 100 μ l of supernatant (n=6) was obtained and the formazan concentration measured. Absorbance was measured at the extinction at 570 nm with a reference at a wavelength of 630 nm by using a microplate photometer. Optical density was normalized to that of the control group (acellular blank scaffolds prepared and incubated in identical conditions). The mean value \pm standard deviation of sixfold measured absorbance values was plotted.

B.3.2 DAPI nucleic acid staining

The nuclei of fixed cells were stained with the fluorescence dye DAPI. The dye binds on the DNA of the nuclei. For DAPI staining seeded scaffolds were transferred in a new 24 well plate at indicated time points and washed once with 1 ml PBS. To fix the cells 1 ml ice cold (-20°C) 96% ethanol was added and incubated for 1 h at 4°C. Thereafter scaffolds were washed again with 1 ml PBS. For staining of the seeded scaffolds were incubated for 15 min in the dark in DAPI-solution (1 μ l DAPI-stock solution in 1 ml DAPI buffer) at 37°C. To eliminate the background the matrices were washed twice with 1 ml PBS. The nuclei were detected and photographed by a fluorescence microscope at 460 nm emission.

B.4 Isolation of adMSCs from abdominoplastic surgery material

The method relies on a collagenase digestion followed by several centrifugal separations using Hanks buffer to isolate the stromal vascular cells from primary adipocytes. All subcutaneous adipose tissue specimens were obtained from abdominoplastic surgeries with informed patient consent. adMSCs were isolated from two donors: a male donor 64 years old (adMSCs(64m)) and a female donor 82 years old (adMSCs(82f)). The tissue was minced into approximately 0.5 cm³ large pieces. Blood vessels and connective tissue was removed from the pieces. 20 g of the tissue material was transferred into 50 ml tubes and digested with 10 ml collagenase type I for 1 h at 37°C. The suspension was homogenized using a vortex shaker and two 15 ml aliquots were sampled from each tube. Then these aliquots were topped up with Hanks buffer I and centrifuged for 5 min at 200 g. The fatty supernatant layers and the pellet was transferred into a new 50 ml tube and topped up with Hanks buffer II. The liquid middle layer was discarded. The adipocytes were separated from the precipitating stromal fraction by two centrifugation steps for 10 min with 400 g. The final pellet was resuspended in 30 ml standard culture medium. 15 ml of the cell suspension was seeded in T-75 cell culture flasks and incubated at 37°C in either normoxic or hypoxic culture conditions. After 24 h non-adherent cells and remaining fat tissue were discarded and the medium was changed. The primary cells (passage 0) were cultivated with medium changes every second day until 80% confluency had been reached, after which the cells were harvested using 2 ml Accutase[®]. After counting, the cells were used for further experiments and the remaining cell suspension centrifuged for 5 min with 300 g. The pellet was resuspended in cryoconservation medium. The cryoconservation

medium consists of 70% human serum, 20% of α MEM and 10% DMSO. adMSCs(64m) and adMSCs(82f) were stored in a final concentration of 1 million viable cells per milliliter of cryoconservation medium. Aliquoted vials were first frozen in an alcohol-cryo-freezing container and stored at -80°C overnight. On the next day the frozen vials were transferred to a liquid nitrogen container for long-term storage.

B.5 Proliferation of adMSCs

Freshly isolated adMSCs(64m) were cultivated in standard culture medium at either normoxic or hypoxic conditions, as described previously in B.4. The growth kinetics of adMSCs(64m) were expanded in quadruple ($n=4$) and monitored over 14 passages. Until passage 4 cells were cultivated in T-75 cell culture flasks to generate a cell stock for further experiments. After passage 4 cells were subcultured in T-25 cell culture flasks. Cells in passage 0 were detached and plated in four cell culture flasks at density of 4,000 cells per cm^2 . The selected time point to evaluate cell expansion was at 80% confluency. Cell viability and cellular morphology were examined in situ using a standard light microscope. Then the cells were washed with PBS and harvested by Accutase[®] treatment. Of each sampled cell suspension, an aliquot of 50 μl was counted using a haemocytometer to obtain growth curves. Cell viability was determined via trypan blue staining. Then all 4 flasks were merged and cells were plated in four new cell culture flasks at the same density. Until passage 4, remaining cell suspension were centrifuged. Then pellets were resuspended in cryoconservation medium and aliquoted for long term storage (1 million viable cells per milliliter of cryoconservation medium).

B.6 Differentiation

For differentiation study adMSCs(64m) and adMSCs(82f) both in passage 2, were plated in 12 well plates coated with human fibronectin at a density of 4,000 cells per cm^2 . The experiment was performed in 3 replicates ($n=3$) for 20 days. Cultivation was conducted in 1 ml standard culture medium at 37°C with 5% CO_2 under normoxy and hypoxy conditions. After cells were grown to confluency, medium of the study group was changed to adipogenic, chondrogenic or osteogenic differentiation medium, depending on the differentiation lineage. As control groups both adMSCs(64m) and adMSCs(82f) were cultured during the whole study time in standard culture medium with no change to differentiation medium. In all groups medium was replaced every 2 to 3 days. To evaluate the general metabolic activity and cell growth, glucose concentration and lactate production were measured in the supernatant. The concentrations were measured using Bioprofile 100 Plus analyzer (Nova Biomedical GmbH). Consumed glucose was calculated by taking the blank values into account. On study day 20, cells were fixed for evaluation and tested with histomorphological stainings to confirm successful cell differentiation. All differentiation assays were examined under a standard inverted light microscope and photographed.

B.6.1 Fixation

After 20 days cell cultures of each culture condition were washed twice with warm PBS at 37°C and incubated for 5 min. Then for histomorphological staining cells were fixed by incubation

for 30 min in 4% PFA. Afterwards the cells were washed and incubated at 4°C over night with PBS.

B.6.2 Oil Red-O

The main histological characteristics of successfully differentiated adipocytes are intracellular triglyceride droplets. Oil Red-O is a red diazo dye which intercalates with neutral triglycerides. To stain these lipid vacuoles, cells were gently washed once with PBS. After incubation for 20 min with Oil Red-O cells were rinsed in 50% ethanol and washed with PBS again.

B.6.3 Alcian blue

Accumulation of chondrocyte matrix and the cartilage-specific proteoglycan synthesis, sulfated GAG were visualized by alcian blue staining. Cells were washed once with 3% acetic acid, stained with 1% alcian blue in 3% acetic acid for 30 min, rinsed three times with 3% acetic acid again and washed twice with ddH₂O.

B.6.4 Von Kossa

Calcium deposits were observed and identified by Von Kossa staining. Von Kossa staining is based on a reaction with silver nitrate and used for the detection of calcium accumulations within the extracellular matrix. A precipitation reaction between silver ions and phosphate occurs. The Ca²⁺ of calcified matrices are substituted with silver ions. Cells were washed three times with ddH₂O. Then stained with AgNO₃ solution for 30 min in the dark. After incubation the cells were washed three times with ddH₂O. To degrade silver phosphate to silver 1 ml developer solution (solution of 5% sodium carbonate and 0.2% formaldehyde) was added and incubated. After 3 min reaction, developer solution was removed and the cells were washed again three times with ddH₂O. Silver atoms appear as black spots under the light microscope.

B.6.5 Alizarin red

As second assay to visualize calcium deposition in osteocytes Alizarin Red staining was used. Alizarin Red forms a chelate complex with calcium ions. After fixation in PFA, cells were rinsed three times with ddH₂O, incubated in 1% Alizarin Red (1% Alizarin Red S w/v) for 15 min and washed five times with ddH₂O to remove excess stain.

B.7 Monitoring of oxygen consumption during differentiation of adMSCs

For this experiment adMSCs(64m) in passage 2 were used. The experimental set up is described in B.2.1. On study day 0, cells were plated with a density of 4,000 cells per cm² in OxoDishes[®]. The study was conducted as described in B.6. Dissolved oxygen was measured and recorded every 5 min over the course of cultivation. Differentiation specific oxygen equilibrium was calculated in % O₂.

B.8 Perfusion system

B.8.1 Perfusion bioreactor design

The bioreactor system consists of a cylindrical chamber and a medium reservoir connected via a tubing circuit (fig. B.4, fig. B.3). In the cylindrical chamber (figure B.2 A, figure B.5) lies the scaffold with seeded side on top. A stainless steel mesh is used to restrict scaffold movement and its aspiration into the tubing (figures B.2 B and C). The medium reservoirs consist of a 100 ml Schott flask with 3 ports in the lid: a feed and sampling port, a sterilfilter port to permit gas exchange and a medium return port to provide recirculating flow. The entire system is stored in the cell culture incubator table IT-3a (Fraunhofer IGB). The IT-3a cell culture incubator table provides a stable gas environment for normoxic (21% O₂) and hypoxic (5% O₂) culture conditions, both at 37 °C and 5% CO₂ atmosphere. The limitation of IT-3a is the lack of technical equipment to assure high humidity. IT-3a has 4 individual drawer systems, 2 for each condition. Furthermore each drawer features its own peristaltic pump and allows the accommodation of up to 4 independent bioreactor systems simultaneously. Medium flow was driven by the peristaltic pump. In all experiments medium flow through the scaffolds was vertical, in a bottom to top direction. The circuit consisted of silicon tubing for all areas except the one passing through the peristaltic pump. It was composed of PharMed[®] (color code: yellow/blue) chosen for its higher mechanical endurance. All tubing had an inner diameter of 1.52 mm and a wall thickness of 0.75 mm. Fittings were Luer-Lock[®] taper connections. For online back pressure measurements one medical pressure transducer in each drawer was used. A sterile disposable dome enabled a serial integration into the tubing circuit.

The complete tubing circuit including medium reservoir and cylindrical chamber is assembled outside the hood and steam sterilized. After final assemblage and loading with the seeded scaffold and 10 ml α MED medium inside a laminar flow cabinet, it was placed in the cell culture incubator table. To permit loss of medium through evaporation every system received 1 ml ddH₂O daily. It was added via syringe directly into each reservoir through a septum. Scaffolds were harvested from the bioreactors by moving the complete system into a laminar flow cabinet. One Luer-Lock[®] connection was opened below the cylindrical chamber to release the pressure in the circuit. After gently pulling out the chambers punch, the mesh was cautiously removed with a surgical forceps. Then the scaffold was carefully obtained with a second forceps and transferred into a 24 well plate.

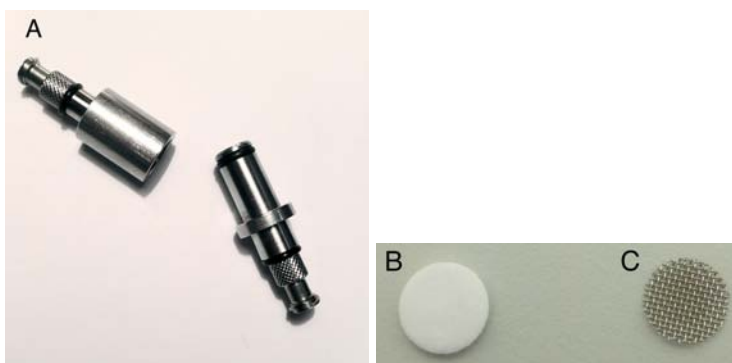


Figure B.2: Mini perfusion bioreactor (A), Matristypt[®] scaffold (B) and stainless steel mesh (C)

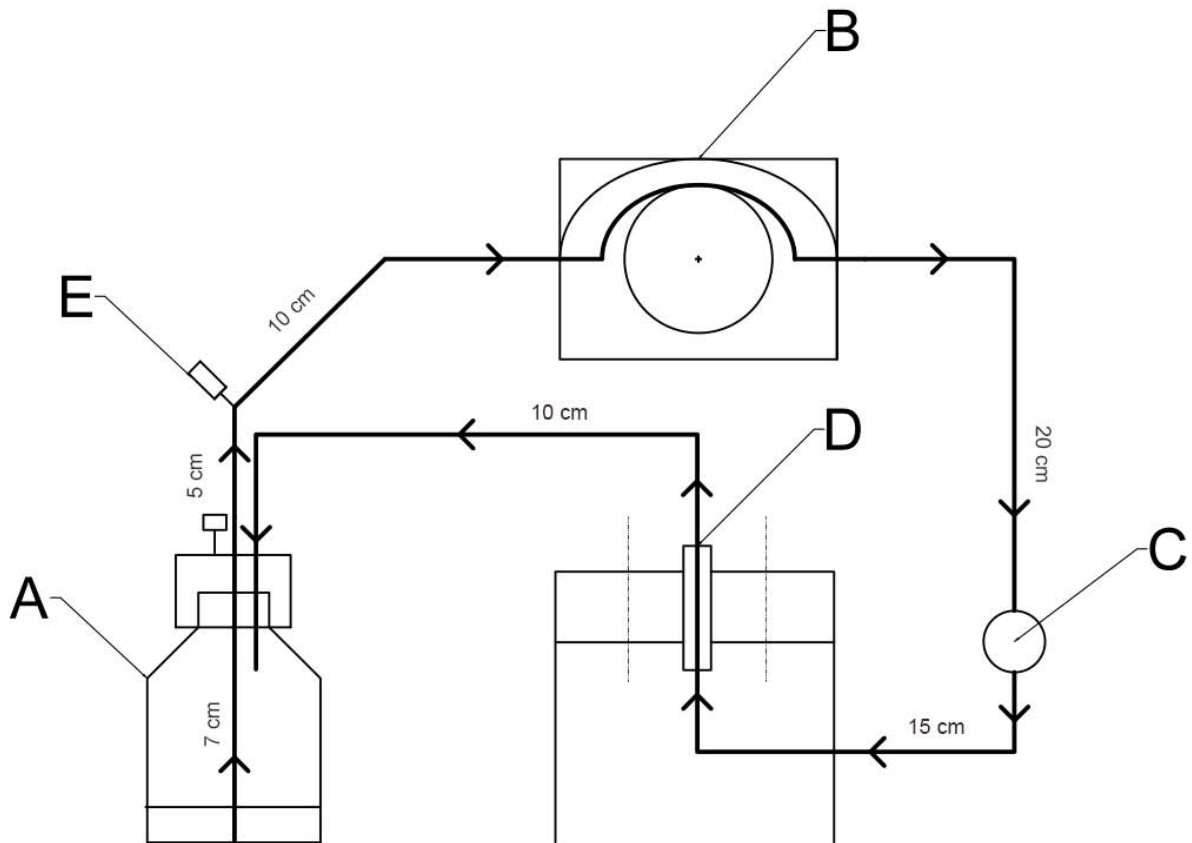


Figure B.3: Scheme of the bioreactor system. The medium is stored in the medium reservoir (A) perfused in the tubing circuit and the perfusion bioreactor (D) by the peristaltic pump (B). A septum allowed medium feeding and sampling (E). In situ online pressure measuring is provided via the pressure transducer (C).

To assure an identical setup of all bioreactors tubing linker had a defined length. Precise tubing length of all linkers is given in figure B.3.

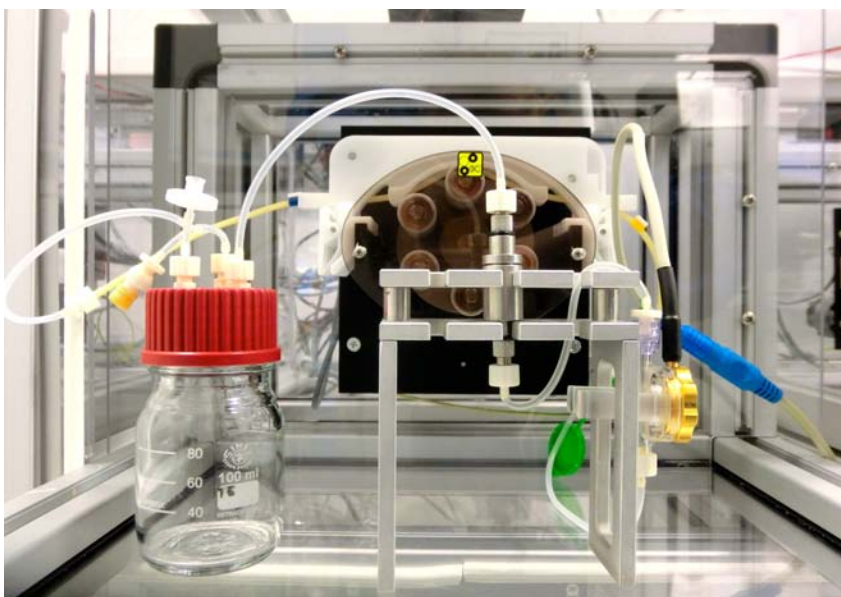


Figure B.4: Image of the bioreactor system stored in the cell culture incubator table

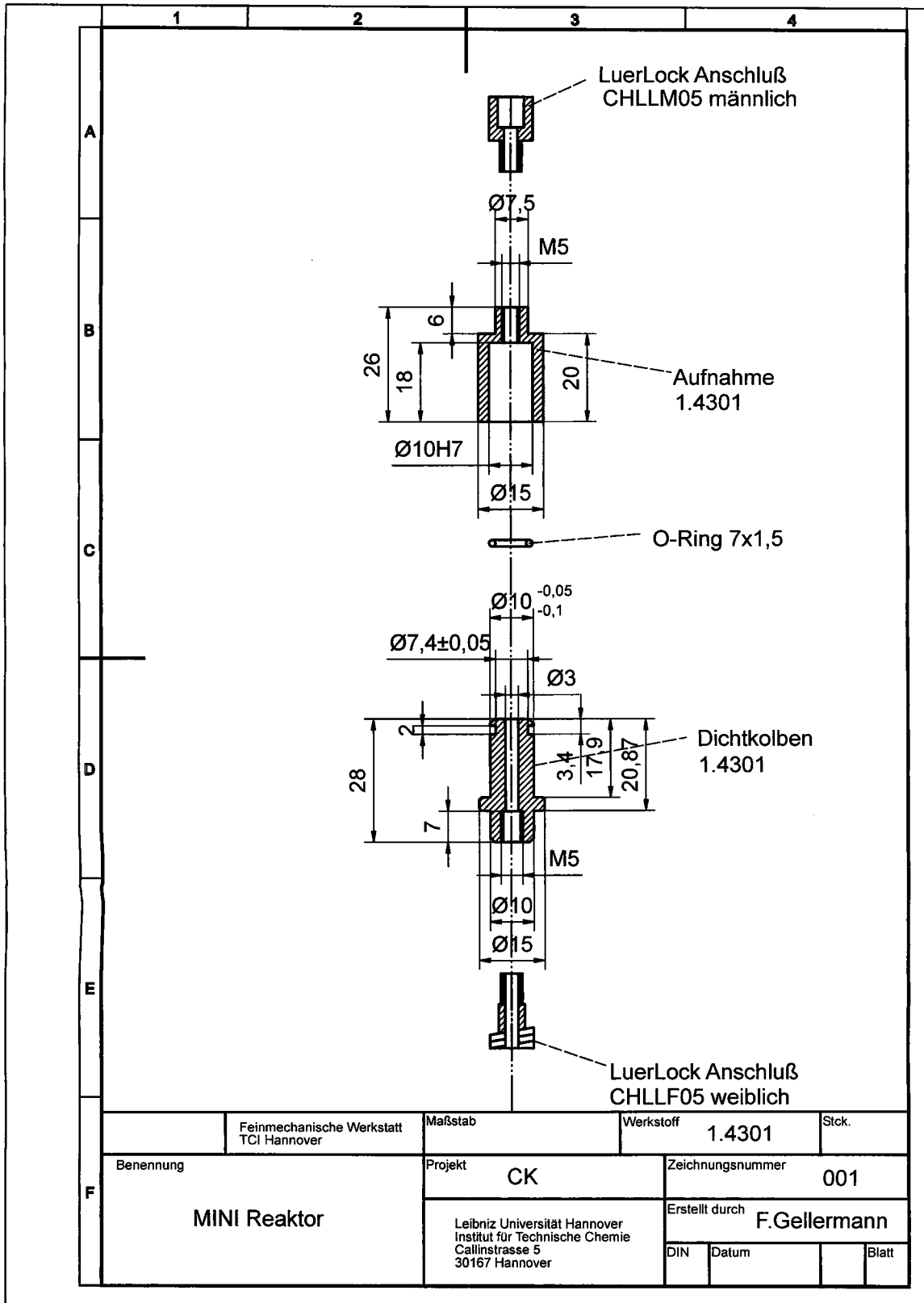


Figure B.5: Technical drawing of the mini perfusion reactor

B.8.2 Experimental Setup

Media evaporation of a bioreactor setup

Four bioreactor systems were assembled as shown in figure B.8.1. To investigate the scale of evaporation 5, 10, 15, and 20 ml PBS were loaded into separate medium reservoirs. On study day 0, one bioreactor system was placed in each drawn of the cell culture incubator table. The experiment was conducted for 10 days with time points every 24 h. To determine the volume of evaporated fluid each bioreactor system was moved entirely onto a scale and its weight determined. The weight loss of the bioreactor system corresponds directly to evaporation of PBS.

B.8.3 Fluid characteristic and shear stress

Fluid characteristic

In order to determine the back pressure behavior in comparison to the fluid flow 2 experiments were completed. First a leak testing study of the bioreactor system was performed. One bioreactor system was completely assembled as described previously in B.8.1. A working solution 25 ml ddH₂O stained with 0.5 ml methylene blue was prepared. For back pressure measuring a non sterile dome was used. The bioreactor system was placed inside the cell culture incubator table and loaded with a Matristypt[®] scaffold (Ø d = 10 mm, h = 2 mm) and 10 ml working solution. At time point 0, the system was exposed to 0.3 ml/min fluid flow. After 10 min the final flow rate of 1.5 ml/min was set. The study was conducted for 25 h with time points every 30 sec.

For the second study another bioreactor system was assembled as described in B.8.1. The experiment was started with a flow rate of 0.3 ml/min. Every 5 min the flow rate was increased by 0.1 ml/min until the final of 1.5 ml/min was reached.

Shear stress and permeability

To get information on permeability of the scaffold and prevailing shear stress following calculations were done.

Following Darcy's law, the intrinsic permeability k [m²] can be obtained as linear relationship between flow rate and drop pressure:

$$k = \frac{\dot{V} \cdot \mu}{A} \cdot \frac{L}{\Delta p} \quad (\text{B.1})$$

k intrinsic permeability [m²]

\dot{V} Flow rate [m³/s]

p Drop pressure [Pa] between 2 points in a specific distance

μ Dynamic viscosity [Pas]

A Cross-sectional area [m²]

L Distance [m]

The prevailing shear stress can be estimated by an assumption based on the Hagen–Poiseuille equation.

$$A \cdot \Delta p = 2 \cdot r \cdot \pi \cdot L \cdot \tau \quad (\text{B.2})$$

$$A = r^2 \cdot \pi \quad (\text{B.3})$$

r Radius [m]

τ Shear stress [N/m²]

The velocity distribution curve of a laminar flow is parabolic and has its vertex at the centerline of the flow channel. In this case shear stress is given by:

$$\tau = \mu \cdot \frac{dv}{dr} \quad (\text{B.4})$$

Following both assumptions leads to:

$$r^2 \cdot \pi \cdot \Delta p = 2 \cdot r \cdot \pi \cdot L \cdot \mu \frac{dv}{dr} \quad (\text{B.5})$$

$$r \cdot \Delta p = 2 \cdot L \cdot \mu \frac{dv}{dr} \quad (\text{B.6})$$

$$\int_0^R r dr = \int_v^0 \frac{2 \cdot L \cdot \mu}{\Delta p} dv \quad (\text{B.7})$$

$$\frac{r^2}{2} = \frac{2 \cdot L \cdot \mu \cdot v}{\Delta p} \quad (\text{B.8})$$

$$\frac{r^2 \cdot \Delta p}{4} = L \cdot \mu \cdot v \quad (\text{B.9})$$

$$\rightarrow v = \frac{r^2 \cdot \Delta p}{4 \cdot L \cdot \mu} \quad (\text{B.10})$$

v Velocity [m/s]

Since the viscous property of fluid follows Newton's law of viscosity, the maximum shear stress τ_{max} is obtained by:

$$V = \frac{r \cdot \Delta p}{2 \cdot L \cdot \mu} \quad (\text{B.11})$$

$$\tau_{max} = \mu \cdot V \quad (\text{B.12})$$

$$\tau_{max} = \mu \cdot \frac{r \cdot \Delta p}{2 \cdot L \cdot \mu} \quad (\text{B.13})$$

$$\Rightarrow \tau_{max} = \frac{r \cdot \Delta p}{2 \cdot L} \quad (\text{B.14})$$

B.8.4 Scaffolds

For all 3D assays the collagen type I material Matristypt® was used. It was kindly provided by Dr. Suwelack Skin and Healthcare GmbH as sheets in the size of 105 x 148 x 2 mm. In order to get disks measuring 10 mm in diameter x 2 mm in thickness and a surface area of 78.5 mm², the collagen matrices were punched out using a hollow punch (Ø d = 10 mm). Before seeding the scaffolds were placed in a 24 well plate. Sterilization was performed inside a laminar flow cabinet via UV-C exposure for 1.5 h on both sides.

Curriculum Vitae

NAME: Anna Marejke Couperus

DATE OF BIRTH: 21-10-1987

PLACE OF BIRTH: Oberpullendorf

EDUCATION

2012-04 to date Master's program
University of Natural Resources and Applied Life Sciences,
Vienna

Field of study: Biotechnology

Master's thesis: Differentiation of adipose derived
mesenchymal stem cells using specialized bioreactors

2011-08 to 2012-02 Erasmus program
Kungliga Tekniska Högskolan KTH Stockholm
School of Biotechnology

2008-10 to 2012-04 Bachelor's program
University of Natural Resources and Applied Life Sciences,
Vienna

Field of study: Food Science and Biotechnology

Bachelor's thesis: Nickel Allergy – Biochemical Pathway

2007-10 to 2008-06 University of Vienna

Field of study: Pharmaceutics

2007-06-06 Supplementary A – level exam in Biology
in a secondary school 1040 Vienna

2002-09 to 2007-06 Federal Higher Technical Institute
HTBLuVA Automation Engineering in 2700 Wiener
Neustadt

A level – passed with credit

Diploma thesis: Modernization of control and feedback
systems

1998-09 to 2002-07 Secondary school in 2560 Berndorf

1994-09 to 1998-07 Primary school in 2763 Pernitz

WORK EXPERIENCE

2013-06 to 2013-09	Boehringer Ingelheim RCV GmbH & Co KG – internship Process Science Downstream
2012-04 to date	Medical University Vienna - Clinic of Surgery Research assistant 10 h per week
2010-01 to 2011-06	Thyroid Resources Centre Vienna – Nuclear Medicine Doctor's receptionist 10 h per week
2009-09 to 2009-09	NUA Umweltanalytik GmbH – internship Microbiology laboratory
2008-10 to 2009-12	Buero.Vogl GmbH Engineer 8 h per week

FOREIGN LANGUAGES

English (Fluent in spoken and written), Swedish (elementary level, A2)